THEORETICAL RESEARCHES ON LASER DRIVEN FUSION

(Laser Plasma Interaction and Implosion Processes)

レーザー核融合の理論的研究
(レーザープラズマ相互作用及び爆縮の研究)

January 10, 1980

Hideaki TAKABE

(Osaka University)

C O N T E N T S

Chapter 1

Introduction

In the laser driven fusion plasma, the problems are roughly separated into the following three titles.

(1) Absorption and Reflection

(2) Transport

(3) Implosion

At the first, irradiated laser light is partially absorbed by collisional or collective processes, while partially reflected by specular reflection or scattered by the stimulated Brillouin scattering. To investigate these phenomena is the foundamental problem to perform the laser fusion. At the second, the absorbed energy, which is mainly deposited near the cut-off as the electron thermal energy, causes the expansion of the target plasma into vaccum. Then, this energy is transported inward through the so-called transport region. To investigate how the absorbed energy is transported and what parcent of this energy is spent to implode the fuel is the second problem. At the third, the transported energy, which does the mechanical work against the non-ablating inner region, causes the super compression of the inner fuel and induces the nuclear reaction near the center of the fusion target. To investigate the implosion phenomena to carry out the optimum implosion is the third and final problem of the laser fusion. These are schematically shown in Fig.1.1.

My theoretical research on laser fusion is mainly devoted to the problem of implosion, so that I intend to introduce the concept of implosion. The necessity of the concept of implosion may be easily understood from the following brief discussion. Let us consider the compressed D.T fuel core with

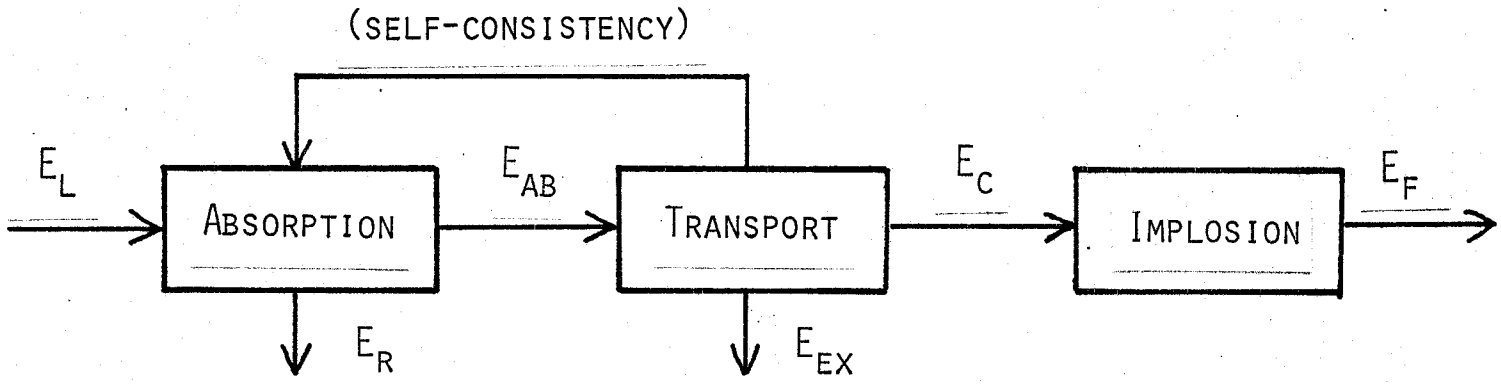

Fig. 1.1 Power flow diagram for essential three mechanisms in the target plasma.
In this diagram, E_l: laser energy, E_r: reflected energy, E_{ex}: energy lossed by ablation, E_c: energy transported in to compressed core, and E_f: fusion energy.

the radius R (cm) and density ρ (g/cm^3). When this core is heated up to 10 keV and begins to expand lowering its density and increasing its radius, the burning rate through the inertially confined time is estimated as follows.

$$f_B = \frac{\rho R}{6 + \rho R}$$

On the other hand, the required laser energy E_L to heat the target up to 10 keV maintaing constant ρR is proportional to $\bar{\rho}^2$, because

$$E_L \propto E_e = \frac{4}{3}\pi \frac{\rho}{M} R^3 \times 10 \ (keV)$$

$$\Rightarrow \quad E_L \propto (\rho R)^3 \cdot \rho^{-2}$$

This indicates that the required energy in order to get the same ρR value becomes lower with increasing the compress core density. The detail estimate yields the following requirement to laser energy in order to reach scientific breakeven.

where ρ_s=0.213 g/cm^3 is the solid D-T density and it is assumed that the 8 % of incident laser energy is transported into the compressed core region through the reflection and ablation losses. As apparent from this discussion, it is necessary to compress the D-T fuel more than 1,000 times solid density in order to perform the laser fusion by the use of practical lasers. (10 $\sim$ 100 k joule) In such a meaning, the laser may be the source driver to induce a piston to compress the fuel rather than to heat it.

In order to clarify what plays the role of a piston in laser fusion, the problem of the laser induced ablation structure is treated in Chaps.2 and 3 by the use of a stationary model (chap.2) and a self-similar model (Chap.3). The detail structures are investigated using the one-fluid two-temperature hydrodynamic equations. The resultant structure provides us the relation between the mechanical power, which gives us the compression efficiency, and the absorbed laser power. The efficiency of the laser driven implosion is discussed.

In connection with implosion, much attention is focused on the transport problem. Since in the high power laser regime the absorption becomes mainly due to the collective processes, where the resonantly induced plasma waves accerelate the electrons to much higher energy, the generated hot elelctrons directly preheat the inner core and prevent it from being compressed. In Chap.4, the hot electron transport is discussed. The following are pointed out. The cold electron return current induced to maintain charge neutrality exceeds the sound velocity and ion wave turbulence is excited near the cut-off. This

turbulence causes an anomalous resistivity, and due to this resistivity the large electrostatic field is generated. This field prevents the hot electrons from penetrating into the compressed region and preheating there.

In Chap.5, the preblem of the resonance absorption is considered associated with the transport problem. Since the transport problem shows the exsistence of the strong expanding motion near the cut-off, or as will be shown in Chap.4, the very strong return current there, the self-consistent inclusion of such flow effects on influencing the resnance absorption processes becomes important. The resonance absorption including these effects are discussed in Chap.5. And it is pointed out that when the flow velocity is sufficiently large, the growth of the plasma wave is saturated due to convection loss.

Chapter 6 is devoted to investigate and discuss the implosion symmetry. In this chapter, attention is focused on the stability of ablation front, since the formation of such front is unavoilable for inertia fusion. The systematic analyses are presented for the compressivity, thermal conduction, ablation, and convention effects, separately. It is pointed out that the compressibility, conduction, and ablation effects reduced the growth of the unstable mode compared with that given by the classical Rayleith-Taylor analysis. In constract to these effects. the convection effect exhibies the interesting role in the stability. In the case where the flow is subsonic the convection effect gives rise to the instability even when the acceleration is absent, while in the case where the flow

Chapter 2

Structure of Stationary Propagating Deflagration Wave

2.1 Introduction

When laser light impinges on a cold solid target, the absorbed energy causes the matter to be heated and set into motion. Since the target is located in a vacuum, an expansion wave will appear. On the other hand, high pressure created by the rapid increase of plasma temperature at the surface can also drive a compression wave which propagates into the solid. The compression wave is maintained by a deflagration wave which separates it from the expansion region. Namely, the deflagration wave can play the role of a piston in laser compression. The electron thermal flux flows into the deflagration region from the laser absorption layer. An increase in the internal energy in this region due to the incoming thermal flux can be regarded as that due to combustion in a chemical reaction wave. Because of the nonlinear thermal conductivity, the deflagration contains a steep temperature gradient as shown in Fig. 2.1. The shock and deflagration fronts propagate into the target. The plasma fluid is accelerated inward across the shock front, and then accelerated outward to the rarefaction region through the deflagration structure. Hence, the deflagration region is often called an ablation layer.

In this chapter we present the structure of the stationarily propagating deflagration wave and a steady compression model in a slab target. Bobin[1)] has investigated the deflagration structure in a one-temperature approximation. We will show by using a two-temperature model that the ion temperature is about half of the electron temperature near the Chapman-Jouguet point of the deflagration. Bobin also assumed that the cut-off density correpsonds to the Chapman-Jouguet point. It will be, however, shown that the

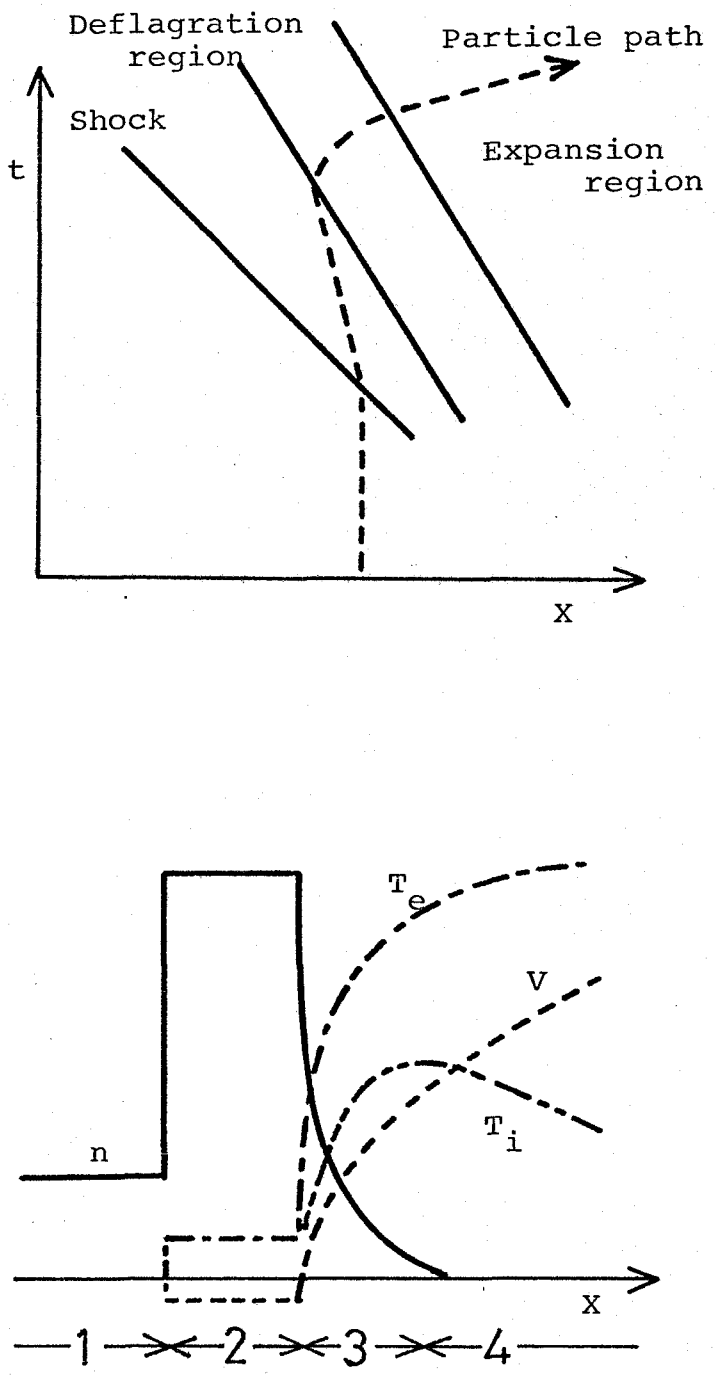

Fig. 2.1 Principal peature of the whole system:

(a) x-t diagram.

(b) Spatial profiles of the electron temperature (T_e), ion temperature (T_i), density (n), and velocity (V). Here, four regions correspond to unperturbed region (1), compressed region (2), deflagration region (3), and rerefaction region (4), respectively.

density at the Chapman-Jouguet is not necessarily the cut-off density and that the density is determined by means of the energy conservation in the whole system.

It is shown in Sec.2-2 that the deflagration can be regarded as a thermal wave accompanied by hydrodynamic motion and that it plays the role of a piston in laser compression. In this section the energy relaxation time between the electrons and the ions is assumed to be small enough for a one-temperature approximation to be used, while the finite relaxation time is taken into account in Sec.2-3 and the deflagration structure is obtained in the two-temperature model. Sec.2-4 is devoted to the shock wave driven by the deflagration. It is shown in Sec.2-5 that a constant energy flux should be absorbed in order to realize the stationary propagation of the deflagration. The compression and ablation profiles are then determined with the aid of the energy conservation.

2.2 Basic Equations and One Temperature Approximation

Since we are interested in the thermal behaviour of the plasma coupled with the fluid motion, the following equations are assumed as the basic ones[2]:

$$\frac{\partial}{\partial t} n + \frac{\partial}{\partial x} nu = 0 \tag{2.1}$$

$$\frac{\partial}{\partial t} u + u \frac{\partial}{\partial x} u = - \frac{1}{m_i n} \frac{\partial}{\partial x} [n (T_e + T_i)] \tag{2.2}$$

$$\frac{\partial}{\partial t} T_i + u \frac{\partial}{\partial x} T_i = - \frac{2}{3} T_i \frac{\partial u}{\partial x} + \frac{T_e - T_i}{\tau_{ei}} \tag{2.3}$$

$$\frac{\partial}{\partial t} T_e + u \frac{\partial}{\partial x} T_e = - \frac{2}{3} T_e \frac{\partial u}{\partial x} - \frac{T_e - T_i}{\tau_{ei}} + \frac{2}{3n} \frac{\partial}{\partial x} \kappa_e \frac{\partial T_e}{\partial x} \tag{2.4}$$

Here n is the number density of the plasma, u is its flow velocity, T_e and T_i are the temperatures of electrons and ions (multiplied by the Boltzmann constant), respectively; τ_{ei} is the temperature equiliblium time between the ions and the electrons, while κ_e is the thermal conductivity of the electrons, namely[3],

$$\tau_{ei} = \frac{3}{8\sqrt{2\pi}} \cdot \frac{m_i T_e^{3/2}}{n m_e^{1/2} e^4 \ln\Lambda} \tag{2.5}$$

$$K_e = 1.89 \left(\frac{2}{\pi}\right)^{3/2} \frac{T_e^{5/2}}{m_e^{1/2} e^4 \ln\Lambda} = K_{e0} T_e^{5/2} \tag{2.6}$$

in which m_e and m_i are the mass of the electron and that of the ion respectively, and $\ln\Lambda$ is the Coulomb logarithm. The first two equations (2.1) and (2.2) are the well-known mass and momentum conservation laws. Here the viscous term is neglected. Equation (2.3) governs the variation of ion temperature, in which the effect of ion thermal conduction is neglected as it is assumed to be small in comparison with that of the electron-ion temperature relaxation. The change of the electron temperature is given by Eq.(2.4).

When the temperature equiliblium time τ_{ei} is small, Eq.(2.3) yields $T_i \simeq T_e$. In this case, Eqs.(2.3) and (2.4) are reduced to

$$\frac{\partial T}{\partial t} + u \frac{\partial}{\partial x} T = -\frac{2}{3} T \frac{\partial u}{\partial x} + \frac{2}{3n} \frac{\partial}{\partial x} K \frac{\partial T}{\partial x} \tag{2.7}$$

in which $T = 2T_e$ and $K = \left(\frac{1}{2}\right)^{7/2} K_{e0} T^{5/2}$. Thus, the basic equations in the one-temperature approximation are given by Eqs.(2.1),(2.2) and (2.7), and the following equations are obtained for the stationary phenomenon in the wave frame.

$$nu = J_0 \tag{2.8}$$

$$u + \frac{1}{m_i}\frac{T}{u} = P_0 \tag{2.9}$$

$$\frac{5}{2}T + \frac{1}{2}m_i u^2 \frac{K_{e0}}{J_0} T^{5/2}\frac{dT}{dx} = Q_0 \tag{2.10}$$

where J_0, P_0 and Q_0 are integral constants, and they can be determined by the boundary conditions. If T and u are normalized by

$$\tilde{T} = \frac{4T}{m_i P_0^2} \quad , \quad \tilde{u} = \frac{2u}{P_0} \tag{2.11}$$

Eq.(2.9) becomes a parabolic form

$$\tilde{T} = \tilde{u}(2-\tilde{u}) \tag{2.12}$$

This curve is drawn in Fig.2-2. By using the local Mach number, $M = u/(T/m_i)^{1/2}$, Eq.(2.12) is also written as

$$M^2 = \frac{\tilde{u}}{2-\tilde{u}} \tag{2.13}$$

Hence, the plasma flow is

subsonic in $0 < \tilde{u} < 1$,

sonic at $\tilde{u} = 1$, and

supersonic in $1 < \tilde{u} < 2$.

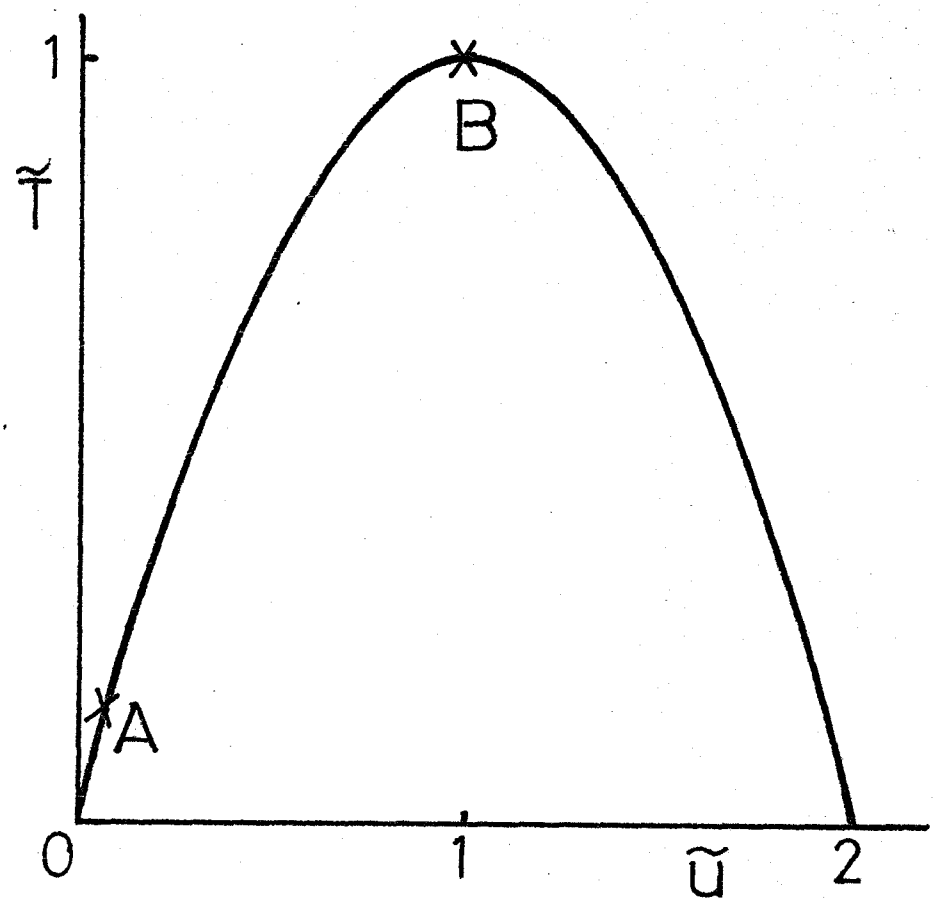

Fig. 2.2 $\tilde{T}$-$\tilde{u}$ diagram obtained from the mechanical equations. Points A and B correspond to the front and rear of the deflagration, respectively.

In general, through the deflagration structure, the plasma flow must be subsonic [4], and the flow velocity increases monotonically. Since the temperature increases with the flow velocity in the subsonic region (see Fig.2-2), in order to realize a stationary deflagration, the tail of the deflagration must be bounded at a critical point, $x=x_p$, where some external heat is supplied. Out of this boundary, the flow is generally non-stationary so that sonic disturbances exist. Therefore, for a stationary deflagration to be realized, it is required that the disturbances do not propagate into the deflagration region. Namely at the boundary $x=x_p$, the flow velocity must be equal to the sound velocity so that the local phase velocities of the sonic disturbances are zero. Thus the critical point must be the sonic point, which is often called the Chapman-Jouguet point. It should be noted that although a constant heat flux should be supplied at the boundary x_p, the cut-off point may not necessarily be the sonic point. We shall assume that the cut-off point is outside of the deflagration. Therefore, the stationary deflagration passes from any subsonic point A to the sonic point B through its structure on the $\tilde{u}$-$\tilde{T}$ plane in Fig.2-2. Under such a regime, the integration constants J_0, P_0 and Q_0 are determined as follows. By the C-J condition, u_p is equal to the sound velocity C_p $(=\sqrt{T_p / m_i})$. (We denote the variables behind and ahead of the deflagration by subscript p and f respectively.) Therefore, from Eq.(2.8) and (2.9),

$$J_0 = M_p \cdot C_p \ , \quad P_0 = 2 C_p \ . \qquad (2.14)$$

We now introduce the parameter a which is the ratio of the density ahead of the deflagration to thatt behind.

$$\alpha \equiv \frac{n_p}{n_f} \tag{2.15}$$

which will be determined in the next section. Using this parameter α, form Eqs.(2.8) and (2.9), we obtain

$$u_f = \alpha c_p , \qquad T_f = (2-\alpha)\alpha \cdot T_p \tag{2.16}$$

In Eq.(2.10), taking note of d/dx = 0 at the front, we obtain

$$Q_0 = (5-2\alpha)\alpha \cdot T_p \tag{2.17}$$

Let us normalize n, u and T in terms of the quantities behind the deflagration : $n = n_p\tilde{n}$, $u = c_p\tilde{u}$ and $T = T_p\tilde{T}$, while the length is normalized in terms of the mean free path $l_p = (5/24\pi)^{1/2}T_p^{\,2}/(n_p e^4 \ln\Lambda)$ as $x = l_p \cdot (m_i/m_e)^{1/2}\tilde{x}$. The normalization for u and T are identical with those employed in Eq.(2.11). Then Eqs.(2.8),(2.9) and (2.10) become

$$\tilde{n}\,\tilde{u} = 1 \tag{2.18}$$

$$\tilde{u} + \frac{\tilde{T}}{\tilde{u}} = 2. \tag{2.19}$$

$$\frac{5}{2}\tilde{T} + \frac{1}{2}\tilde{u}^2 - a\tilde{T}^{5/2}\frac{d\tilde{T}}{d\tilde{x}} = \alpha(5-2\alpha), \tag{2.20}$$

$$a = 0.33.$$

In general the density ratio α is small enough to neglect the right hand side of Eq.(2.20). We then obtain

$$\frac{a\tilde{T}^{5/2}}{\frac{5}{2}\tilde{T} + \frac{1}{2}\tilde{u}^2}\, d\tilde{T} = d\tilde{x}. \tag{2.21}$$

Before integrating this equation, we show that the temperature structure of the deflagration can be approximately given by that of the thermal wave[5]. Since the flow is subsonic through the structure, Eq.(2.21) can be easily integrated with neglecting the flow term.

$$\tilde{T} = \left(\frac{5}{2}\right)^{4/5}\left(\frac{\tilde{x}}{a}\right)^{2/5} \tag{2.22}$$

This temperature structure is that of the well-known thermal wave. Integration Eq.(2.21) with the aid of Eq.(2.19), we obtain

$$\frac{\tilde{x}}{a} = \frac{1}{5} w^5 - \frac{1}{3}(1+\tilde{u}) w^3 - \left(\frac{3}{2}+\tilde{u}\right) w - \frac{33}{16} \sin^{-1}\sqrt{\frac{\tilde{u}}{2}}$$

$$- \frac{15\sqrt{5}}{32} \sin^{-1}\left(\frac{5-3\tilde{u}}{5-2\tilde{u}}\right) + 1.6464. \qquad (2.23)$$

Here w^2 denotes u(2-u) (=T), and the integration constant is estimated by setting u=0 at x=0. The width of the deflagration Δx can be obtained by putting u=1 in Eq.(2.23),

$$\Delta x = 0.049\, l_p \cdot \left(\frac{m_i}{m_e}\right)^{1/2} \qquad (2.24)$$

On the basis of Eq. (2.23), n and T are calculated as functions of x, which are plotted in Fig.2.3. One can see that for most of the deflagration, all the quantities change gently (almost linearly). However, in the vicinity of the front all the quantities vary very rapidly as in a thermal wave. At the sonic point, du/dx becomes infinite, but dT/dx is finite. This singularity is well-known as a bifurcation, but in fact, must vanish due to the non-stationary effect. From Eqs.(2.1) and (2.2),

$$\frac{\partial u}{\partial x} = \frac{-\frac{u}{m_i}\frac{\partial T}{\partial x} + \frac{c^2}{n}\frac{\partial n}{\partial t} - u\frac{\partial u}{\partial t}}{u^2 - c^2}$$

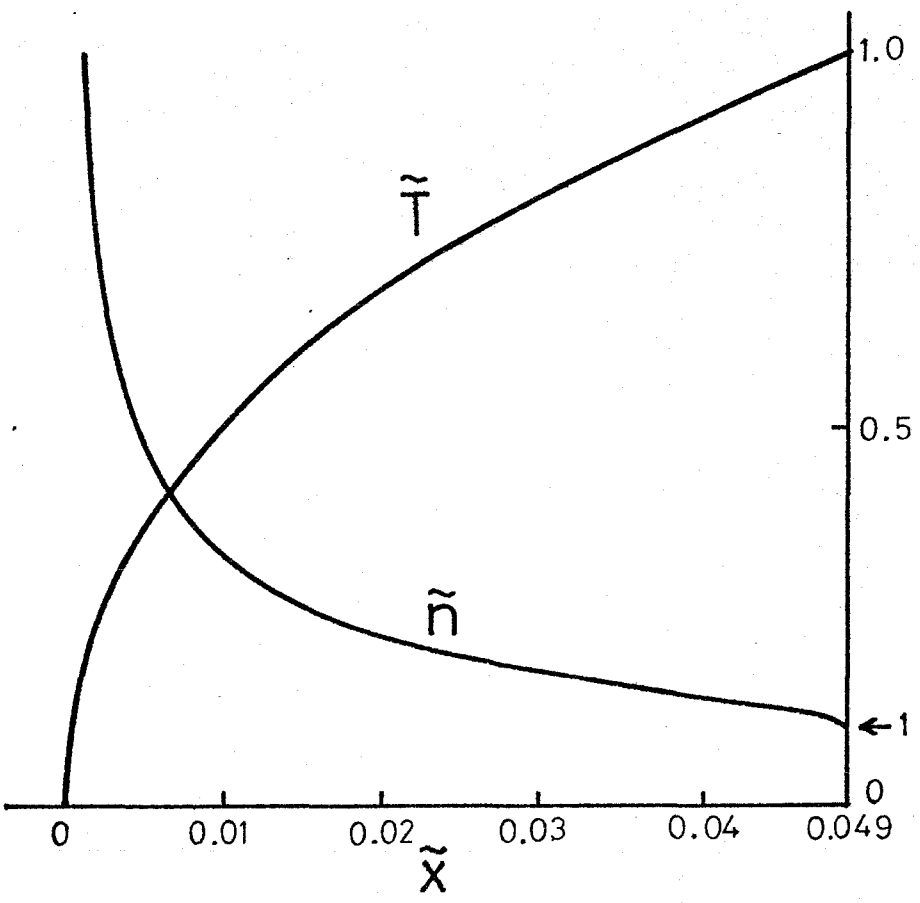

Fig. 2.3 Normalized deflagration structure in the one temperature approximation given in Eq.(2.23). $\tilde{x} = 0$ and $\tilde{x} = 0.049$ correspond to the front and sonic point, respectively.

here C means the sound velocity, $(T/m_i)^{1/2}$. Since the denominator vanishes at the sonic point, the numerator should also vanish. As the result, the relation

$$\frac{\partial C}{\partial X} = \frac{1}{2}\left(\frac{C}{n u}\frac{\partial n}{\partial t} - \frac{1}{C}\frac{\partial u}{\partial t}\right)$$

should be established at this sonic point. It will become obvious in chapter 3 that this singularity appearing at the sonic point has no physical meaning and taking the non-stationary effect into account by considering the self-similar motion allows the continuous extention to the super sonic region.

It shound be noted from Eqs.(2.15) and (2.16) that the change in the pressure through the deflagration is approximately given by $P_f = n_f T_f \quad 2n_p T_p = 2P_p$, which is very small compared with those of the desity and the temperature for small α . The incoming flow velocity into the deflagration u_f is αC_p from Eq.(2.16), while the propagation velocity of the deflagration λ_D is propotional to $\alpha^{1/2} C_p$, which will be obtained in Sec.2.4. Consequently, if the density at the front is large enough compared with that at the sonic point, that is, if α is small, the pressure is kept nearly constant and the incoming mass flux into the deflagration is small. Thus, the fluid ahead the deflagration is pushed with the velocity $\lambda_D - u_f \simeq \lambda_D$ in the laboratory frame. This is the reason why the deflagration plays the role of a piston in laser compression.

2.3 Structure of Stationary Deflagration in Two Temperature Model

As shown in the previous section, the plasma temperature behind the deflagration is high, while its desity is low. Thus the one temperature approximation may not be valid in the rear of the deflagration, since the temperature equilibrium time τ_{ei} is propoerional to $n^{-1}T_e^{3/2}$. In this section, we take into account the effect of the finite temperature equilibrium time. Equations (2.1) (2.4) can be integrated, assuming a stationary propagation of the deflagration. The resultant equations in the wave frame are the following with the same mornalization employed in the previous sections.

$$\tilde{n}\tilde{u} = 1. \tag{2.25}$$

$$\tilde{u} + \frac{\tilde{T}_e + \tilde{T}_i}{\tilde{u}} = 2. \tag{2.26}$$

$$\frac{d\tilde{T}_i}{d\tilde{x}} + \frac{2}{3}\frac{\tilde{T}_i}{\tilde{u}}\frac{d\tilde{u}}{d\tilde{x}} - \nu_0 \frac{\tilde{T}_e - \tilde{T}_i}{\tilde{u}^2 \tilde{T}_e^{3/2}} = 0. \tag{2.27}$$

$$\frac{5}{2}(\tilde{T}_e + \tilde{T}_i) + \frac{1}{2}\tilde{u}^2 - \kappa_0 \tilde{T}_e^{5/2}\frac{d\tilde{T}_e}{d\tilde{x}} = \alpha(5-2\alpha) \tag{2.28}$$

Equation (2.28) is obtained by adding Eq. (2.3) to Eq. (2.4). ν_0 and κ_0 are constants equal to 1.72 and 3.73, respectively. The boundary conditions used at the sonic point are $T_e + T_i = 1$

and u = 1, by which the conditions at the front become $\tilde{T}_e = \tilde{T}_i = \frac{1}{2}(2-\alpha)$ and $\tilde{u} = \alpha$. From Eq. (2.26) $\tilde{T}_i$ is given in terms of $\tilde{u}$ and $\tilde{T}_e$, which is then substituted into Eqs. (2.27) and (2.28) to give the set of two differential equations for $\tilde{T}_e$ and $\tilde{u}$.

$$\frac{d\tilde{T}_e}{d\tilde{x}} = \frac{1}{K_0}(\tilde{u}-\alpha)(5-2\alpha-2\tilde{u})\,\tilde{T}_e^{-5/2} \tag{2.29}$$

$$\frac{d\tilde{u}}{d\tilde{x}} = \frac{3}{2}\frac{1}{K_0}\,\frac{\tilde{u}^2(\tilde{u}-\alpha)(5-2\alpha-2\tilde{u}) + K_0\nu_0(2\tilde{T}_e - 2\tilde{u} + \tilde{u}^2)\tilde{T}_e}{\tilde{u}(5\tilde{u}-4\tilde{u}^2-\tilde{T}_e)\tilde{T}_e^{5/2}} \tag{2.30}$$

Here we note that in contrast to the one temperature case, the sonic point is not a sigular point; equating $\tilde{u}$ to unity on the right hand side of Eq. (2.30) yields a finite $d\tilde{u}/d\tilde{x}$, because $d\tilde{T}_e/d\tilde{x} = -d\tilde{T}_i/d\tilde{x}$ is established at this point so that the singularity disappears.

The independent variable $\tilde{x}$ is next eliminated by dividing Eq. (2.29) by Eq. (2.30). The resultant differential equation,

$$\frac{d\tilde{T}_e}{d\tilde{u}} = \frac{2}{3}\cdot\frac{\tilde{u}(\tilde{u}-\alpha)(5-2\alpha-2\tilde{u})(5\tilde{u}-4\tilde{u}^2-\tilde{T}_e)}{\tilde{u}^2(\tilde{u}-\alpha)(5-2\alpha-2\tilde{u}) + K_0\nu_0(2\tilde{T}_e - 2\tilde{u} - \tilde{u}^2)\tilde{T}_e} \tag{2.31}$$

may then in principle be integrated from the front $(\tilde{u},\tilde{T}_e) = [\alpha, \frac{\alpha}{2}(2-\alpha)]$ (point A) to the rear $\tilde{u} = 1$ (point B) in the $(\tilde{u}, \tilde{T}_e)$ plane to give a relation $\tilde{T}_e = \tilde{T}_e(\tilde{u})$. However, the point A is obviously a singular point of Eq. (2.31). To obtain the slope of

the integral curve at the singular point we assume that, near the singular point the solition is of the form

$$\tilde{u} = \alpha + K_1 \exp(s\tilde{x})$$

$$\tilde{T}_e = \frac{\alpha}{2}(2-\alpha) + K_2 \exp(s\tilde{x}) \qquad (2.32)$$

where K_1 and K_2 are assumed small. On inserting these assumed forms into Eqs. (2.27) and (2.28) in which T_i is eliminated by using Eq. (2.26), and retaining only those terms linear in K_1 and K_2, one then obtains a homogeneous system foir these quantities. The characteristic equation of the system given by Eqs. (2.27) and (2.28) at the singular point A is

$$s^2 - \left\{ \frac{1}{4-\frac{7}{2}\alpha}\left[5-4\alpha-K_0\gamma_0\frac{(2-\alpha_0)(1-\alpha)}{\alpha}\right]\right\} s$$

$$-\left\{\frac{2}{3}K_0\gamma_0\frac{(2-\alpha)(5-4\alpha)}{\alpha(4-\frac{11}{3}\alpha)}\left[\frac{\alpha}{2}(2-\alpha)\right]^{5/2}\right\} = 0 \qquad (2.33)$$

Since $\alpha<1$ the characteristic equation has two roots with opposite sign. Such a singular point is called a saddle point. A saddle point provides a good starting point for the munerical integration because there is a unique integral curve passing through the saddle

point for each characteristic direction.

The numerical results are shown in Fig.2.4. In Fig.2.4-(a), the whole deflagration structure is shown, while in Fig.2.4-(b) the front structure is shown in an expanded scale. For several α values which are sufficiently small compared with unity, it is found that the deflagration structures are almost the same, and the following characteristics of the deflagration are obtained. Near the front, the temperatures and the flow velocity increase steeply but the pressure is almost constant, thereby demonstrating that the thermal wave approximation is valid. The one temperature approximation also holds in the front. The heat is efficiently imparted to the ions through electron-ion collisions. In the course of the expansion, the ions still get some energy from the electrons. However, the expansion cooling makes the ion temperature lower, so that it becomes, half of the electron temperature in the rear of the deflagration. At the sonic point, $T_e = 0.68$ and $T_i = 0.32$, and ions are heated up to 50 % of the electron temperature due to electron-ion collisions. The width of the deflagration, Δx, is given by

$$\Delta x = 0.32\, l_{ep} \left(\frac{m_i}{m_e}\right)^{1/2} \qquad (2.34)$$

where l_{ep} is the electron mean free path at the sonic point. It should be also noted that the pressure changes gently through the deflagration and the pressure behind the deflagration is about the half of that at the front.

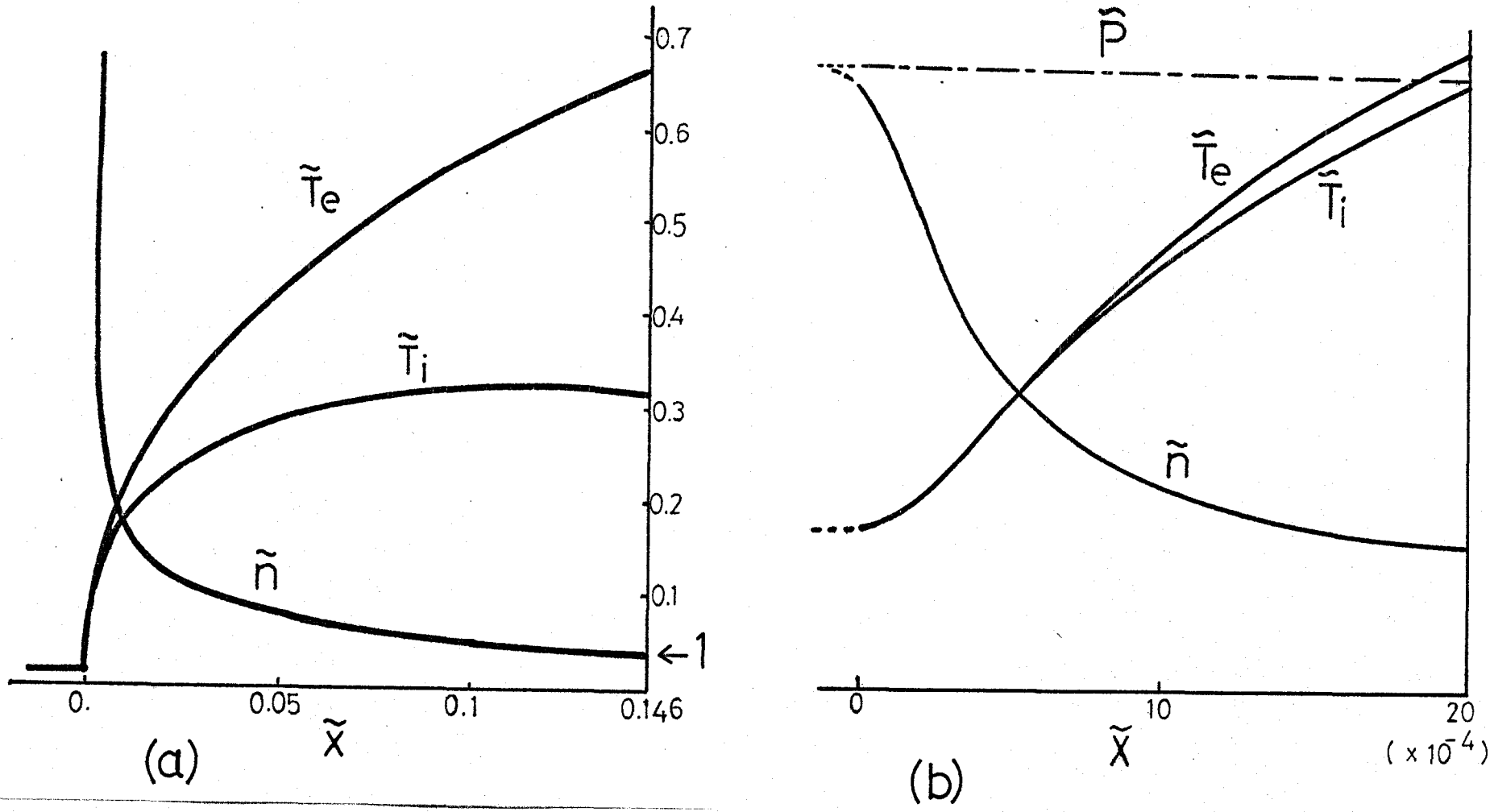

Fig. 2.4 Normalized deflagration structure in the twe temperature model:

(a) Whole structure of deflagration.

(b) Structure near the front in an expanded scale.

2.4 Shock Wave Driven by Deflagration

The deflagration plays the role of a piston in laser driven compression, as was shown in the previous sections. A shock wave can therefore be driven ahead the deflagration. We can determine the propagation velocities of both the shock and the deflagration in terms of n_p, C_p, and the states ahead of the shock. From Eqs. (2.15) and (2.16), the ratios of plasma desity and tempareture ($T_e + T_i$) across the shock are written as

$$\mu = \frac{n_f}{n_s} = \frac{1}{\alpha}\frac{n_p}{n_s}, \qquad \delta = \frac{T_f}{T_s} = \alpha(2-\alpha)\frac{T_p}{T_s} \tag{2.35}$$

respectively, where the states ahead the shock are denoted by the subscript s. The Rankine-Hugoniot relation[6] can be then reduced to the form.

$$4\alpha^2 - \left(\delta + \frac{n_p}{n_s} + \frac{n_s T_s}{n_p T_p}\right)\alpha + 2\left(\frac{n_p}{n_s} + 2\frac{T_s}{T_p}\right) = 0 \tag{2.36}$$

from which the parameter α is determined as a function of the plasma desities and temperatures in the unperturbed region and at the C-J point. The solution of Eq. (2.36) can be given approximately by

$$\alpha \cong \frac{2n_p T_p + 4 n_s T_s}{\delta n_p T_p + n_s T_s} \tag{2.37}$$

From the definition of the deflagration[4], $\alpha<1$, the condition for the pressure,

$$P_p > \frac{1}{2} P_s$$

is required to realize the deflagration wave.

Thus, with the knowledge of n_p and T_p, which will be determined in the next section, the plasma motion can be uniquely determined. The shock speed λ_s given by

$$\lambda_s = \mu \left[\frac{5 T_f}{(4\mu-1) m_i} \right]^{1/2} = \mu \left[\frac{5\alpha(2-\alpha)}{4\mu-1} \right]^{1/2} C_p \qquad (2.38)$$

where Eq.(2.16) is used to eliminate T_f. The downstream flow velocity of the shock wave u_f' is calculated in the laboratory frame as

$$u_f' = \left(1 - \frac{1}{\mu}\right) \lambda_s \qquad (2.39)$$

When one sees this velocity in the deflagration frame moving with the velocity λ_D, it corresponds to the inflow velocity u_f. Thus,

$$u_f' - \lambda_D = - u_f \tag{2.40}$$

Using Eqs. (2.16), (2.38) and (2.39), we obtain the propagation velocity of the deflagration,

$$\lambda_D = \left\{ (\mu-1) \left[\frac{5\alpha}{4\mu-1} (2-\alpha) \right]^{1/2} + \alpha \right\} \cdot c_p \tag{2.41}$$

Since α is small compared to unity, as long as δ is small enough we can obtain the followings for λ_s and λ_D, i.e.,

$$\lambda_s, \lambda_D \propto \alpha^{1/2} \cdot c_p \tag{2.42}$$

Since the plasma is initially at rest, the kinetic energy aquired by a particle passing through the shock front is equal to

$$\mathcal{E}_{kin} = \frac{1}{2} m_i u_f'^2 \tag{2.43}$$

Also, the increase of the internal energy of a particle is given by

$$\mathcal{E}_{in} = \frac{3}{2}(T_f - T_s) \tag{2.44}$$

With the aid of Eqs. (2.16), (2.35), (2.36), (2.38) and (2.39), the total enerty increase of a particle passing through the shock front is written as

$$\begin{aligned}\mathcal{E} &= \mathcal{E}_{kin} + \mathcal{E}_{in} \\ &= (\mu-1)(2-\alpha)\alpha\, T_p\end{aligned} \tag{2.45}$$

Although the deflagration can be regarded as a piston in laser compressin, the plasma flowing into the shock compressed region is escaping to the deflagration regions. This is different from the usual gas shock proceeding ahead of a piston in a tube. The flux J_0 given by Eq.(2.15) escapes from the compressed region into the deflagration region. Thus the energy increase in the whole compressed region in unit time is given by

$$\begin{aligned}\dot{\mathcal{E}}_{comp} &= (M_s \lambda_s - J_0)\,\mathcal{E} \\ &= \left\{ \left[\frac{5\alpha}{4\mu-1}(2-\alpha) \right]^{1/2} - \alpha \right\} (\mu-1)(2-\alpha)\, n_p T_p \zeta_p\end{aligned} \tag{2.46}$$

2.5 Energy Conservation

Isothermal expansion is assumed to follow the deflagration. Since the deflagration propagates with the velocity λ_D, the flow velocity and the density in the expansion region can be, therefore, expressed as follows in the laboratory frame,

$$u = c_p + \frac{x}{t}, \quad n = n_p \exp\left[-\left(\frac{x}{t} + \lambda_D\right)^2 / c_p\right] \tag{2.47}$$

where the point $x = -\lambda_D t$ corresponds to the Chapman-Jouget point. The energy increase in this region is given by

$$\dot{\mathcal{E}}_{iso} = \frac{d}{dt} \int_{-\lambda_D t}^{\infty} n \left(\frac{3}{2} T_p + \frac{1}{2} m_i u^2\right) dx \tag{2.48}$$

Substituting Eq.(2.47) into Eq.(2.48) and using Eq.(2.41), the increase is written as

$$\dot{\mathcal{E}}_{iso} = \left(4 - 2\beta + \frac{\beta^2}{2}\right) T_p n_p c_p \tag{2.49}$$

where $\beta = \{(\mu-1)[5\alpha(2-\alpha)/(4\alpha-1)]^{1/2} + \alpha\}$.

The energy increase in the whole system is the sum of $\dot{\varepsilon}_{comp}$ and $\dot{\varepsilon}_{iso}$ given by Eqs.(2.46) and (2.49), respectively. Since for

small values of α, $\dot{\varepsilon}_{comp}$ and $\dot{\varepsilon}_{iso}$ can be approximately given by

$$\dot{\mathcal{E}}_{comp} = \left(\frac{40\alpha}{4\mu-1}\right)^{1/2}(\mu-1)\, n_p T_p C_p + O(\alpha) \tag{2.50}$$

$$\dot{\mathcal{E}}_{iso} = \left[4-(\mu-1)\left(\frac{40\alpha}{4\mu-1}\right)^{1/2}\right] n_p T_p C_p + O(\alpha) \tag{2.51}$$

the energy increase in the whole system is

$$\begin{aligned}\dot{\mathcal{E}}_{tot} &= \dot{\mathcal{E}}_{comp} + \dot{\mathcal{E}}_{iso} \\ &\simeq 4 n_p T_p C_p + O(\alpha)\end{aligned} \tag{2.52}$$

One can estimate the energy partition ratio which is defined as the ratio of the enegy increase in the compressed region to that in the whole system. This ratio can be regarded as the efficiency of energy transport to the compressed region. Using Eqs.(2.50) and (2.51), we obtain

$$\eta_{comp} = \frac{\dot{\mathcal{E}}_{comp}}{\dot{\mathcal{E}}_{tot}} \simeq \left[\frac{5}{2(4\mu-1)}\right]^{1/2}(\mu-1)\,\alpha^{1/2} \tag{2.53}$$

It should be noted that the compression efficiency is proportional to $\alpha^{1/2}$.

The steady propagation of the deflagration can be realized only in the case where constant energy flux is supplied to the plasma to compensate for the energy increase $\dot{\varepsilon}_{tot}$. Thus, $\dot{\varepsilon}_{tot}$ should be equal to the absorbed energy flux Φ near the cut-off density. The absorbed energy flux is carried out from the cut-off region by the electrons. The electron temperature is sufficiently high in the cut-off region, and hence the energy transported by the electron can be given by the form

$$\Phi = f\,(n_e T_e V_{the})_{\text{at cut-off}} \tag{2.54}$$

where the numerical factor f should be determined by the microscopic phenomena in the cut-off region. Using Eqs.(2.52), (2.54) and $\Phi = \dot{\varepsilon}_{tot}$, $T_e \sim T_p$, we obtain

$$n_p \simeq 0.25\, f \left(\frac{m_i}{m_e}\right)^{1/2} n_c, \quad T_p \simeq \left(\frac{m_e^{1/2}}{f n_c}\Phi\right)^{2/3} \tag{2.55}$$

where n_c is the cut-off density. Thus, if the flux Φ is specified, the plasma motion of the whole system can be determined uniquely.

2.6 Conclusion and Discussion

Now, let us consider the case of a D-T solid target whose density, n_s, is 4.7×10^{22} cm^{-3}. With the conditions $T_s \ll T_p$ and $\alpha \ll 1$, the following relations can be obtained from Eqs.(2.35), (2.36), (2.37), (2.41) and (2.55) in the previous sections,

$$n_p \simeq 1.9\times10^{22} f \lambda_L^{-2}$$

$$T_{ep} \simeq 0.82 f^{-2/3} \lambda_L^{4/3} \Phi^{2/3}$$

$$\lambda_s \simeq 2.3\times10^{7} f^{1/6} \lambda_L^{-1/3} \Phi^{1/3}$$

$$\lambda_D \simeq 1.7\times10^{7} f^{1/6} \lambda_L^{-1/3} \Phi^{1/3}$$

here the laser wave length λ_L in μm and the laser flux Φ in units of 10^{15} W/cm^2 are used. The efficiency η_{comp} is also given as

$$\eta_{comp} \simeq 0.38 f^{1/2} \lambda_L^{-1}$$

For a Nd-glass laser and f = 0.6, the efficiency becomes approximately

$\eta_{comp} \sim 0.3$.

Let us estimate the time lag Δt to establish the stationary deflagration structure. It can be of the order of

$$\Delta t = \frac{\Delta X}{C_p} = 1.1 \times 10^{10} \frac{T_{ep}^{3/2}}{n_p} \quad (sec)$$

where T_{ep} is in keV, n_p in cm^{-3} and $\ln \Lambda$ is assumed to be 10. If n_p is equal to n_c as is assumed in Ref. 1, for the Nd-glass laser light of $\dot{\Phi}=10^{15}$ W/cm^2 we have $\Delta x=0.84$ cm and $\Delta t=14$ nsec. These width and time lag are not realistic for the short pulse laser light. However, in our theory n_p is much greater than n_c, hence we can obtain realistic results. For example, if we assume $f=0.6$, then $\Delta x=24$ μm and $\Delta t=85$ psec. This result is cofirmed by computer simulations.

References

1. J. L. Bobin, Phys. Fluids 14, 2341(1971)
2. M. S. Chu, Phys. Fluids 15, 413(1972)
3. L. Spitzer, "Physics of Fully Ionized Gases."(Interscience, New York, 1962), Chap.5.
4. R. Courant and K. O. Friedrichs, "Supersonic Flow and Shock Waves."(Interscience, New York, 1948), Chap.III-E.
5. Ya. B. Zel'dovich and Yu. P. Raiser, "Physics of Shock Waves and High -Temperature Hydrodynamic Phenomena." (Academic, New York, 1967), Chap.X.
6. L. D. Landau and E. M. Lifshitz, "Fluid Mechanics." (Pergamon, New York, 1959), Chap.9.

Chapter 3

Self-Similar Motion in Laser Produced Plasma

3.1 Introduction

To achieve break-even conditions in microfusion, a laser pulse must compress a D-T fuel to densities well above that of a solid density n_s, and strongly heat its core[1),2)]. The radiation is absorbed near the critical density where the electron plasma frequency is equal to the laser frequency. Rarefied coronal plasma is produced and hydrodynamic motion of ablation gives a reaction force to implode the central fuel. Hydrodynamics is therefore essential to the ablation and implosion phenomena.

The hydrodynamics of laser plasma interaction has already been investigated both in theoretical analysis[3),4),5),6)] (see Chap.2) and by the extensive computer simulation[7),8),9)]. The theoretical analysis has concentrated on the stationary problem for constant laser irradiation, which cannot clarify time-dependent hydrodynamic phenomena. In order to clarify how the hydrodynamics evolve with time and how these behaviours depend on the irradiated laser prameters(pulse shape, its duration, and frequency), we consider to solve the hydrodynamic equations by reducing them to the ordinary differential ones, which gives us the self-similar motion for hydrodynamics of ablating plasma.

Anisimov[10)] noted the exsistence of self-similar motion including electron conduction and ion-electron energy relaxation, and Barero and Sanmartine[11),12)] extensively analysed the self-similar motion for the hydrodynamics under the absorption of linearly increasing laser flux. We here consider the self-similar motion for the hydrodynamics of laser produced plasma. It is pointed out that one fluid, two temperature hydrodynamic equations including nonlinear electron thermal conduction and ion-electron

energy relaxation terms reduce to ordinary differential equations in general. Solving these equations under appropriate(idealized) boundary condition gives us various self-similar motions according to the difference of similarity parameter α.

In Sec.3.2, similarity properties of basic hydrodynamic equation are pointed out and the resultant ordinary differential equation are obtained. The way in which these reduced equations should be integrated under the idealized boundary condition to the ablation front is considered. An unique integral path which gives us a phsically meaningful ablation structure is found. To determine a similality parameter α and dimensional constant A is devoted to Sec.3.3. By considering the energy consevation relation through the system, the parameter α and dimensional constant A are determined. In terms of these α and A, an ablation front pressure, which gives a mechanical power to compress an inner solid region, is obtained. In Sec.3.4, an application of this analysis to an ablating plasma produced through an inverse-bremmstrahlung absorption of a constant laser flux is considered. Using the resultant ablation structure and considering strong shock formation in front of the ablation region, an x-t diagram for the characteristics is shown. In Sec.3.5, the relation between absorbed laser flux and ablation front pressure is considered. It is found that due to an expansion of the ablating region, the absorbed laser energy should be increased in proportion to one sixth power of time in order to maintain a constant pressure at the ablation front.

3.2 Similarity of Basic Equations

We consider a fully ionized plasma produced by the incidence of laser radiation on a solid target. The produced plasma may be described by the one-fluid equation as long as the characteristic scale length for spatial variation is much smaller than the Debye distance λ_D, and this condition is usually satisfied. However, the temperature relaxation time τ_{ei} between electrons and ions is long enough and the ions cannot get sufficient energy from the electrons to compensate an energy loss due to expansion cooling. We therefore employ the two temperature model with the electron thermal conduction and electron-ion energy relaxation. Then basic equations are shown as follows.

$$\frac{\partial}{\partial t} n + \frac{\partial}{\partial x} nu = 0 \tag{3.1}$$

$$\frac{\partial}{\partial t} u + u \frac{\partial}{\partial x} u + \frac{1}{n} \frac{\partial}{\partial x}\left(n \frac{Z T_e + T_i}{m_i} \right) = 0 \tag{3.2}$$

$$\frac{\partial}{\partial t} T_i + u \frac{\partial}{\partial x} T_i + \frac{2}{3} T_i \frac{\partial}{\partial x} u + \nu_0 Z^3 \frac{n (T_e - T_i)}{T_e^{3/2}} = 0 \tag{3.3}$$

$$\frac{\partial}{\partial t}(Z T_e + T_i) + u \frac{\partial}{\partial x}(Z T_e + T_i) + \frac{2}{3}(Z T_e + T_i) \frac{\partial}{\partial x} u - \frac{2}{3} \frac{K_0}{Z n} \frac{\partial}{\partial x}\left(T_e^{5/2} \frac{\partial}{\partial x} T_e \right) = 0 \tag{3.4}$$

where n, u, T_i, and T_e are the ion number density, flow velocity, ion temperature, and electron temperature, respectively. The

coefficients ν_0 and κ_0 are defined[13] by

$$\nu_0 = 6.667 \times \frac{m_e^{1/2}}{m_i} e^4 \ln\Lambda$$

$$\kappa_0 = 0.30 \times \alpha \left(m_e^{1/2} e^4 \ln\Lambda \right)^{-1} \qquad (3.5)$$

where m_i and m_e are ion and electron masses, and $\ln\Lambda$ is the Coulomb logarithm (This is assumed constant here). In the above equations we made use of the fact that the plasma is neutral, writting $n = n_i = n_e/Z$. We also exploit the fact that the ratio m_e/m_i is small. These equations describe the plasma motion in the frame moving with the ablation front (x=0), and an inertia force coming from an acceleration of the ablation front is neglected.

Let us investigate the similarity involved in Eqs.(3.1)∿(3.4). In order to do this we shall resort to dimensional considerations[14),15] Equations(3.1)∿(3.4) do not contain any dimensional parameters without the dependent variables n, u, T_e, and T_i and the independent variables x and t and the dimensional constants m_i and κ_0. (The dimension of ν_0 is constructed by $\kappa_0^{-1} m_i^{-1}$.) bearing in mind the dimensions od functions, n, u, T_e, and T_i, we can represent them in the form

$$n = \kappa_0 m_i^{5/2} \frac{x^3}{t^4} N$$

$$u = \frac{x}{t} V \qquad (3.6)$$

$$T_{e,i} = m_i \left(\frac{x}{t}\right)^2 \theta_{e,i}$$

where N, V, θ_e, and θ_i are dimensionless functions that depend on only the dimensionless variable constructed by x, t, and parameters in the problem. It is noted that Eqs.(3.1) and (3.2) are homogeneous to the density n, so that its form is determined by the energy equation (3.3) or (3.4) and in this case it is given by the density dependence of the electron heat conduction term.

In general self-similar motion has a power-law dependence on time, and the nondimensional similarity variable ξ with the form

$$\xi = \frac{x}{At^\alpha} \tag{3.7}$$

is introduced. Here A and α are constants (A is dimensional and α is a pure number). Substituting $x = At^\alpha \xi$ into the relations (3.5) and integrating new variables g, v, τ_e, and τ_i

$$g(\xi) = \xi^3 N, \quad v(\xi) = \xi V, \quad T_{e,i}(\xi) = \xi^2 \theta_{e,i} \tag{3.8}$$

,then Eq.(3.6) is rewritten in the form

$$n = K_0 m_i^{5/2} A^3 t^{3\alpha-4} g(\xi)$$

$$u = A t^{\alpha-1} V(\xi) \qquad (3.9)$$

$$T_{ei} = m_i A^2 t^{2(\alpha-1)} \tau_{ei}(\xi)$$

Taking account of the definition of the similarity variable (3.7), we substitute the above relations into Eqs.(3.1)∿(3.4). After some arrangement we obtain the following ordinary differential equations.

$$(V-\alpha\xi) g' + \{V' + (3\alpha-4)\} g = 0 \qquad (3.10)$$

$$(V-\alpha\xi) V' + \frac{1}{g}\{g(Z\tau_e + \tau_i)\}' + (\alpha-1) V = 0 \qquad (3.11)$$

$$(V-\alpha\xi)\tau_i' + \left\{\frac{2}{3}V' + 2(\alpha-1)\right\}\tau_i - \mu_0 Z^3 \frac{g(\tau_e-\tau_i)}{\tau_e^{3/2}} = 0 \qquad (3.12)$$

$$(V-\alpha\xi)(Z\tau_e+\tau_i)' + \left\{\frac{2}{3}V' + 2(\alpha-1)\right\}(Z\tau_e+\tau_i) - \frac{2}{3}\frac{1}{Zg}(\tau_e^{5/2}\tau_e')' = 0 \qquad (3.13)$$

where μ_0 is a dimensionless constant defined by $\mu_0 = K_0 \nu_0 m_i$.

The differantiation of the reduced functions with respect to the similarity variable ξ is denoted by a prime.

Before solving the above equations, we set aboundary condition to the reduced variables. It is well known[3] that as long as the target density is much higher than the cut-off density, the deflagration structure exhibits steep gradients of density n, velocity u, temperature T_e and T_i in the vicinity of the front, while the pressure nT and mass flow density nu are held almost constant there. Therefore, we set the following idealized boundary condition at the front $\xi = 0$.

$$g = \infty$$
$$v, \tau_e, \tau_i = 0$$
but
$$gv, g\tau_e, g\tau_i \neq 0, \infty \qquad (3.14)$$

Taking account of the structure of stationary deflagration[3] which says that the flow is sufficiently subsonic, the temperature relaxation is effective enough to give $T_e = T_i$, and the electron thermal conduction play the most significant part to determine the ablation structure, then we can reduce Eqs.(3.10)-(3.13) to an approximate form near the ablation front:

$$v g = J_0 \ (= 1) \quad : \text{const.} \tag{3.15}$$

$$\tau_e = \tau_i \tag{3.16}$$

$$g \tau_e = P_0 \quad : \text{const.} \tag{3.17}$$

$$(z+1) v \tau_e' + \frac{2}{3}(z+1) v' \tau_e - \frac{2}{3} \frac{1}{z g} (\tau_e^{5/2} \tau_e')' = 0. \tag{3.18}$$

It is evidient from the relation (3.9) that one of the constants of integration J_0 and P_0 can be adjusted by varing the prameter A. We set therefore J_0 to be unity. Using Eqs.(3.15),(3.18), and (3.14), the equation (3.18) is solved giving the form

$$\tau_e = \left[\frac{25}{4} \left(1 + \frac{1}{z}\right) \xi \right]^{2/5}$$

$$g = v^{-1} = P_0 \left[\frac{25}{4} \left(1 + \frac{1}{z}\right) \xi \right]^{-\frac{2}{5}} \tag{3.19}$$

$$\tau_i = \tau_e$$

The temperature profile in the above form is identical with that of the well-known thermal wave[16].

Here, a new problem to determine the constant P_0 appears when we integrate Eqs.(3.10)-(3.13) starting from the approximate solutions(3.19). The front pressure P_0 should not be chosen arbitrally. If we specify some arbitrary value of this constant P_0 and start the integral of Eqs(3.10)-(3.13), the integral curves will in general diverge, and the curves will not correspond to the correct solution. Only for a particular value of P_0 will

the integral curves converge and give a reasonable profile. This is one of eigen value problems, which are well treated for the Schrodinger equation, and the finitness of the wave function is , in this case , correspond to the energy conservation of the whole system.

If we consider the assymptotic behaviour of the solution given by Eqs.(3.10)-(3.13), we can specify a reasonable, unique integral path by the following procedure. In order for the solution to conserve the total energy, the electron thermal flux coming from the infinite ($\xi\to\infty$) must be finite ($S=\kappa_0 T_e^{5/2} Z^{-1}\frac{\partial T_e}{\partial x}$ is finite at $\xi = \infty$ and this also means $\tau_e^{5/2}\tau_e'$ is finite at $\xi=\infty$) In order to satisfy this asymptotic relation, the electron temperature increases as follows.

$$T_e \propto \xi^{2/7} \quad \text{for } \xi\to\infty \tag{3.20}$$

But, due to expansion cooling the ion temperature decreases monotonically.

$$T_i \to 0 \quad \text{for } \xi\to\infty \tag{3.21}$$

By use of the transformed variables $G(\xi) = \xi g(\xi)$, $V(\xi) = v(\xi)/\xi$, and $\theta(\xi) = (Z\tau_e+\tau_i)/\xi^2$, the equations (3.10) and (3.11) are

rewritten by the form

$$(V-\alpha)\frac{d\ln G}{d\ln\xi} + \frac{dV}{d\ln\xi} = 4(1-\alpha) \tag{3.22}$$

$$\theta\frac{d\ln G}{d\ln\xi} + (V-\alpha)\frac{dV}{d\ln\xi} = -\frac{d}{d\xi}(\xi\theta) - (V-1)V \tag{3.23}$$

The first term of the right side of Eq.(3.23) can be neglected for $\xi \to \infty$ as obvious from the asymptotic relations (3.20) and (3.21). Consequently, Eqs.(3.22) and (3.23) reduce to the following form for $\xi \to \infty$.

$$\frac{d\ln G}{d\ln\xi} = \frac{(V-1)V + 4(1-\alpha)(V-\alpha)}{(V-\alpha)^2 - \theta} \tag{3.24}$$

The left hand side must be negative for $\xi \to \infty$, because the density $g(\xi) = G(\xi)/\xi$ should decrease faster than ξ^{-1} to maintain the total mass finite. For $\alpha > 9/8$ the numerator of Eq.(3.24) is always positive. Therefore, to satisfy the above relation the denominator must be negative, namely $\theta > (V-\alpha)^2$. The equation (3.21) also denotes that the reduced temperature θ must be equal to zero at $\xi = \infty$. These two requirements give us the unique

integral path, which is drawn schematically in Fig.3.1. The equation (3.24) also denotes the exponential decrease of the density g. It is easily shown that the situation is the same for $1 < \alpha \leq 9/8$.

in the case of $\alpha < 1$, the temperaturs and flow velocity are infinite at time $t = 0$, obviously from the relations(3.9). This case corresponds to that of the collapse problem and may be, for example, applied to investigate an adiabatic compression by the use of the tailored pulse. The origin for time (t=0) is taken at the instant of collapse. We analyse the system for negative time. In this regard, we slightly modify the definitions. These collapse problems contain much interest, but we do not treat them here.

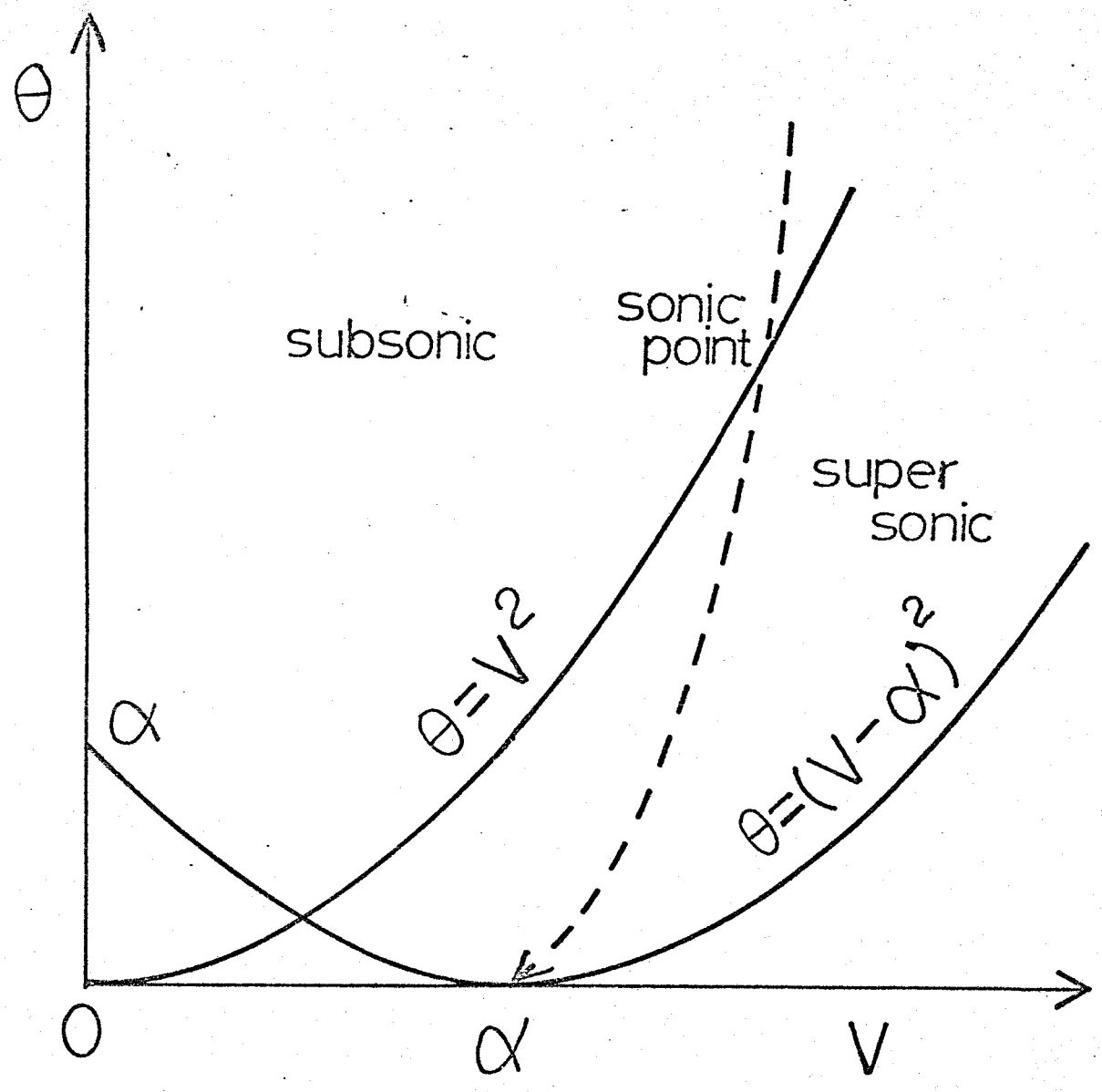

Fig. 3.1 Integral path in (V,θ) space.

Dotted curve means the schematic integral path. The integral path should pass a sonic point and converge into the point $(\alpha,0)$ for $\xi \to \infty$ with positive value of $T-(v-\alpha)^2$. Here, the curve, $\theta=V^2$, is a sonic one.

3.3 Energy Conservation and Determination of Similarity Parameter α and Dimensional Constant A

By considering the energy conservation for the system, the similarity prameter α and dimensional constant A can be uniquely determined as follows. Multiplying Eq.(3.4) by the density n and using Eqs.(3.1) and (3.2), we obtain the energy equation as a conservation form.

$$\frac{\partial}{\partial t}\left[\frac{1}{2}m_i n u^2 + \frac{3}{2}n(ZT_e + T_i)\right]$$

$$+ \frac{\partial}{\partial x}\left[\frac{1}{2}m_i n u^3 + \frac{5}{2}n(ZT_e + T_i)u - \frac{K_0}{Z}T_e^{5/2}\frac{\partial T_e}{\partial x}\right] = 0.$$

Integrating this equation over the space from the origin to the infinte yields the total energy conservation:

$$\frac{\partial}{\partial t}E_T = \frac{K_0}{Z}T_e^{5/2}\frac{\partial T_e}{\partial x}\Big|_{x=\infty} \qquad (3.25)$$

where

$$E_T = \int_0^\infty \left[\frac{1}{2}m_i n u^2 + \frac{3}{2}n(ZT_e + T_i)\right] dx$$

where to evaluate the integral, we made use of the fact that no energy convection exsists at x=0 and ∞. The energy increase in the whole system is compensated with the thermal conduction from the infinite. From Eq. (3.9), Eq.(3.25) is rewritten as

$$\frac{\partial}{\partial t} E_T = \frac{K_0}{Z} m_i^{7/2} A^6 S_\infty t^{6\alpha-7} \qquad (3.26)$$

where S_∞ is the nondimensional thermal flux at $\xi = \infty$ [$S_\infty = \tau_e^{5/2} \tau_e'(\xi=\infty)$], which should be given after integrating Eqs. (3.10)-(3.13). Let us assume that the incident laser flux is absorbed arround the underdense region and the absorbed power is given by $I_{ab} = \phi_0 t^\beta$ (β is a pure number and ϕ_0 is a constant). The energy conservation requires the relation

$$\frac{\partial}{\partial t} E_T = \phi_0 t^\beta$$

Comparing this equation with Eq.(3.26), we can determine the similarity prameter α and dimensinal constant A:

$$\alpha = \frac{\beta+7}{6}$$

$$A = \left(\frac{Z \phi_0}{K_0 m_i^{7/2} S_\infty} \right)^{1/6} \qquad (3.27)$$

Substituting this prameter into Eqs.(3.10)-(3.13) and integrating them according to the procedure mentioned in the previous section, we get the nondimensional ablation structure. The dimensional structure is obtained by substituting the constant A given in Eq.(3.27) into the relation (3.9).

It is important to consider how this resultant ablation implode the inner solid region. Up to now, we treated only the ablation region and the meaningful quantities to construct the compressed region are given by the mass flow nu and tht ablation front pressure P. These values provide us with the boundary condition to construct the dynamics occuring in the compressed region. From Eqs.(3.15)-(3.17) and relations(3.9), the pressure and mass flux at the ablation front are given as

$$P_f = (1+Z) P_0 K_0 m_i^{g/2} A^{5} t^{5\alpha-4}$$

$$J_f = K_0 m_i^{5/2} A^{4} t^{4\alpha-5} \qquad (3.28)$$

where the constant P_0 should be given after the integral. These boundary condition correspond to the problem of the compression with the porous piston. We do not here treat the problem to construct the compressed region, but the simple analysis will be shown later. It is noted that if we could determine the dynamics of the compressed region we get the prpagation velo-

city of the ablation front and we can transform the variables from in the frame propagating with the ablation front velocity to in the laboratory frame, obtaining the whole dynamics of the implosion and ablation.

3.4 Application to Ablating Plasma Produced by Classical Absorption

Let us consider the case where the incident laser with constant power I_0 is absorbed through the inverse-bremsstrahlung absorption process by a D-T plasma (Z=1). In this case the absorbed power I_{ab} will be given as the form

$$I_{ab} = \left[1 - \exp\left(-2\int_{x_c}^{\infty} K_{cl}\, dx\right)\right] I_0$$

$$\approx 2\int_{x_c}^{\infty} K_{cl}\, dx \cdot I_0 \qquad (3.29)$$

where

$$K_{cl} = 2.2\times 10^{-11} \ln\Lambda \frac{1}{\lambda_L^2 T_e^{3/2}} \frac{(n/n_c)^2}{(1-n/n_c)^{1/2}}$$

Here, n_c and λ_L are the cut-off density and laser wavelength, respectively. The absorption rate is assumed to be small in Eq.(3.29). As mentioned in Sec.3.2 the density exhibits an exponential profile in the underdense region, so that we can perform the integral to Eq.(3.29).

$$I_{ab} = 2.2\times10^{-11}\frac{\ln\Lambda\cdot I_0}{m_i^{3/2}\lambda_L^2 A^2}\frac{\delta}{3}L\cdot\tau_e(\xi_c)^{-3/2}\,t^{3-2\alpha} \qquad (3.30)$$

where L and $\tau_e(\xi_c)$ are non-dimensional density scale length, $n/n_c = \exp[-(\xi-\xi_c)/L]$, and the temperature at cut-off. In this case, β in Eq.(3.27) is equal to $3-2\alpha$ and ϕ_0 is also given in Eq.(3.30), so that the similarity prameter α and the dimensional constant A are

$$\alpha = 5/4 \qquad (3.31)$$

$$A = \left(\frac{2.2\times10^{-11}\ln\Lambda\,\frac{\delta}{3}L}{K_0 m_i^5\lambda_L^2\tau_{ec}^{3/2}(\xi)S_\infty}I_0\right)^{1/8}$$

Fig.3.2 shows the resultant profile obtained by integrating Eqs.(3.10)-(3.13) with $\alpha=5/4$. The integral was carried out numerically using Runge-Kutta method. The meaningful integral required $P_0 = 1.361$ and the resultant profile gave L=1.30, $\tau_{ec}{}^{3/2}S_\infty=75.0$.

Let us consider to make an x-t diagram for the implosion dynamics. Calculation of the ablation front velocity will be simply carried out if we assume a strong shock formation in front of the ablation region. The ablation pressure caluculated in Eq.(3.28) make ashock in the solid region, and its propagation

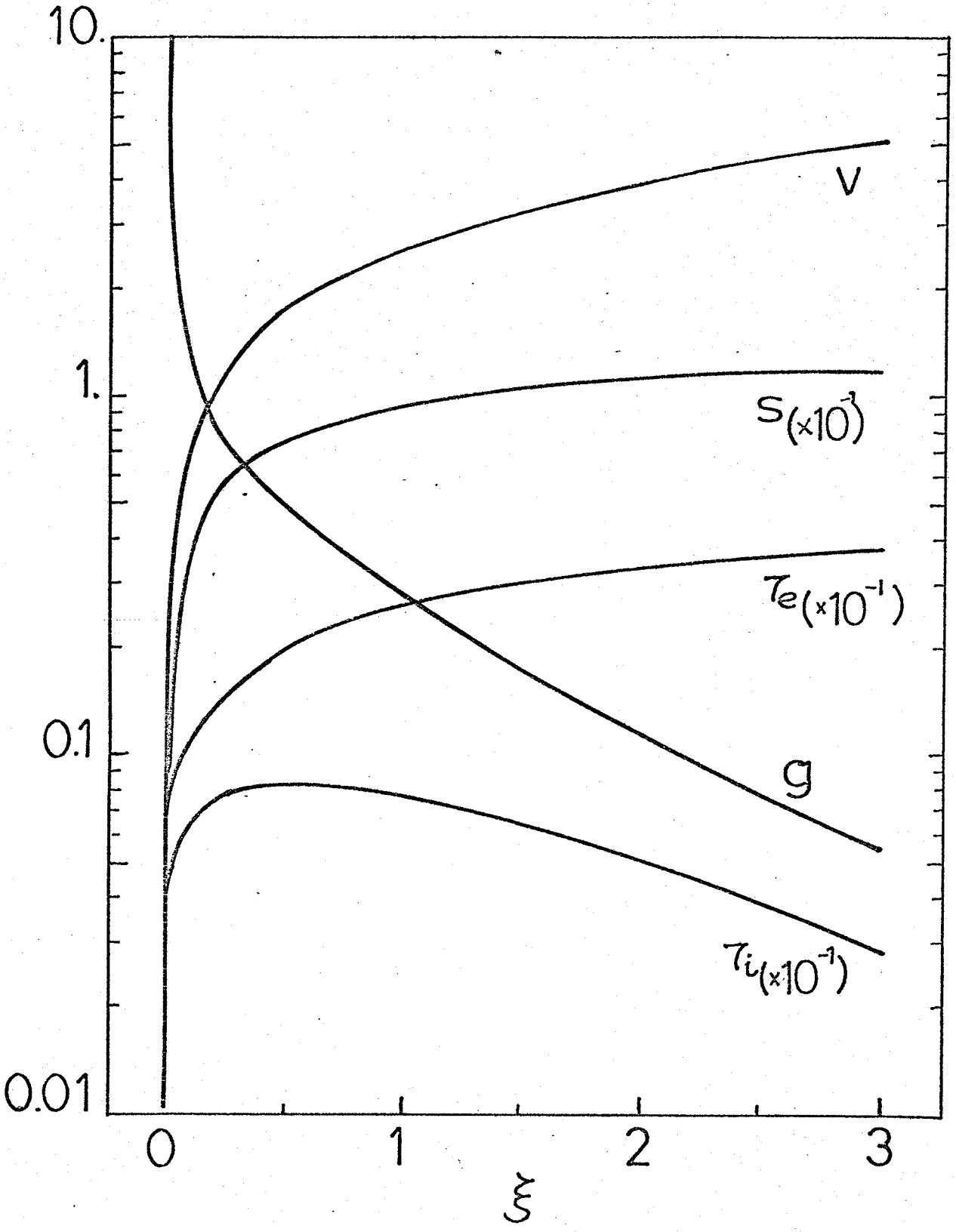

Fig. 3.2 Nondimensional ablation structure in the case where $\alpha=5/4$. Here, g, v, τ_e, τ_i, and S are the density, velocity, electron and ion temperature, and electron thermal flux, respectively. These nondimensional quantities are converted into the dimensional ones by the use of relation (3.9) after determination of constant A.

velocity λ_s may be given[17] as

$$\lambda_s = \left(\frac{4}{3} \frac{P_f}{m_i n_s} \right)^{\frac{1}{2}}$$

where n_s is the initial solid density, and a specific heat γ is assumed to be equal to 5/3. Moreover, considering the mass conservation across the ablation front, the propagation velocity of the ablation front λ_a is calculated.

$$\lambda_a = \frac{3}{4} \left(\frac{8}{3} P_0 \frac{K_0 m_i^{5/2} A^5}{n_s} \right)^{\frac{1}{2}} t^{\frac{1}{8}} + \frac{1}{4} \frac{K_0}{n_s} m_i^{5/2} A^4$$

where the mass flow given in Eq.(3.28) and the well-known shock relations[11] are used. Using this propagation velocity we can construct the x-t diagram in the laboratory frame, which is shown in Fig.3.3. This figure shows the case in which $I_0 = 10^{15}$ W/cm^2 and $\lambda_L = 1.06$ μm. Here, $\ln\Lambda$ is set to be 10. In Fig.3.3, the symbols S, A, S_p, and C denote the shock front, ablation front, so-called Chapman-Jouguet point (which means a sonic point in the frame moving with the ablation front), and the cut-off point, respectively.

The structure shown in Fig.3.2 and the dynamics given by Fig3.3 exhibit good agreements with those obtained by computer simulations, which are shown in Fig.3.4[18]. (Take care that

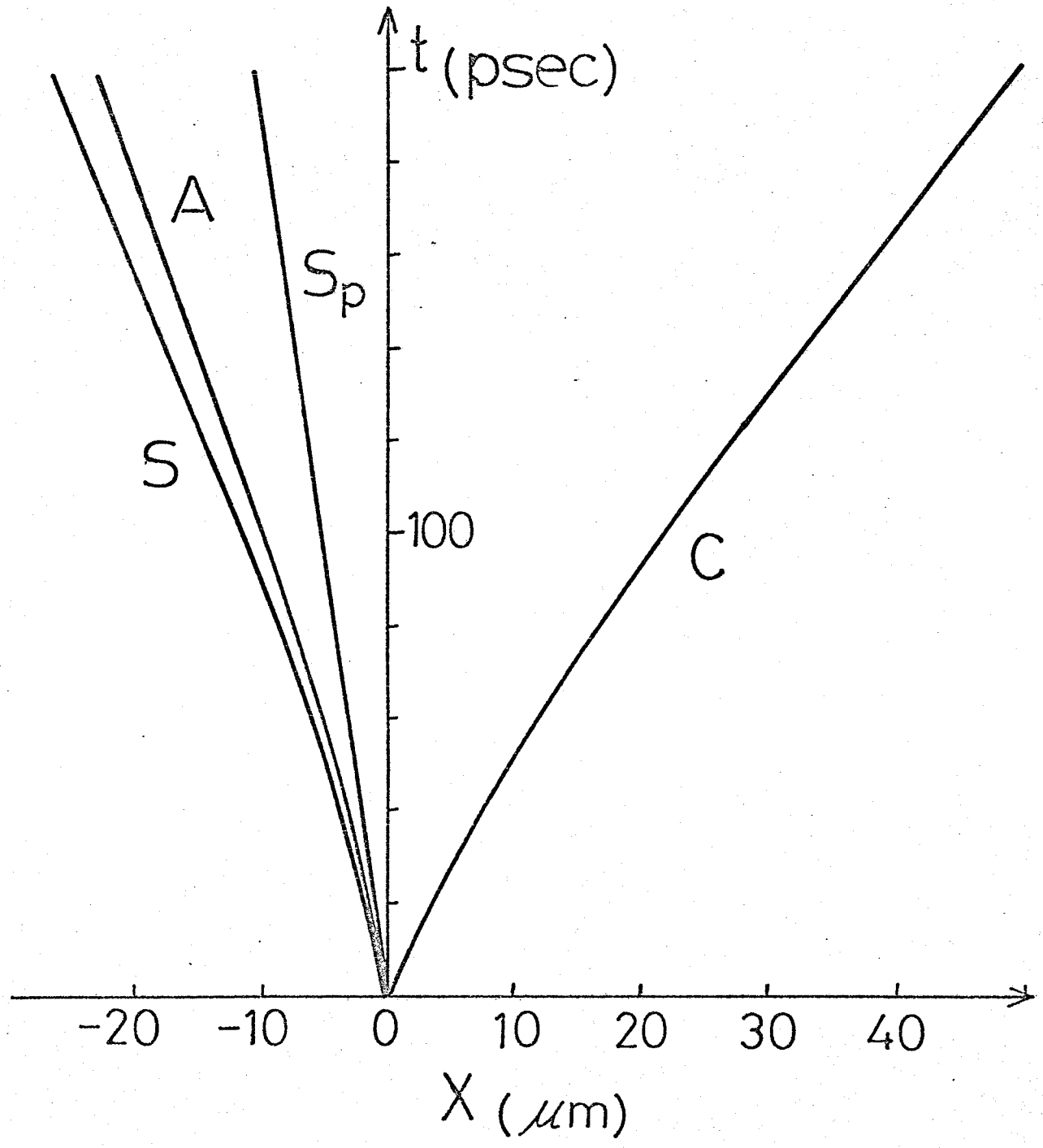

Fig. 3.3 Resultant x-t diagram for the case where 1.06 μm laser with power 10^{15} W/cm^2 is absorbed through the inversebremsstrahlung by a D-T plasma which is initially solid.

Here, the characteristics of the shock front (S), ablation front (A), Chapman-Jouguet point (S_p), and cut-off (C) are shown respectively.

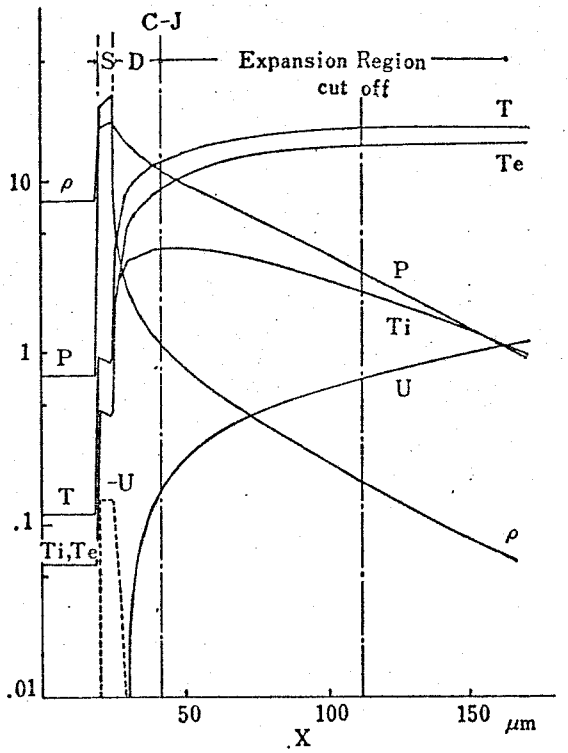

A typical implosion structure obtained by computer simulation. p denotes plasma pressure ($\times 10^{10}$ kg/m sec^2), ρ mass density ($\times 10^2$ kg/m^3), u flow velocity ($\times 10^5$ m/sec), T_e electron temperature ($\times 10^6$ °K), T_i ion temperature ($\times 10^6$ °K) and $T = T_e + T_i$. S corresponds to the shock compressed region and D the deflagration region.

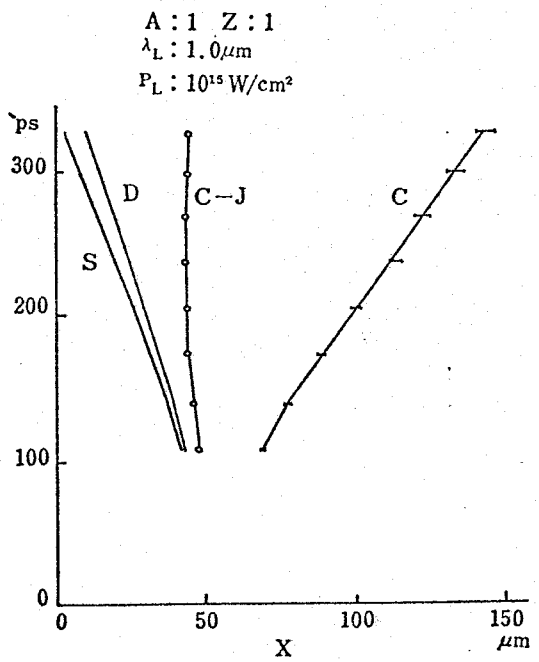

A x-t diagram of implosion. S corresponds to the shock compressed region ad D the deflagration front, C-J the Chapman-Jouguet point and C the cut-off point.

Fig. 3.4 Typical example of the dimensional ablation structure and the x-t diagram for the corresponding characteristics, obtained by a computational calculation (Ref.18). These computational results support the accuracy of the present self-similar analysis to the laser produced plasma behaviour.

the target material used in this simulaion is different from that employed in the present analysis, and the simulation employed a hydrogen solid target.)

3.5 Concusion and Discussion

Imploding a fuel target is required to achieve the inertia fusion within the usage of the practical laser. In order to achieve the super compression, the controlled compression , especially adiabatic one, is necessary. The irradiation of laser light gives rise to a formation of the ablation region, and through this region the absorbed energy is transfered toward the overdense region. This transported energy causes the implosion by doing the mechanical work against the inner non-ablating region. As mentioned in Sec.3.3, between the absorbed power and ablation pressure there are such time dependences.

$$I_{ab} \propto t^{6\alpha-7}$$
$$P_f \propto t^{5\alpha-6} \qquad (3.32)$$

Namely, there is the difference in time response by $t^{-\alpha+1}$ between them. Let us consider the case of a constant absorbed power (I_{ab} = const.). In this case, Eq.(3.32) says

$$\alpha = \frac{7}{6} \rightarrow P_f \propto t^{-1/6}$$

This relation means that due to the expansion of the deflagration

region in proportion to $t^{7/6}$, the absorbed energy can not be transported directly to the ablation front but is spent so as to compensate the expansion of the deflaglation region. This is analogeous to pushing a wall in roller skates. Under the constant power absorption, the formed shock wave will be weakened by the following rarefactive perturvations. In order to sustain the shock, we must therefore require for the absorbed power to increas as follows.

$$P_f : const \rightarrow \quad \alpha = \frac{6}{5} \quad , \quad I_{ab} \propto t^{1/5}$$

In such a case, the absorbed power is transported to maintain the constant ablation pressure suppling more energy to the expanding deflagration region. What was mentioned above is one of the significant differences compared with the result given by the stationary analysis shown in Chp.2.

It may be interesting to compare these different model analyses. The treatment with the stationary model has advantages in the simplicity of the basic equations and moreover being easily taken account of various anormalous effects. However, in intending to enclose the system self-consistently, we face the problem to determine the unknown prameter as seen in Chp.2. And, the restriction coming from the momentum conservation causes an appearance of singularity near the sonic point, which prevents the solution from extending into the super sonic region. Morever, the stationary solution says nothing about the time

evolution of the phenomena. Therefore, we have to pay attention to under what conditions the stationary analysis provides us with well approximated solutions.

In contrast to the stationary treatment the analysis with the self-similar method provides the ablation structure which exhibits the continuous structure over the ablation region from the front to the vaccum without showing any singularities. Moreover, the time dependent dynamical evolution of the ablation phenomena can be obtained for the various cases.

It is interesting to point out that not only the case treated here but also the others including, for example, the effects of hot electron transport or heat inhibition ... may exhibit the self-similer type time evolution in the ablating region. So, the applications of this self-similar method to the various problems will provide us with the more realistic ablation and implosion phenomena.

References

1. J. Nuckolls, L. Wood, A. Thiessen, and G. Zimmerman, Nature 239, 139(1972)
2. K. A. Brueckner and S. Jorna, Rev. Mod. Phys. 46, 325(1974)
3. H. Takabe, K. Nishihara, and T. Taniuti, J. Phys. Soc. Japan 45, 2001(1978)
4. F. S. Felber, Phys. Rev. Lett. 39, 84(1977)
5. J. L. Bobin, Phys. Fluids 14, 2341(1971)
6. S. G. Gitomer, R. L. Morse, and B. S. Newberger, Phys. Fluids 20, 234(1977)
7. J. Nuckolls, in"Laser Interaction and Related Plasma Phenomena."(Plenam, New York, 1974).
8. R. J. Mason and R. L. Morse, Phys. Fluids 18, 814(1975)
9. R. L. McCrory and R. L. Morse, Phys. Rev. Lett. 38, 544(1977)
10. I. Anisimov, JETP Lett. 12, 287(1970)
11. A. Barrero and J. R. Sanmartin, Phys. Fluids 20, 1155 (1977)
12. J. R. Sanmartin and A. Barrero, Phys. Fluids 21, 1957(1978), and 21, 1967(1978)
13. S. I. Braginskii, in "Reviews of Plasma Physics." edited by M. A. Leontovich, Vol. I, P.205. (Consultant Bureau, New York, 1965).
14. Ya. B. Zel'dovich and Yu. P. Raiser, "Physics of Shock Waves and High-Temperature Hydrodynamic Phenomena." (Academic, New York, 1967), Chap.XII.

15. L. I. Sedov, "Similarity and Dimensinal Methods in Mechanics." (Infoseach, London, 1957).

16. see Chap.X in Ref.14.

17. L. D. Landau and E. M. Lifshitz, "Fluid Mechanics," Chap.IX. (Pergamon,London, 1959).

18. N. Kimura, "Annual Progress Report on Laser Fusion Program Sep. 1976 - Aug. 1977," p.105. ILE, Osaka University.

Chapter 4

Hot Electron Energy Flux Limitation by Electrostatic Field

4.1 Introduction

When intense laser light is irradiated on a target, collective processes, for instance, parametric instabilities[1),2)], and/or resonance absorption[3),4)] become more important than inverse-bremsstrahlung. In conection with the collective absorption, hot electrons are generated[5),6),7)]. When the hot electron energy exceeds about 10 kev, the mean free path is longer than the scale length of target plasma. In such a case, those electrons penetrate into the core plasma and preheat it[8)]. Furthermore, they expand out into the corona region generating fast ions there[9)]. Therefore, we have to understand how due to those long mean free path electrons implosion efficiency, preheating, and corona-core decoupling are affected[10)]. In this chapter, we point out the electrostatic field generation, which redudes the hot electron heat conduction.

A qualitative explanation of the electrostatic field genaration, is as follows. When the hot electrons expand into the overdense region, a return current of background cold electrons toword the critical layer is induced to maintain charge neutrality. The electrostatic field is then built up because of finite electrical resistivity of the return current. Moreover, if the electron drift velocity exceeds the ion sound velocity, ion waves become unstable and the turblent state appears. When this is the case, the electrical resistivity is enhanced by electron-ion wave scattering. As a result, the strong electric field is generated by anomalous resistivity, and the electrostatic potential energy at cut-off reaches a few times the hot electron energy. This electric field insulates the hot electrons from the core region. (This is shown schemalically in Fig.6.1.)

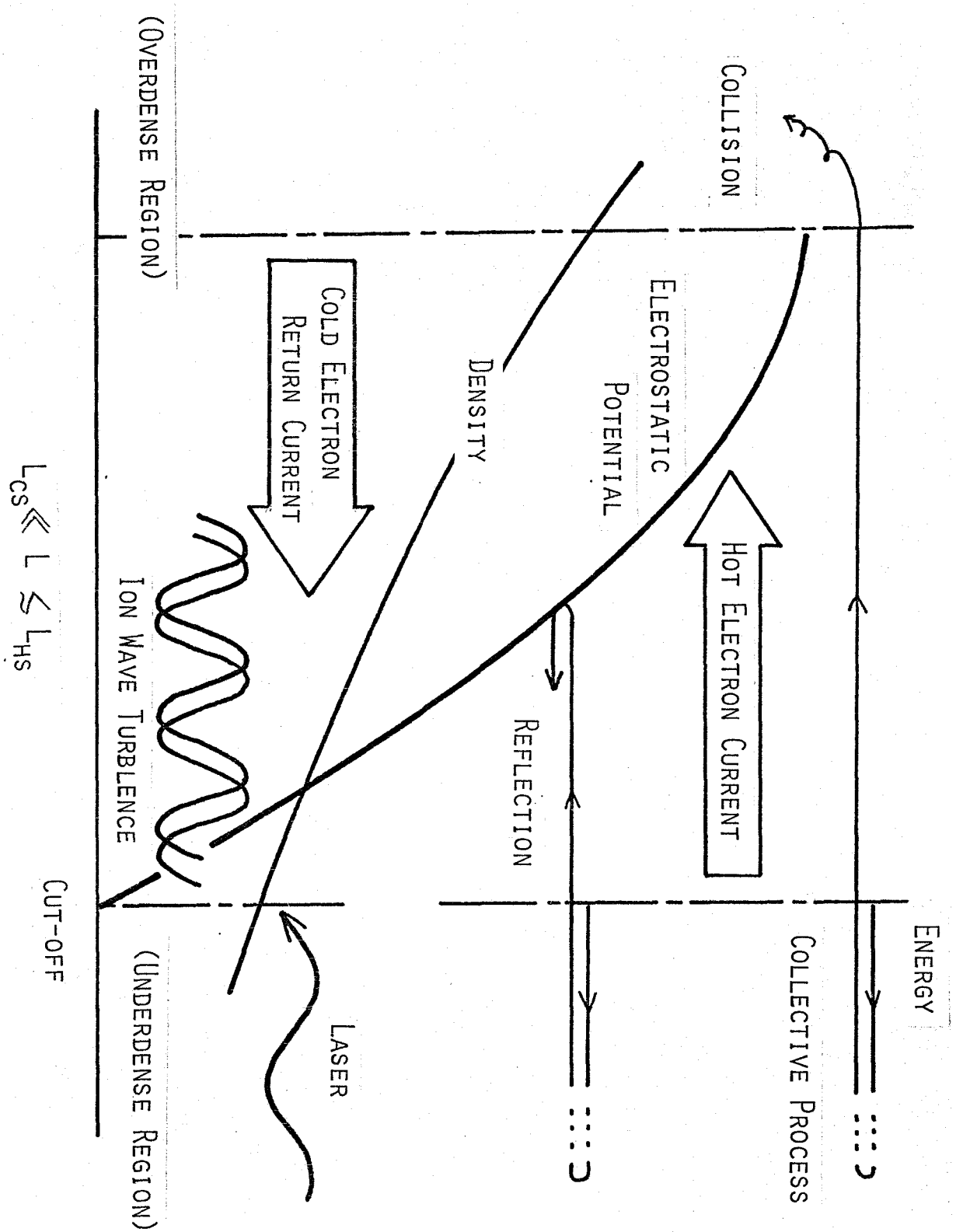

Fig. 4.1 Conceptial diagram for the electrostatic field generation mechnism.

Here, the hot electrons are assumed to be collisionless because the hot electron-ion collision frequency, ν_{hi} is approximately related to the cold electron collision frequency, ν_{ei} by $\nu_{hi} \simeq \nu_{ei}(T_c/T_h)^{3/2} << \nu_{ei}$, where T_c and T_h mean the temperatures of the hot and cold electrons, respectively. Note that this relation is maintained even if the electrons are scattered by the ion waves. Therefore, the ratio of the hot electron mean free path l_h to the cold electron path l_c is $l_h/l_c \simeq (T_h/T_c)^2$. When T_h/T_c is sufficiently greater than unity and our consideration is restricted to a region of width, $l_c << L \lesssim l_h$. We can assume that the hot electrons are collisionless whereas the cold ones are collisional. Therefore, the Vlasov equation is used to describe the hot electrons and the cold electrons are described by the fluid equations.

The phenomena are assumed to be stationary, because the electrons re-distribution time scale is much shorter than the time scale of ion motion and/or laser pulse length. Two models are considered. One is the one dimensional slab geometry and the other is the spherical geometry. (Note that the one dimensional slab model is a limiting case of the spherical case.) For simplicity, we consider the slab case at first in order to clarify the mechanism of electrostatic field generation.

The hot electron distribution is then given by the BGK solution of the Vlasov equation. The velocity moments of the distribution give the hot electron density and current. Using the hot electron density and current which are now only the functions of potential, the cold electron equation of motion is reduced to an equation for the electrostatic potential. This equation contains the cold electron-ion collision frequency. When the electron drift velocity

is smaller than the sound velocity, the well-knowned Spitzer's formula for the collision frequency may be used. For a supersonic drift velocity, an anomalous collision frequency due to the ion wave turbulence has to be used. In order to obtain the anomalous collision frequency, the wave kinetic equation for ion waves involving the nonlinear Landau damping is discussed and so-called Kadomtsev spectrum is used. Inserting the resultant spectrum into the quasilinear equation of cold electron, the anomalous collision frequency is determined.

For the typical parameters of laser produced plasmas, the potential profile is determined and tne potential jump $|e\Phi/T_h| \sim 1 \sim 2$ is obtained in the vicinity of the critical layer. Such a potential jump is mainly attributed to appearance of the ion wave turbulence near the critical layer. The hot electron flux reduction is then found to be about 10 % (spherical) or 20 % (plane) of the free streaming limit.

The dependence of heat flux reduction on hot electron density is also investigated and the flux reduction is found to be enhanced with increasing hot electron density. It is interesting, however, that in spite of such a reduction, the total thermal flux of hot electrons penetrating into the core region is approximately constant. The effect of an anisotropy of the hot electron distribution function on the flux reduction is also considered. Finally, the flus rediction in the high Z material is considered. In such a case, electrostatic field effects on the flux reduction seems to be important even without ion wave turbulence.

4.2 Equations for Slab Model

The Vlasov equation for the hot electron distribution function f_h in the one dimensional slab potential $\Phi(x)$ is

$$v \frac{\partial}{\partial x} f_h + \frac{e}{m_e} \frac{\partial \phi}{\partial x} \frac{\partial}{\partial v} f_h = 0 \quad . \tag{4.1}$$

The fluid equations are employed to describe the cold electrons.

$$n_e u_e = J_o \quad : \text{ const. in } x \ , \tag{4.2}$$

$$e n_e \frac{d\phi}{dx} = - m_e \nu_{ei} n_e u_e - T_e \frac{dn_e}{dx} \quad . \tag{4.3}$$

Here, n_e, u_e, and T_e are the density, velocity, and temperature of the cold background electrons, where T_e is assumed constant, and J_0 is a constant of integrations. The ions are assumed to be the stationary background with charge Z and density $n_i(x)$, and the quasi-condition for the plasmas is then shown to be

$$\begin{aligned} Z n_i &= n_e + \int_{-\infty}^{\infty} f_h \, dV \\ n_e u_e &+ \int_{-\infty}^{\infty} V f_h \, dV = 0 \end{aligned} \tag{4.4}$$

Note that the charge neutrality condition is required since the scale of spatial variation L is much longer than the elcetron Debye length λ_D.

Now let us solve the Vlasov equation for the hot electron by the BGK procedure[11]. Here, we assume that the hot electron distribution function at the critical surface $x=x_c$ is given by a Maxwellian one with temperature T_h.

$$f_h = \frac{m_e^{1/2}}{(2\pi)^{1/2} T_h^{1/2}} n_{h0} \exp\left(-\frac{m_e}{2T_h} v^2\right) \qquad (4.5)$$

Here, n_{h0} is a density of the hot electrons at cut-off. The assumption of the Maxwellian distriburion is based on the fact that the hot electrons are produced due to the stochastic heating by the electric field of plasma waves resonantly generated at cut-off. It is obvious that the equation (4.1) conserves the total energy for s single electron,

$$E = \frac{m_e}{2} v^2 - e\phi_{(x)} : \text{const.}$$

The potential $\phi(x)$ is considered to decrease monotonically from $\phi=0$ at cut-off to $\phi=\phi_0$ at a inner boundary ($x=x_0$) where the Coulomb collision between hot electrons and ion becomes significant. In such a case, electrons climbing over the potential barrier are assumed to penetrate into the collisional region and deposit their energies.

On the other hand, the electrons satisfying the following condition are reflected by the potential toword the critical layer.

$$V < V_c(x) \equiv \frac{2e}{m}\left[\phi(x) - \phi_0\right] \qquad (4.6)$$

Here, v_c is the velocity with kinetic energy equal to the difference of the potential energy. The condition (4.6) is obvious from the energy consevation for Eq.(4.1). Under the boundary condition (4.5), the BGK solution for (4.1) is easily obtained to be

$$f_h = \begin{cases} \dfrac{n_{h0}}{\sqrt{2\pi}\,v_h} \exp\left[-\dfrac{m}{2T_h}V^2 + \dfrac{e}{T_h}\phi(x)\right] & ; (V < V_c) \\ 0 & ; (V > V_c) \end{cases} \qquad \cdots\cdots (4.7)$$

The schematic feature of this distribution is shown in Fig.4.2. Note here that the distribution(4.7) has a net current and a heat flow from cut-off toward inner overdense region.

Taking the zeroth and first velocity moments of this distribution, we obtain hot electron density $n_h(x)$ and current $j_h(x)$

$$n_h(x) = n_{h0} \exp\left[\frac{e}{T_h}\phi(x)\right] \cdot \Phi\left[V_c(x)/V_h\right]$$

$$j_h(x) = -\frac{1}{\sqrt{2\pi}} n_h v_h \exp\left(e\phi_0/T_h\right) \qquad (4.8)$$

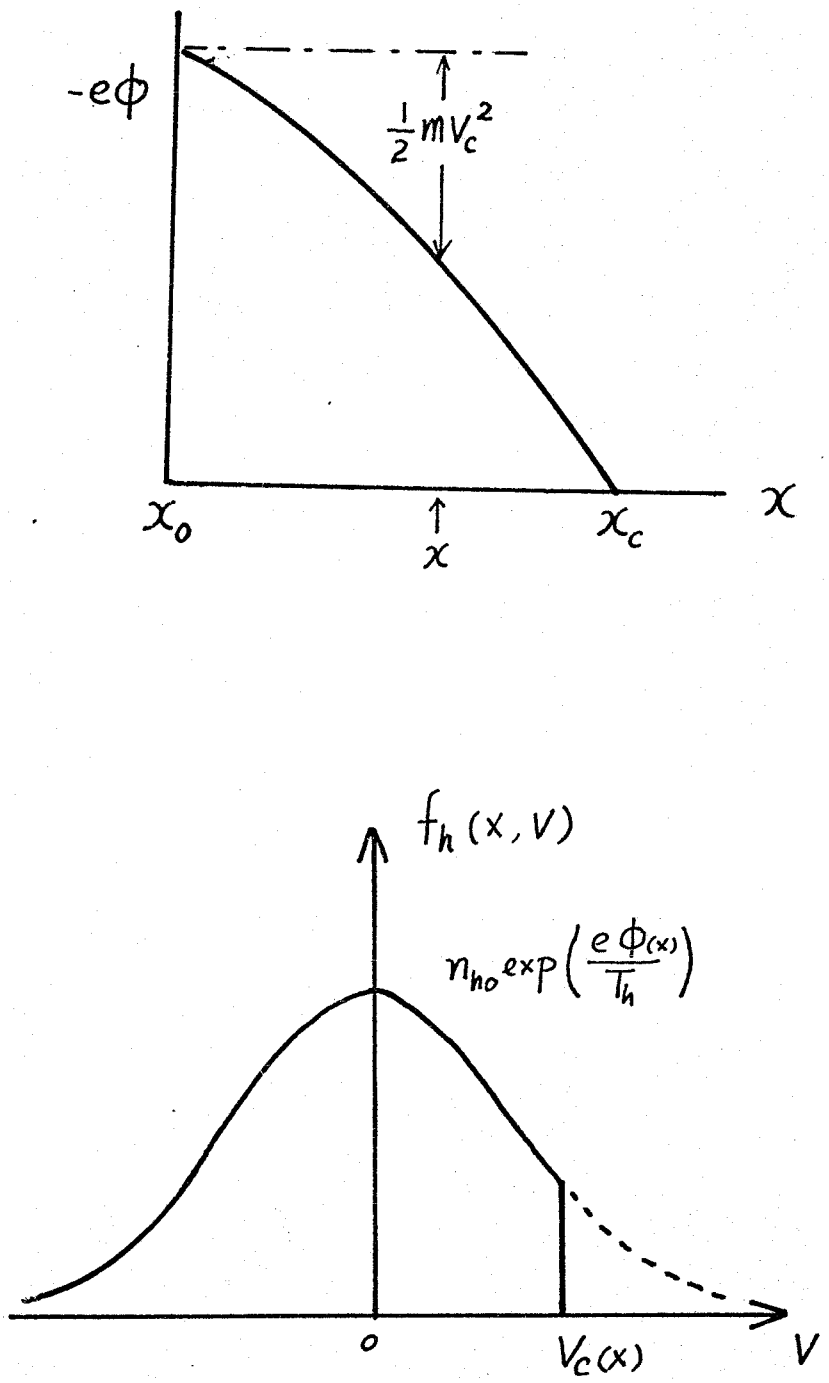

Fig. 4.2 Schematic picture of hot electron distribution function given by Eq.(4.7).

Here, $V_h = \sqrt{T_h/m_e}$ and a function $\Phi(\xi)$ is an error function defined by

$$\Phi(\xi) = \frac{1}{\sqrt{2\pi}} \int_{-\infty}^{\xi} \exp\left(-\frac{t^2}{2}\right) dt \tag{4.9}$$

Eliminating n_e and u_e in Eq.(4.3) by the use of Eqs.(4.4) and (4.8), the equation (4.3) reduces to the equation for ϕ.

$$\frac{d\tilde{\phi}}{d\tilde{x}} = \frac{\tilde{\nu}_{ei} + Z \frac{d\tilde{n}_i}{d\tilde{x}}}{\frac{T_h}{T_e} Z \tilde{n}_i + \frac{\tilde{n}_{h0}}{\sqrt{2\pi}\tilde{v}_c} e^{-\tilde{\phi}_0} - \tilde{n}_{h0} \Phi(\tilde{v}_c)\left(\frac{T_h}{T_e} e^{-\tilde{\phi}} - e^{-\tilde{\phi}_0}\right)} \tag{4.10}$$

Here, the nondemensional variables are introduced by

$$\tilde{\phi} = -e\phi(x)/T_h$$

$$\tilde{n} = n(x)/n_c \tag{4.11}$$

$$\tilde{x} = (x_c - x)/(x_c - x_0)$$

and also

$$\tilde{\nu}_{ei} = \nu_{ei}/\nu_0$$

$$\tilde{v}_c = [2(\tilde{\phi}_0 - \tilde{\phi})]^{1/2} \tag{4.12}$$

where ν_0 is defined by $\nu_0 = v_h^2 n_c J_0^{-1}(x_c - x_0)^{-1}$. The eqation (4.10) gives us a spatial structure of the electrostatic potential $\tilde{\phi}(\tilde{x})$. Note that Eq.(4.10) involves the peak potential value ϕ_0 at the overdense boundary, so that the equation is solved as an eigenvalue problem.

For solving the Eq.(4.10), we have to determine the electron-ion collision frequency ν_{ei}. This problem will be considered in Sec.4.4. Before considering ν_{ei}, we will derive the basic equations for the spherical symetric model in the following section.

4.3 Equations for Spherical Model

In a spherical plasma sustaining spherically synmetric potential $\phi(r)$, the Vlasov equation for a hot electron distribution function f_h is given by

$$V_r \frac{\partial}{\partial r} f_h + \left[\frac{1}{r^3} \left(V_\theta^2 + \frac{V_\phi^2}{\sin^2\theta} \right) + \frac{e}{m_e} \frac{d\phi}{dr} \right] \frac{\partial}{\partial V_r} f_h = 0 \qquad (4.13)$$

For cold electron, the fluid equations are

$$r^2 n_e u_e = J_{os} : \text{const} \qquad (4.14)$$

$$e n_e \frac{d\phi}{dr} = - m_e \nu_{ei} n_e u_e - T_e \frac{dn_e}{dr} \qquad (4.15)$$

We also require charge neutrality condition same as Eq.(4.4).

Now, let us set the hot electron distribution function at cut-off to be a bi-Maxwellian with temperatures T_h in the radial direction and $T_\perp$ in the azimuthal direction, namely,

$$f_h = \frac{n_{ho} \cdot m_e^{3/2}}{(2\pi)^{3/2} T_\perp T_h^{1/2}} \exp\left(- \frac{m_e}{2T_h} V_r^2 - \frac{m_e}{2T_\perp} V_\perp^2 \right) \qquad (4.16)$$

Here, $v_\perp$ is the azimuthal velocity component, $v_\perp^2 = (v_\theta^2+v_\psi^2/\sin^2\theta)/r^2$. The reason why we take anisotropic distribution for hot electron is due to the fact that the electron acceleration by resonance field is mainly along the density gradient direction, and in general, the hot electron distrubution is not isotropic. Considering the constants of motion of electrons for the central force in Eq.(4.13), we have the following conservation relations for the energy E and the angular momentum M for a single electron,

$$E = \frac{m_e}{2}(V_r^2+V_\perp^2) - e\phi(r) : \text{const.} \tag{4.17}$$

$$M = rV_\perp = (V_\theta^2 + V_\varphi^2/\sin^2\theta)^{1/2} : \text{const.}$$

If the potential $\phi(r)$ varies monotonically from $\phi=0$ at cut-off ($r=r_c$) to $\phi=\phi_0$ at the overdense radius ($r=r_0$), the electrons climbing over the potential penetrate into the collisional region and deposit their energies by collisions with the backgroud plasma. On the other hand, the electrons satisfying the following condition are reflected by the potential toward the critical layer.

$$V_\perp^2 \gtrsim \frac{r^2}{r^2-r_0^2}\left[V_r^2 - V_c^2(r)\right] \tag{4.18}$$

Here, the definition of $v_c(r)$ is the same given in Eq. (4.6) with $\phi(r)$ instead of $\phi(x)$, namely, $v_c^2(r) = 2e[\phi(r)-\phi_0]/m_e$. The condition(4.18) is obvious from the energy and angular monentum conservation, Eq.(4.17). In Fig.4.3.a, the achematic feature of the hot electron distrivution at a radius r is shown. Note here that the distribution has a loss cone according to the condition (4.18). This is partly due to an efective potential (centrifugal force) associating with electron angular momentum. Under the boundary condition (4.16) the BGK solution for the hot election distribution function is derived from the conservation laws for energy and angular momentum as follows:

$$f_h = \frac{n_{h0}}{(2\pi/m_e)^{3/2} T_\perp T_h^{1/2}} \exp\left[-\frac{E}{T_h} - \frac{m_e}{2}\left(\frac{M}{r_c}\right)^2\left(\frac{1}{T_\perp} - \frac{1}{T_h}\right)\right] \tag{4.19}$$

Substituting relation(4.17) into E and M of this equation, the BGK solution of the hot electrons is obtained under the reflection condition(4.18). We can also reduce the distribution function(4.19) to a radial velocity distribution function, by integrating the distribution over $v_\perp$;

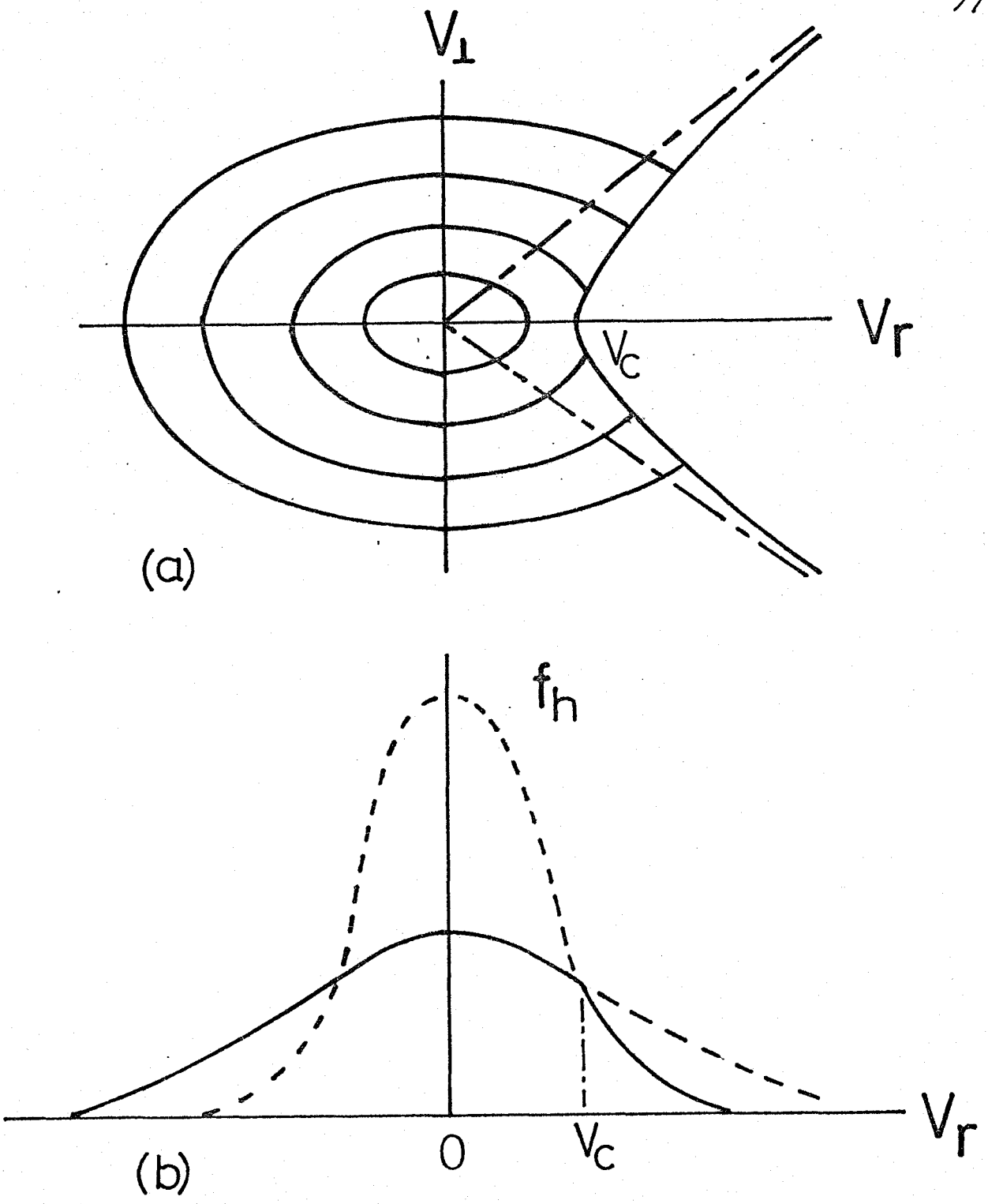

Fig. 4.3 Schematic picture of hot electron distribution at a radius r:

(a) Contours of the distribution in V_r, V .
The reflected component has a loss cone to satisfy condition (4.18).

(b) The hot electron distribution function versus V_r.
The distribution consists of two Gaussian profiles of diferent halfwidths, given by Eq.(4.20).

$$f_h(r,V_r) = \begin{cases} \dfrac{n_{ho}}{\sqrt{2\pi}V_h}\dfrac{1}{(1-\tilde{r}^2)\beta+\tilde{r}^2}\exp\left[-\dfrac{m_e}{2T_h}V_r^2+\dfrac{e}{T_h}\phi(r)\right] ; & (V_r<V_c) \\ \dfrac{n_{ho}}{\sqrt{2\pi}V_h}\dfrac{1}{(1-\tilde{r}^2)\beta+\tilde{r}^2}\exp\left[-\dfrac{m_e}{2T_h}\dfrac{V_r^2}{\mathcal{E}^2}+\dfrac{e}{T_h}\dfrac{(\phi-\phi_o)}{\mathcal{E}^2}+\dfrac{e}{T_h}\phi_o\right] : & (V_r>V_c) \end{cases} \tag{4.20}$$

Here, v_h is the radial hot electron thermal velocity $(T_h/m)^{1/2}$, β is the temperature anisotropy defined by $T_\perp/T_h$, and $\tilde{r}$ is the radius normalized by cut-off radius, $\tilde{r}=r/r_c$. The nondimensional function ε is defined by

$$\mathcal{E}^2 = \frac{1-\tilde{r}_o^2/\tilde{r}^2}{1-\tilde{r}_o^2+\tilde{r}_o^2/\beta}$$

This hot electron distribution function versus v_r is shown in Fig. 4.3.b. Taking the zeroth and the first velocity moments of this distribution, the hot electron density $n_h(r)$ and current $j_h(r)$ are obtained as follows.

$$n_h(r) = n_{ho}\frac{\exp\left(\frac{e}{T_h}\phi\right)}{(1-\tilde{r}^2)\beta+\tilde{r}^2}\left[\Phi(\tilde{V}_c)+\mathcal{E}\cdot\exp\left(\frac{1-\mathcal{E}^2}{2\mathcal{E}^2}\tilde{V}_c^2\right)\cdot\Phi\left(-\frac{\tilde{V}_c}{\mathcal{E}}\right)\right]$$

$$j_h(r) = -\frac{n_{ho}V_h}{\sqrt{2\pi}}\exp\left(\frac{e}{T_h}\phi_o\right)\frac{\tilde{r}_o^2}{(1-\tilde{r}_o^2)\beta+\tilde{r}_o^2}\cdot\frac{1}{\tilde{r}^2} \tag{4.21}$$

Here, v_c is normalized as $\tilde{v}_c = v_c/v_h$, and $\Phi(\xi)$ is the error function defined by Eq.(4.9).

For the spherical case, we also obtain the differential equation of $\Phi(r)$ using the charge neutral condition through the same process as the slab case. However, since the meaning of the equation becomes clear by the use of the integral form, we stop deriving the deffential form explicitly.

Using the integration constant J_{0s} of Eq.(4.14), we solve Eq. (4.15) to obtain the cold electron density as the function of $\Phi(r)$,

$$n_e = \left[\frac{J_{0s}}{T_e} m_e \int_r^{r_c} \frac{\nu_{ei}}{r^2} \exp\left(\frac{e}{T_e} \phi(s) \right) ds + n_{e0} \right] \exp\left(-\frac{e\phi(r)}{T_e} \right) \qquad (4.22)$$

where n_{eo} is an integration constant, representing the cold electron density at the cut-off. We normalize the potential and the densities by the hot electron temperature T_h and the cut-off density n_c according to the slab case normalization. Using Eqs. (4.14), (4.21) and (4.22), we can rewrite the neutrality condition(4.4) as follows.

$$J_{0s} = \frac{n_c}{\sqrt{2\pi}} V_h \cdot \frac{\tilde{n}_{h0} \exp(-\tilde{\phi}_0)}{(\tilde{r}_0^{-2} - 1)\beta + 1} \qquad (4.23)$$

and

$$\left[\frac{n_{h0}\alpha\cdot\exp(-\tilde{\phi}_0)}{\sqrt{2\pi}\,(\tilde{r}_0^{-2}-1)\beta+1}\int_{\tilde{r}}^{1}\frac{\gamma_c\nu_{ei}}{V_h s^2}\exp\left(-\alpha\tilde{\phi}(s)\right)ds+\tilde{n}_{e0}\right]\exp(\alpha\tilde{\phi})$$

$$+\ \tilde{n}_{h0}\,\frac{\exp(-\tilde{\phi})}{(1-\tilde{r}^2)\beta+\tilde{r}^2}\left[\Phi(\tilde{V}_c)+\varepsilon\cdot\exp\left(\frac{1-\varepsilon^2}{2\varepsilon^2}\tilde{V}_c^2\right)\cdot\Phi\left(-\frac{\tilde{V}_c}{\varepsilon}\right)\right]$$

$$=\ Z\cdot\tilde{n}_i \qquad (4.24)$$

where $\alpha = T_h/T_e$. Eq.(4.24) determines the spatial structure of the electrostatic potential $\tilde{\phi}(\tilde{r})$. If we differentiate this with respect to $\tilde{r}$, we get the differential form corresponding to Eq.(4.10). Note that the equation for the slab case is obtained by taking the limit, $r_c - r_0$ = fixed and $r_c \to \infty$ in Eq.(4.24).

4.4 Anomalous Resistivity due to Ion Wave Turblence

Before solving Eq.(4.10) or (4.24), it is necessary to determine the collision frequency ν_{ei}. When the return current velocity u_e is smaller than the sound velocity $C_s = (ZT_e/m_i)^{1/2}$, the electrical resistivity is equal to Spitzer's formula[13]. However, when the drift velocity associated with the return current exceeds the sound velocity, ion waves are unstable and the electron scattering is then dominated by the ion waves. In such a case, the electrical conductivity is reduced anomalously. Therefore, we must determine the collision frequency ν_{ei} in the ion acoustic turbulence regime.

When the ion acoustic turbulence with spectrum $I_{\underline{k}}$ builds up, transport coefficients like electrical conductivity should be estimated from the quasi-linear equation for the coarse-grained velosity distribution function.

$$\frac{\partial}{\partial t} f_e + v \frac{\partial}{\partial r} f_e + \frac{e}{m_e} \frac{\partial \phi}{\partial r} \frac{\partial}{\partial v} f_e + \pi \left(\frac{e}{m_e}\right)^2 \sum_{\underline{k}} \underline{k} \frac{\partial}{\partial v} \left(I_{\underline{k}} \delta(\omega - \underline{k}v) \right.$$

$$\left. \underline{k} \frac{\partial}{\partial v} f_e \right) = 0. \qquad (4.25)$$

Thereby $\underline{k}$ is the wave vector of an ion wave, $\delta(\omega - \underline{k}v)$ is the Dirac delta function, and the wave number spectrum $I_{\underline{k}}$ is the mean square of the oscillating potential $\phi_{\underline{k}}$ of the ion wave ($I_{\underline{k}} = \langle |\phi_{\underline{k}}|^2 \rangle$).

Taking the first velocity moment of Eq. (4.25) and comparing it

with Eq.(4.3), we obtain the following expression for the anomalous collision frequency ν_{ei},

$$\nu_{ei} = \pi\left(\frac{e}{m_e}\right)^2 \frac{1}{\int v f_e dv} \int v \sum_{\underline{k}} k \frac{\partial}{\partial v} I_{\underline{k}} \delta(\omega - \underline{k}v) k \frac{\partial}{\partial v} f_e dv \qquad (4.26)$$

The turbulence spectrum $I_{\underline{k}}$ should be determined by the wave kinetic equation, in which the nonlinear Landau damping is taken into account as a saturation mechanism of ion wave instability. When the deviation of the cold electron distribution function from the thermodynamic equilibrium is small enough, the distribution function with the flow velocity u_e and thermal flux Q may be approximated by [14]

$$f_e = \frac{n_e}{(2\pi v_e)^{3/2}} \exp\left[-\left[\frac{(v_r - u_e)^2 + v_\perp^2}{2v_e^2}\right]\left\{1 + \frac{Q}{3 n_e m_e v_e^3}\right.\right.$$
$$\left.\left.\left[\left(\frac{v_r - u_e}{v_e}\right)^3 - 3\frac{v_r - u_e}{v_e}\right]\right\}\right] \qquad (4.27)$$

where v_e is the cold electron thermal velocity. Using this distribution under the condition $ZT_e \gg T_i$, the wave kinetic equation[15] is

$$\frac{\omega_{pi}^2}{\omega_k^3}\frac{\partial I_k}{\partial t} = \sqrt{\frac{\pi}{2}}\frac{\omega_{pe}^2}{k^2 v_e^3}\left(u_e\cos\theta - c_s - \frac{Q}{m_e n_e v_e^2}\right) I_k$$

$$+ \frac{16\pi^2 (ze)^4}{m_i^3 k^2}\cdot\frac{v_i^2}{\omega_{|k}^3}\sum_{|k'}\frac{(|k'\cdot|k)^2\,(|k\times|k')^2}{|k''^2\,\omega_{|k'}}$$

$$\times\ |k''\cdot\frac{\partial f_i}{\partial v}\,\delta(\omega_{|k}-\omega_{|k'}-|k''v)\,dv\cdot I_{|k'} \qquad (4.28)$$

Here, ω_{pi} and ω_{pe} are the plasma frequencies of ions and electrons, v_i and f_i are the thermal velocity and the distribution function of ions, $\underline{k}'' = \underline{k}-\underline{k}'$, and the angle θ is the propagation angle of an ion wave with respect to the electron current. We average Eq. (4.28) with respect to θ over the unstable cone to obtain the stationary spectrum $I_{\underline{k}}$. The thermal flux Q in Eq.(4.27) is described by $Q = K_e dT_e/dr \simeq m_e n_e v_e^3 l_c/L_T$, where l_c is the cold electron mean free path and L_T is the spatial scale of the temperature variation. Consequently, $Q/m_e n_e v_e^3 \simeq v_e l_c/L_T$. Thus, since the condition $l_c/L_T < (Zm_e/m_i)^{1/2}$ is satisfied, we can neglect the term induced by the thermal flux Q in Eq.(4.28) and obtain

$$I_{|k} = \left(\frac{\pi}{2}\right)^{1/2}\frac{\omega_{pe}^2}{v_e^3}\cdot\frac{m_i^3 c_s^4 u_e}{2(ze)^4 n_i v_i^2}\cdot\frac{(1-\delta)^2}{2F(\delta)}\cdot\frac{1}{k^3}\ln\left(\frac{k_c}{k}\right)$$

where δ is the velocity ratio C_s/u_e (<1), the function $F(\delta)$ is the correction factor of order unity, and k_c is the upper limit of the wave number of the ion wave turbulence where linear growth rate due to the current balances the linear ion Landau damping. Substituting this spectrum into Eq.(4.26), we obtain the anomalous collision frequency ν_{ei} by the use of the electron distribution function (4.27).

$$\nu_{ei} = \frac{1}{\delta} \cdot \frac{T_e}{T_i} \cdot \frac{u_e n_e}{n_i} k_c H(\delta) \tag{4.29}$$

where $H(\delta)$ is a function which comes from the angular average over the unstable cone. The function $H(\delta)$ is plotted with respect to δ in Fig.4.4.

When the ion fluctuation is superthermal, namely, $\delta < 1$, the electron-ion effective collision frequency is given by Eq. (4.29). On the other hand, when the drift velocity is subsonic, i.e., $\delta < 1$, the collision frequency is given by Spitzer's formula,[16] that is,

$$\nu_{ei} = 1.70 \cdot Z^2 \frac{e^4 \ln \Lambda}{m_e^{1/2} T_e^{3/2}} n_i \tag{4.30}$$

where $\ln \Lambda$ is the Coulomb logarithm.

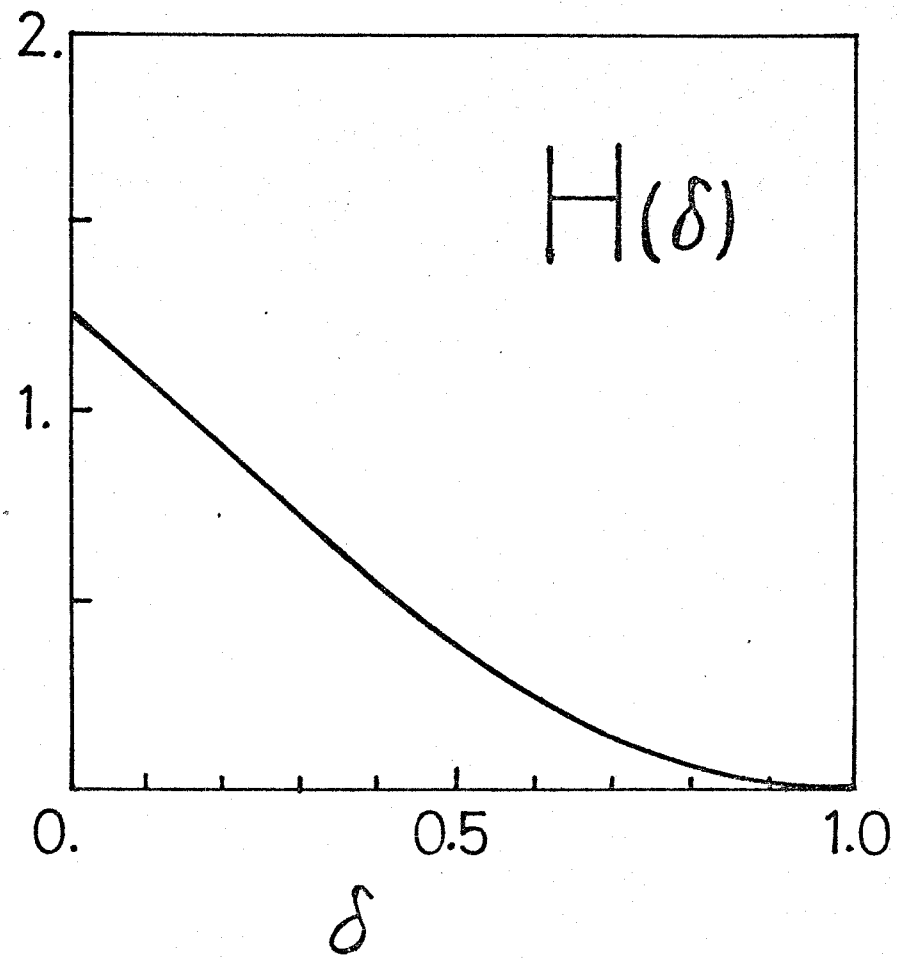

Fig. 4.4 $H(\delta)$ is a function which comes from the anguler average over the unstable cone, δ being the velocity ratio c_s/u_e.

4.5 Self-consintent Electrostatic Field Generation and Reduced Hot Electron Heat Flux

Using the coliision frequency obtained in the previous section, we solve Eqs. (4.10) and (4.24) with respect to ϕ. Here, we assume that the ion density n_i in Eqs. (4.10) and (4.24) has an exponential profile, $n_i = n_c/Z \exp[(r_c - r)/L_i]$, where L_i is the density scale length. In such an ion density, the hot electrons are not subjected t Coulomb collisions with the ions over a distance l_s from the cut-off;

$$l_s = L_i \ln(l_{hc}/L_i + 1) \tag{4.31}$$

Thereby l_{hc} is the hot electron mean free path at the critical surface. Over the distance l_s the hot elelctrons can be described by the collisionless Vlasov equation as shown previously. Therefore, we take the system size L to be smaller than the distance l_s. It is noted, however, that Eqs. (4.10) and (4.24) contain the maximum value of the potential ϕ_0 which should be determined self-consistently. Therefore, they have to be solved as an eigenvalue problem. We solved them numerically.

In the slabe case, following parameters are used,

$$n_c = 10^{21}\ cm^{-3}, \quad x_c - x_0 = 50\mu m, \quad T_h = 10\ keV$$
$$\tilde{n}_{h0} = 0.5, \quad T_e = 500\ eV, \quad T_i = 250\ eV,$$
$$L_i = 10\mu m, \quad Z = 5 \tag{4.32}$$

A resultant profile of the potential is shown in Fig.4.5. It is found from this figure that the turbulent state appears in the vicinity of the critical layer and the potential ϕ decreases (or $\tilde{\phi}$ increses) rapidly due to anomalous resistivity. In the spherical model, the corresponding potential profile is shown in Fig.4.6, where additional parameters, $\beta=1$, $r_c=100\mu m$, $r_0=50\mu m$, are used. In Fig.4.6, we see that the potential height is reduced by the geometrial effect compared with the slab case.

Let us now investigate the reduction of the hot electron energy flux. The inward going energy flux of the hot electrons over the electrostatic potential is evaluated to be

$$Q_o = \int_{-\infty}^{\infty} \frac{1}{2} m_e v^3 f_h(v)\, dV \Big|_{at\ x=x_o}$$

$$= Q_c \cdot \exp(-\tilde{\phi}_0) \qquad (4.33)$$

in the slab case, and

$$Q_{oS} = 4\pi r_0^2 \int_{-\infty}^{\infty} \frac{1}{2} m V_r^3 f_h(V_r)\, dV_r \Big|_{at\ r=r_o}$$

$$= Q_{cS} \frac{\tilde{r}_0^2}{\beta + (1-\beta)\tilde{r}_0^2} \cdot \exp(-\tilde{\phi}_0) \qquad (4.34)$$

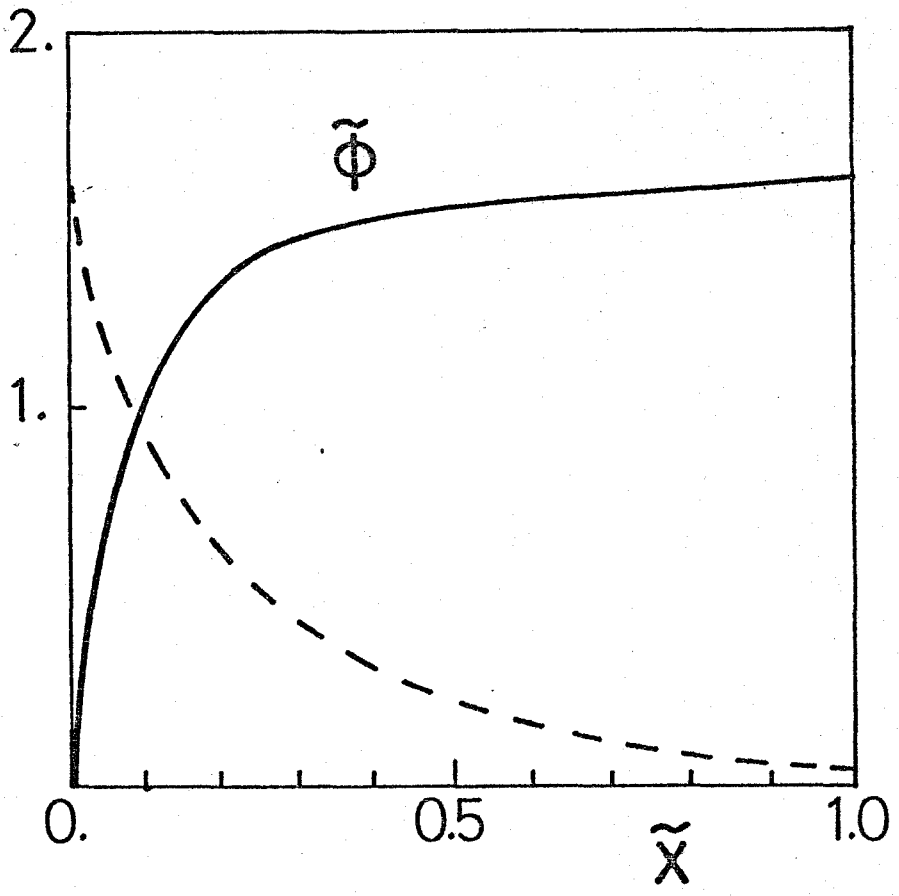

Fig. 4.5 The electrostatic potential and return current velocity in the slab model.
The normalized potential $\tilde{\phi} = -e\phi/T_h$ and flow velocity $\tilde{u}_e = 10^{-1}u_e/C_s$ are drawn by the solid and dotted lines. The turblence appears near the critical layer ($\tilde{x}=0$).

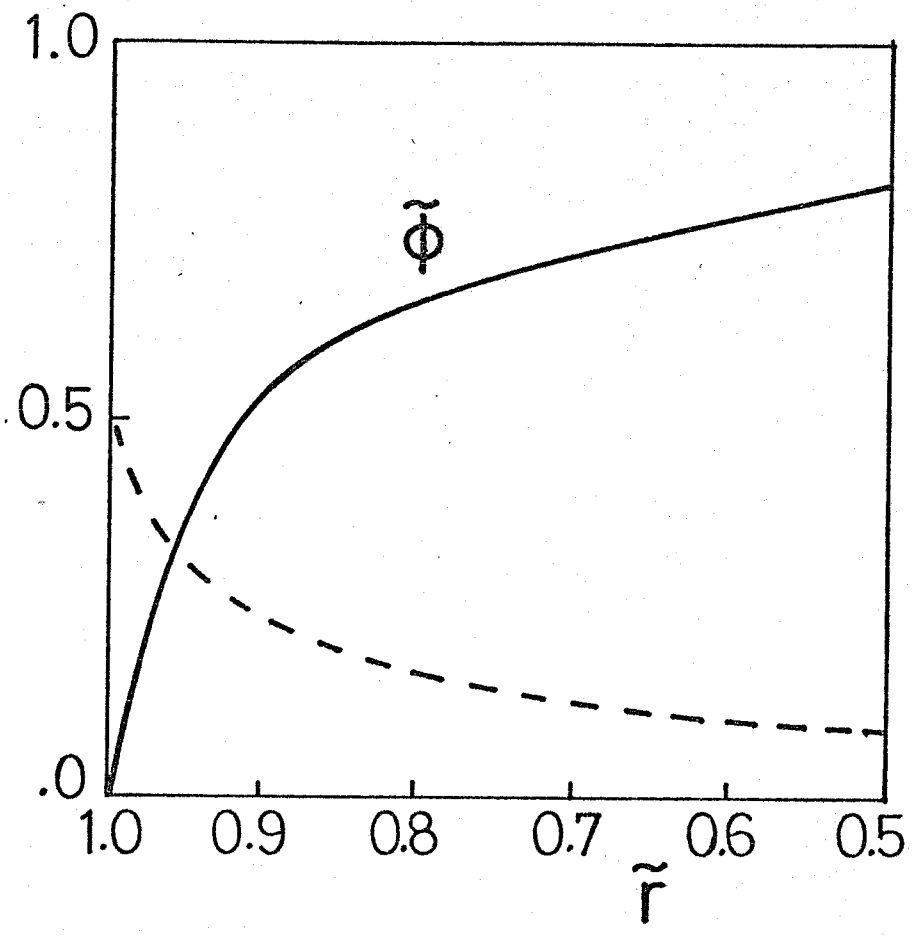

Fig. 4.6 The electrostatic potential and the return current velocity in the spherical model.
The normalized potential $\tilde{\phi}= -e\phi/T_h$ and the flow velocity $\tilde{u}_e = 10^{-1}u_e/C_s$ are shown by the solid line and the dotted line, respectively. The turblent state appears near the critical layer ($\tilde{r}$=1) and the large electric field is produced due to the anomalous resistivity.

in the spherical case. Here, $Q_c = (2\pi)^{-1/2} n_{h0} v_h T_h$ is the heat flux density of the half Maxwellian distribution at cut-off, and $Q_{cs} = (2\pi)^{-1/2} n_{h0} v_h T_h 4\pi r_c^2$ is the total heat flux emitted from the cut-off sphere. From Eqs. (4.33) and (4.34), we define a flux reduction coefficient f by

$$f \equiv \frac{Q_o}{Q_c} = \exp(-\tilde{\phi}_o) \tag{435}$$

in the slab case, or

$$f \equiv \frac{Q_{os}}{Q_{cs}} = \frac{\tilde{\gamma}_o^2}{\beta + (1-\beta)\tilde{\gamma}_o^2} \exp(-\tilde{\phi}_o) \tag{436}$$

in the spherical case.

Eqs.(4.39) and (4.36) clearly indicate that the electrostatic field effect, say $\exp(-\tilde{\phi}_0)$, reduces f both in the slab and sperical case. However, in the spherical case, the effect of the anisotropy of hot electron distribution β and the geometrical effect $\tilde{r}_0^2$ are also effective for the inhibition. From figs.4.5 and 4.6, it is found that the reduction coefficient f is 0.20 in the slab case and 0.11 in the spherical sace, respectively. Note that the generated electrostatic potential has the height almost equal to hot electron thermal energy T_h.

Let us now investigate hot electron density dependence of f at the critical layer. Fig.4.7 shows the result. Although one

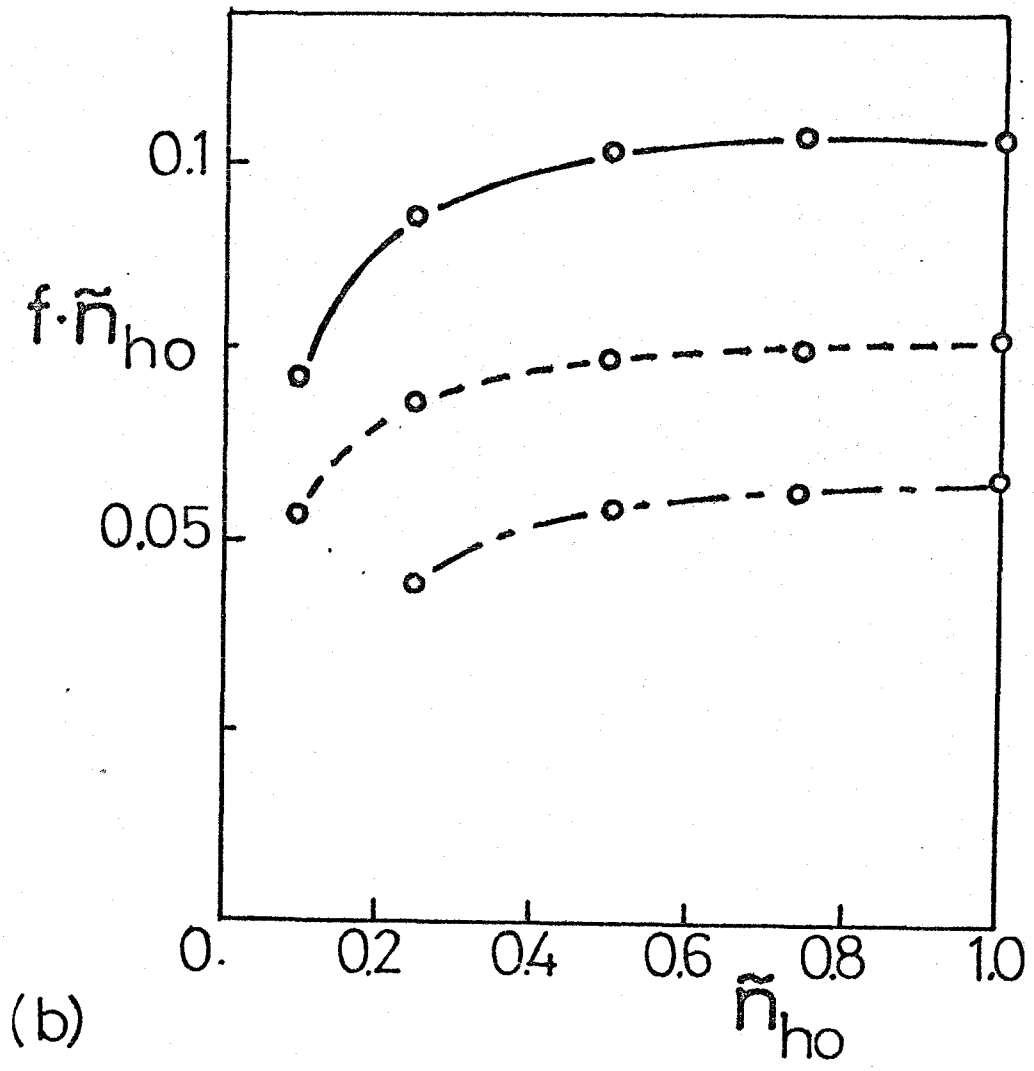

Fig. 4.7 Reduction coefficient of hot electron heat flux versus hot electron density.

The solid line corresponds to the reduction coefficent in the slab model. The dotted and dash-dot lines correspond to those in the spherical model with $\beta=0.1$ and $\beta=1$, respectively.

(a) Reduction coefficient f versus hot electron density $\tilde{n}_{h0}$ where f is given by Eq.(4.35) or (4.36).

(b) Total energy flux penetrating into the core region versus hot electron density $\tilde{n}_{h0}$. This flux, which is proprtional to the quantity $\tilde{n}_{h0}f$, is insensitive to variation of the hot electron density.

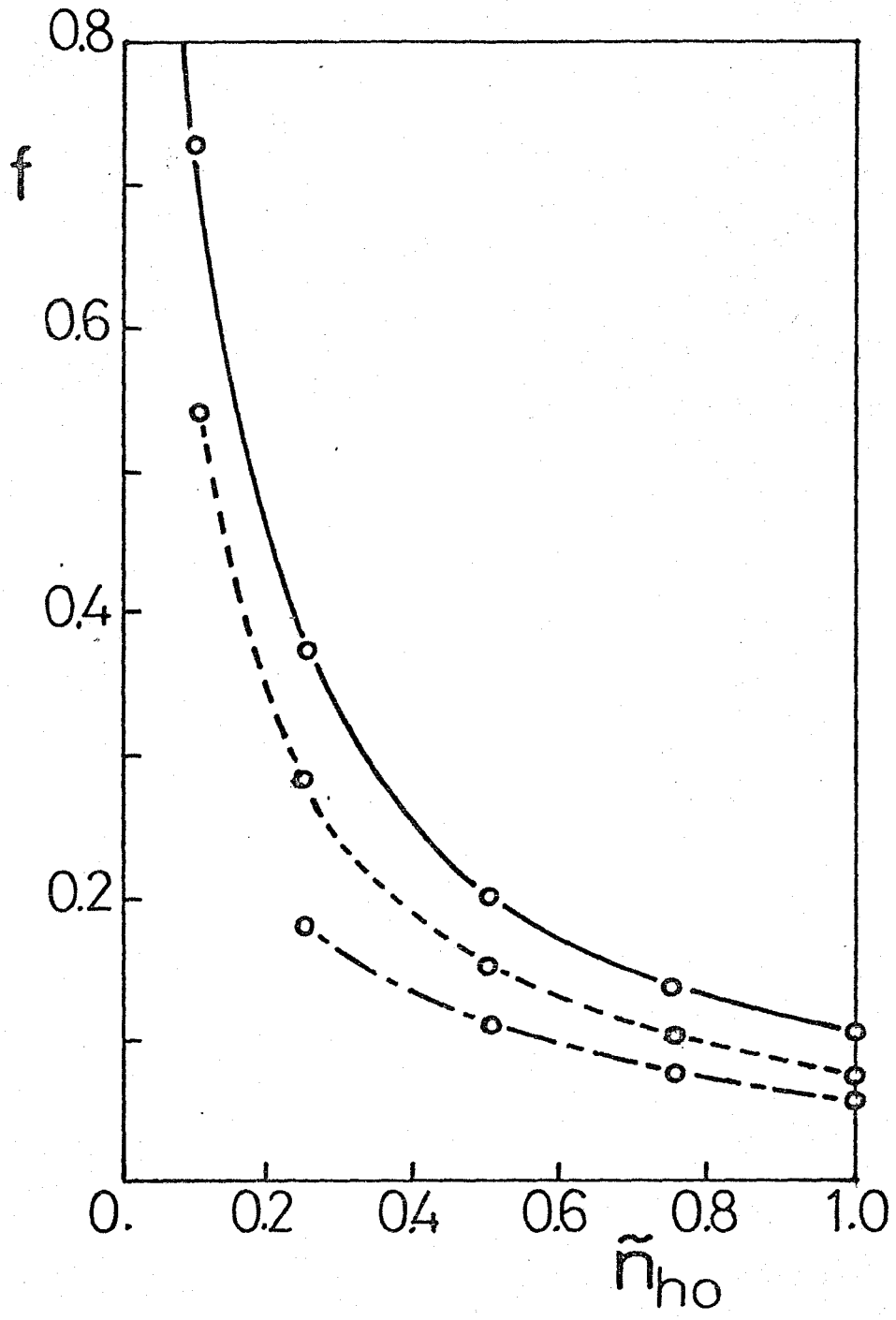

(a)

of the most important problems in the laser produced plasma is how the hot electron density is related to other physical quantities such as T_h and T_c, we have restricted our considerarion to the density dependence of the reduction coefficient f without changing the other parameters used in obtaining Fig. 4.5 and 4.6 previously.

Fig.4.7.a shows the n_{ho} dependence of the reduction coefficient f and Fig.4.7.b shows the n_{ho} dependence of the total eregy flux penetrating into the core region, which is proportional to $n_{ho}f$. It should be emphasized that the potential depth becomes larger in proportion to the hot electron desity n_{ho} and the reduction coefficient f decreases. However, the tatal energy flux penetrating into the core region is independent of n_{ho} and is maintained almost constant as $\tilde{n}_{h0}f = 0.11$ in the slab model and $\tilde{n}_{h0}f = 0.06$ in the spherical model.

Let us now investigate the effects of the anisotropy of the hot electron velocity distribution on the flux reduction. When we consider the machanisms of hot electron generation; for instance, the resonance absorption the electrons are accelerated mainly along the density gradient which is the radial derection. When this is the case, the relation $T_h >> T_\perp \tilde{=} T_c$ is generally established. From such a point of view, the β dependence of the reduction coefficient f was investigated and the results are shown in Fig.4.8. This figure clearly indicates that f is insensitive to β. This fact is interpreted as follows. For small β, the hot electron number for the large angular momentum is small and the average hot electron kinetic energy in the radial direction is relatively large. However, a large electrostatic potential is built up and strong reflection occurs due to the electrostatic

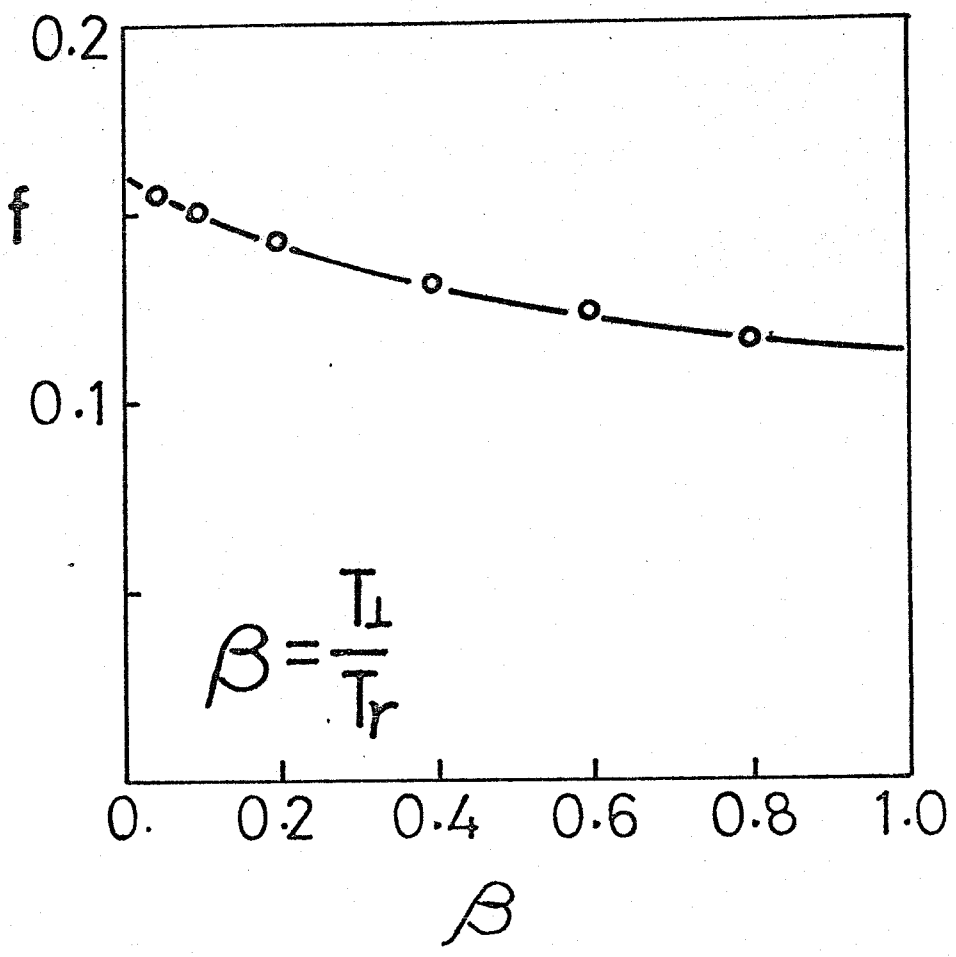

Fig. 4.8 Reduction coefficient f as a function of the anisotropy β of the hot electron distribution function.

filed. On the other hand, for large β, hot electrons are effectively reflected both by centrifugal force and a modereate electrpstatic filed. Because of the self-consistent behavior of the elcetrostatic filed as mentioned here, the reduction coefficint f is maintained constant.

We also investigated the dependence on the ion charge state Z of the hot electron flux reduction. Althought the hot elcectrons are free from collisions over the distance l_s from cut-off given by Eq.(4.31), the cold elctron return current depends upon the coulomb collision frequency, namely, Z and the electrostatic potential then depends on Z. Therefore, even if our consideration restricted to the region where hot electrons are collisonless, it is meaningful to look at the Z dependence of the hot elctron heat flux. The Z dependence of f is shown in Fig.4.9 for the slab mode. From this figure it is found that within the collisionless region the heat flux is further reduced by a factor about 0.2 with respect to that generated at cut-off. So, the heat shielding by the elctrostatic field is very important even if high Z materials are used.

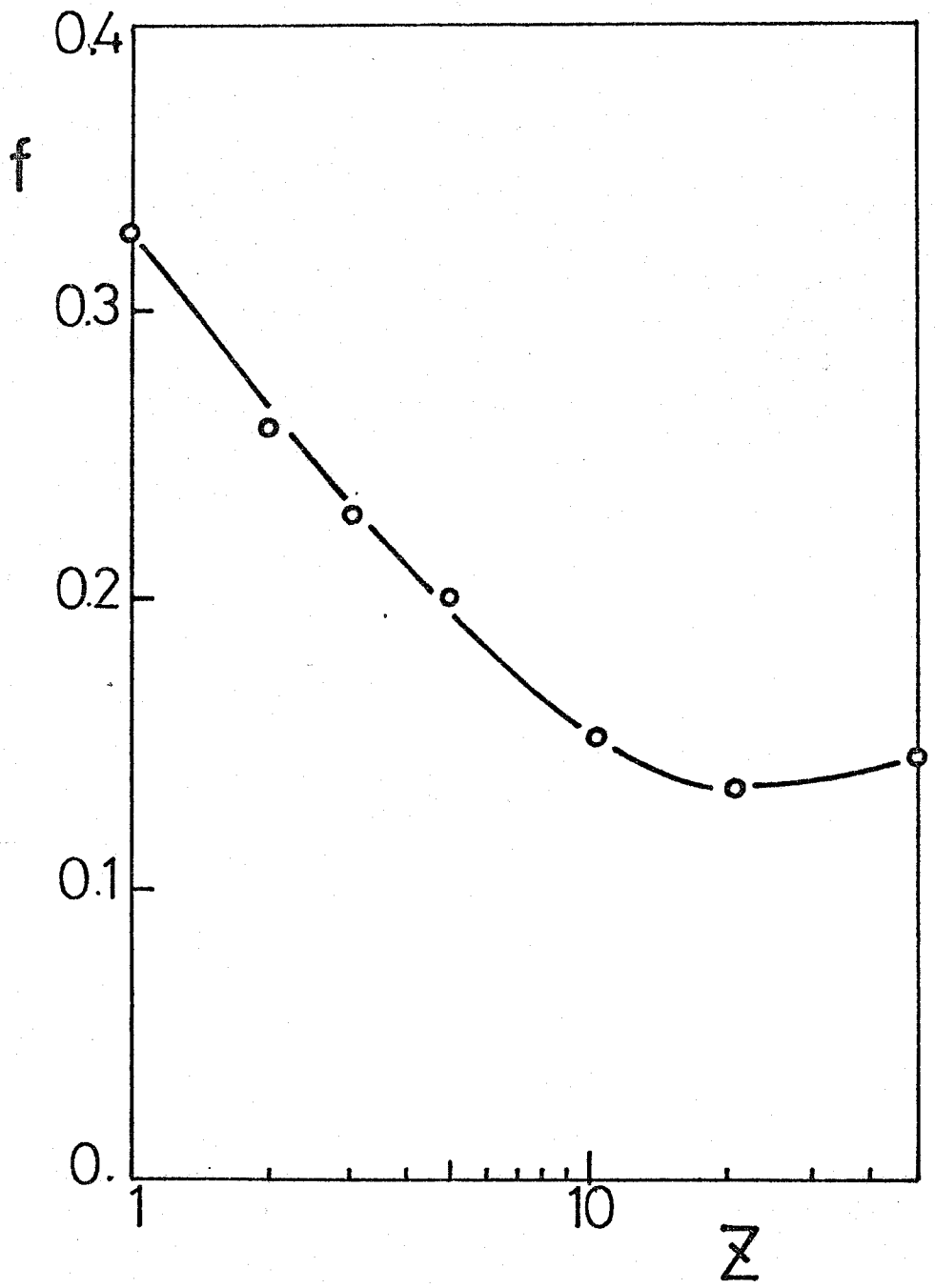

Fig 4.9 Dependence of the hot electron flux reduction on the ion charge state Z.

The heat flux is reduced by a factor of about 0.2 by the electrostatic field.

4.6 Conclusion and Discussion

In the stationary production of the hot electrons, a cold electron return current is induced and an electrostatic field is built up due to finite electrical resistivity. We investigated the elctrostatic field effects on the hot elctron heat flux. It is found that ion turblence is produced locally in the vicinity of the critical layer to enchance the elctrical resistivity. The induced potential depth $|e\phi/T_h|$ is found to be larger enough to reduce the hot electrons. The flux reduction coefficient f depends strongly on the hot electron density. The heat flux of the hot electrons ($\propto n_{h0} f$) is, however, nearly constant, which is about 0.04 $n_c v_h T_h$ for the slab model and $0.02(r_c r_0)^2 n_c v_h T_h$ for the spherical model.

We should also emphasize that the geometrical structure of the target plasma is important not only for the transport of hot elctrons but also for the general transport problems of energetic particles. Finally, we claim that the electrostatic field is also important for hot electron shielding by high Z materials.

Joule heating of the cold electrons was not taken into account in this paper. In the case of a rest plasma, the stabilization of turbulence due to Joule heating would be possible and important. However, there always exists the ablative flow in laser produced plasmas, and the energy deposited by the Joule heating is convected out into the underdense region. Therefore, the backgroud electrons can remain cold. This fact is interpreted as follows. The

energy balance between Joule heating and convcntive loss gives us the approximate cold electron temperature, $e\phi_0/(M^2/2+5/2)$, where M is the Mach number of the ion flow at cut-off. Therefore, the cenvention loss for $M \tilde{=} 3$ keeps elecctron temperature. In such a case, we can justify the neglection of Joule heating and expect anomalous heat flux reduction.

References

1. W. L. Kruer and J. M. Dawson, Phys. Fluids 15, 446(1972)
2. J. J. Thomson, R. J. Faehl, and W. L. Kruer, Phys. Rev. Lett. 31, 918(1973)
3. J. P. Freidberg, R. W. Mitchell, R. L. Morse, and L. I. Rudshinski, Phys. Rev. Lett. 28, 795(1972)
4. K. G. Estabrook, E. J. Valeo, and W. L. Kruer, Phys. Fluids 18, 1151(1973)
5. D. V. Giovanielli, J. F. Kephart, and A. H. Williams, J. Appl. Phys. 47, 2907(1976)
6. J. F. Kephart, R. P. Godwin, and G. H. MaCall, Appl. Phys. Lett. 25, 108(1974)
7. B. H. Ripin, et. al, Phys. Rev. Lett. 34, 1313(1975)
8. K. A. Brueckner and S. Jorna, Rev. Mod. Phys. 46, 325(1974)
9. E. J. Valeo and I. B. Bernstein, Phys. Fluids 19, 1348(1976)
10. J. D. Lindl, Nucl. Fusion 14, 511(1974)
11. R. C. Davidson, "Methods in Nonlinear Plasma Theory." (Academic, New York, 1972).
12. K. Kato, J. Phys. Soc. Jpn 41, 1050(1976)
13. L. Spitzer, Jr., "Physics of Fully Ionized Gases." (Interscience, New York, 1965).
14. W. L. Manheimer, Phys. Fluids 20, 265(1977)
15. B. B. Kadomtsev, "Plasma Turbulence."(Academic, London,1965)

16. S. I. Braginskii, in "Reviws of Plasma Physics," edited by M. A. Leontovich, Vol.I, p.205. (Consultant Bureau, New York, 1965)

Chapter 5

Flow Effects on Breaking of Resonantly Produced Plasma Wave

5.1. Introduction

At high laser intensity the interaction between laser and coronal plasma of fusion target appears to be dominated by the coupling of electromagnetic wave with plasma wave. Thus, the dominant absorption mechanism is likely to be the linear conversion of the transverse electron magnetic wave to a longitudinal plasma wave. This occurs in the vicinity of the critical density in the case of the obliquely incident P-polarized laser light. The microscopic analysis of the linear conversion is necessary associated with the determination of the hot electron energy spectrum, which has direct effect upon transport problems as shown in the previous chapter. In the case of strongly driven plasma oscillation, the growth of the plasma wave is saturated by the onset of wavebreaking and the production of energetic electrons.

The wavebreaking amplitude in a cold, spatially uniform rest plasma without an external pump field has been calculated by Dawson[1]. The corresponding amplitude in a cold, spatially inhomogeneous rest plasma has computed by Koch and Albritton[2], and the investigation of the wavebreaking regime where collective osillation energy is converted into random energy of the electron motion has also been done by them[3]. Plasma temperature effect on reducing the wavebreaking amplitude has been calculated by Kruer[4] by the use of the results calculated by Coffey[5] with the "water bag" model. "Paricle code" similation has been also employed to investigate the dynamics of the resonance absorption[6),7),8)], giving good agreements with theoretical

results. Using this particle code, the correspondence between simulation and experimental results has been investigated[9),10)] to get, especially, a scaling law to the hot electron temperature. And it seems that a good agreement exsistes between these results.

However, the laser produced plasma is not an ideal rest plasma but is a plasma expanding into a vacuum. Moreover, as we have seen in the previous chapter the generation of hot electron induces the cold electron return current toward the underdense region. The exsistence of this flow will influence the resonantly excited plasma wave, and hence the hot electron generation. In this chapter, we take flow effect into account to investigate the linear conversion and the plasma wave excitation.

In Sec.5.2, the Lagrangian description is employed to investigate the dynamics of resonant excitation of plasma wave and the oscillation is expressed in this frame. Inversion from Lagrangian to Eulerian variables is carried out in Sec.5.3 and a distortion of the wave profile is demonstrated, as well as an appearence of wavebreaking. In Sec.5.4, the resonance field amplitude limited by the convection loss is obtained, including the amplitude limitation due to wavebreaking. Finally, the comparison with the other, finite temperature effect and time dependent wavebreaking effect at rest plasma, is shown to investigate what effect is most significant for our practical plasma.

5.2 Basic Equations in Lagrangian Frame.

We consider an obliquely incident electro magnetic wave on a plasma with a monotonically increasing plasma density. The laser electric field is polarized in the plane of incidence (P-polarization). The electromagnetic wave is reflected by the density gradient so that it does not reach the critical surface, where the laser frequency equals the plasma frequency. However, some of the electromagnetic energy tunnels into the critical surface. Thus an obliquly incident electrmagnetic wave results in an electric field along the density gradient with the frequency near the local plasma frequency at the critical surface and resonantly excites an electrostatic plasma wave.

We use the Maxwell equations and the equation for the electron motion to see the resonant excitation of the plasma wave.

$$\nabla \times \mathbf{B} = \frac{4\pi}{c}\mathbf{j}^{0} + \frac{1}{c}\frac{\partial}{\partial t}\mathbf{E} \tag{5.1}$$

$$\nabla \cdot \mathbf{E} = 4\pi e\,(Z n_i - n_e) \tag{5.2}$$

$$m\left(\frac{\partial}{\partial t} + V\frac{\partial}{\partial x}\right)V = -e\,\mathbf{E} \tag{5.3}$$

We do not consider the ion motion because the wave excitation occures much faster than the time scale of ion motion. The effect of the electron temperature which gives rise to the dispersion effect on the excited plasma wave is neglected. Near the critical surface the tunneled magnetic field shown ih the left hand side of Eq.(5.1) corresponds to the driver field. The amplitude of this field is almost homogeneous near the critical layer along the density-inhomogeneous direction (x-direction) and the vector component of $\nabla\times\mathbb{B}$ is dominant in the x-direction. Therefore, the induced plasma wave oscillates in the x-direction. We here consider the motion only in the density-inhomogeneous, x-direction. Then, Eqs.(5.1)-(5.3) are rewritten as the form

$$\frac{\partial}{\partial t}E = -4\pi j + C\cdot(\nabla\times\mathbb{B})_x \qquad (5.1)'$$

$$V\frac{\partial}{\partial x}E = 4\pi e Z n_i V + 4\pi j \qquad (5.2)'$$

$$\left(\frac{\partial}{\partial t} + V\frac{\partial}{\partial x}\right)V = -\frac{e}{m}E \qquad (5.3)'$$

where $(\nabla\times\mathbb{B})_x$ is the x-component of the vector $\nabla\times\mathbb{B}$ and E, V, and j is the electric field, electron velocity, and current in the x-direction, respectivrly.

By representing the aboube equations in the Lagrangian

frame, we can easily treat large amplitude oscillation without considering various nonlinear effcts. From Eqs(5.1)' and (5.2)' the variation of the electric field in the Lagrangian frame is descrided by

$$\frac{dE}{dt} = \frac{m}{e}\omega_{p0}^2 V + c\,(\nabla\times B)_x \qquad (5.4)$$

where $d/dt = \partial/\partial t + v\partial/\partial x$ is the total derivative following the electron motion, and ω_{p0}^2 is the electron plasma frequency given by the initial electron density ($n_e = Zn_i$ at t=0). Operating the total derivative to Eq(5.3)' and eliminating dE/dt by the use of Eq.(5.4), the following model equation is obtained.

$$\frac{dV}{dt^2} + \omega_{p0}^2 V = -\frac{e}{m} c\,(\nabla\times B)_x \qquad (5.5)$$

The driver term of the right hand side in the equation is approximately given by the form

$$B = B_c \cdot \cos(\omega t + k_y y)\, \hat{e}_z \qquad (5.6)$$

where ω is the frequency of the electromagnetic wave; k_y =

$\frac{\omega}{c}\sin\theta$ is the wavenumber in the y-direction with the incident angle θ; B_c is the magnetic field amplitude at the critical point and assumed constant, and $\hat{i}_z$ means the unit vector perpendiculer to the plane of incidence. Substituting Eq.(5.6) into (5.5) and neglecting the sinusoidal y-dependence of the variables, Eq.(5.5) reduces to

$$\frac{d^2}{dt^2}V + \omega_{p0}^2 V = -\omega^2 V_d \sin(\omega t) \qquad (5.7)$$

where $v_d = \frac{eB_c}{m\omega}\sin\theta$ is the driver strength.

In the above equation the plasma frequency ω_{p0} defined by thefixed ion density is the function of time in genral, since the electron has a mean velocity. Noticing this and using a complex representation for the oscillation velocity v with $v=f(t)\exp(i\omega t)$, where f(t) varies slowly in time, Eq.(5.7) reduces to an equation for f(t).

$$\frac{d^2}{dt^2}f + 2i\omega\frac{df}{dt} + [\omega_{p0}^2(t) - \omega^2]f = -\omega^2 V_d$$

Since the function f(t) is slowly varing in time, the second derivative in this equation is sufficiently smll. Neglecting this term and integrating the above equation, the resultant oscillation velocity for Eq.(5.7) is obtained in the form

$$V_{os} = \frac{1}{2}\omega V_d \exp(i\omega t)\int_0^t \exp\left[-i\int_t^{t'} \frac{\omega_{p0}^2(t'') - \omega^2}{2\omega} dt''\right] dt' \tag{5.8}$$

where $\omega_{p0}(t)$ is the plasma frequency in the Lagrangian frame moving with the electron fluid element.

Let us assume that the background plasma has a linear density profile near the critical surface where x=0, i.e.,

$$\omega_{p0}^2 = \omega^2\left(1 - \frac{x}{L}\right) \tag{5.9}$$

where L is the density scale length. In the Lagrangian frame, relation between the Eulerian coordinate x and time t is shown as

$$x = \int_0^t V_{os}(t,a)\, dt + V_0 t + a \tag{5.10}$$

where a=x(t=0) is an initial position of an electron fluid element and $v_{os}(t,a)$ is an oscillation velocity of this element, which may be given after solving Eq.(5.8). Since we are interested in the oscillation behaviour near the critical surface, the mean velocity can be assumed constant.

When we carry out the integral of Eq.(5.8), the plasma frequency ω_{p0} is given by substituting Eq(5.10) into (5.9). In this case, the inclusion of variation for the background

plasma frequency due to the quivering motion, which is given by the first term of the right hand side in Eq.(5.10), allows the appearence of some nonlinear phenomena, in particuler, the generation of higher harmonic oscillations. Although such nonlinear effects are important near the critical layer[11], we neglect these effects and focus our attention on the effect coming from the exsistence of mean electron velocity.

Let us introduce nondimensional variables to the time, coordinate, and velocity.

$$\tilde{V}_{os} = \frac{V_{os}}{V_0} , \quad \xi = \frac{t}{t_D} , \quad \tilde{x} = \frac{x}{x_D} \tag{5.11}$$

Where t_D and x_D are defined by $\beta\omega^{-1}$ and $\beta v_0\omega^{-1}$ respectively using a nondimensinal prameter $\beta=2(\omega L/v_0)^{1/2}$ which means a square root of the ratio between the time interval L/v_0 and the oscillation period. Note that the parameter β is much larger than unity within the context of our interest. By the use of the nondimensional variables defined by Eq.(5.11), the oscillation velocity of Eq.(5.8) is shown as

$$\tilde{V}_{os} = \frac{\beta}{2}\frac{V_d}{V_0} Re\left[e^{i(\beta\xi - \frac{a}{2L}\beta\xi - \xi^2)} \int_0^{\xi} e^{i(\frac{a}{2L}\beta\xi' + \xi'^2)} d\xi' \right] \tag{5.12}$$

where Re means taking a real part. Introducing the nondimen-

sional initial position $\tilde{a}=a/x_D$ and a new time coordinate $\eta = \xi + \tilde{a}$ (The origin of this time $\eta=0$ is set to be the time when the electron fluid element which is located initially at a passes the critical surface x=0.), Eq.(5.12) is rewritten as

$$\tilde{V}_{os}(\eta,\tilde{a}) = \left(\frac{\pi}{8}\right)^{1/2}\beta\frac{V_d}{V_0}\left\{\cos(\beta\eta-\eta^2-\tilde{a}\beta)\left[C\left(\sqrt{\tfrac{2}{\pi}}\eta\right)-C\left(\sqrt{\tfrac{2}{\pi}}\tilde{a}\right)\right]-\sin(\beta\eta-\eta^2-a\beta)\left[S\left(\sqrt{\tfrac{2}{\pi}}\eta\right)-S\left(\sqrt{\tfrac{2}{\pi}}\tilde{a}\right)\right]\right\} \tag{5.13}$$

where the functions C and S are defined by the well-known Fresnel integrals as

$$C(z) = \int_{-\infty}^{z}\cos\left(\frac{\pi}{2}t^2\right)dt$$

$$S(z) = \int_{-\infty}^{z}\sin\left(\frac{\pi}{2}t^2\right)dt$$

respectively. Profiles of these functions are shown in Fig. 5.1. For example, the oscillation profile given by Eq.(5.13) is shown in Fig.5.2 where $\beta=50$. In Fig 5.2.a, the case where $\tilde{a}=0$, say, initially located at the resonance point, is shown and the other case where $\tilde{a}=-\infty$ is shown in Fig.5.2.b. The

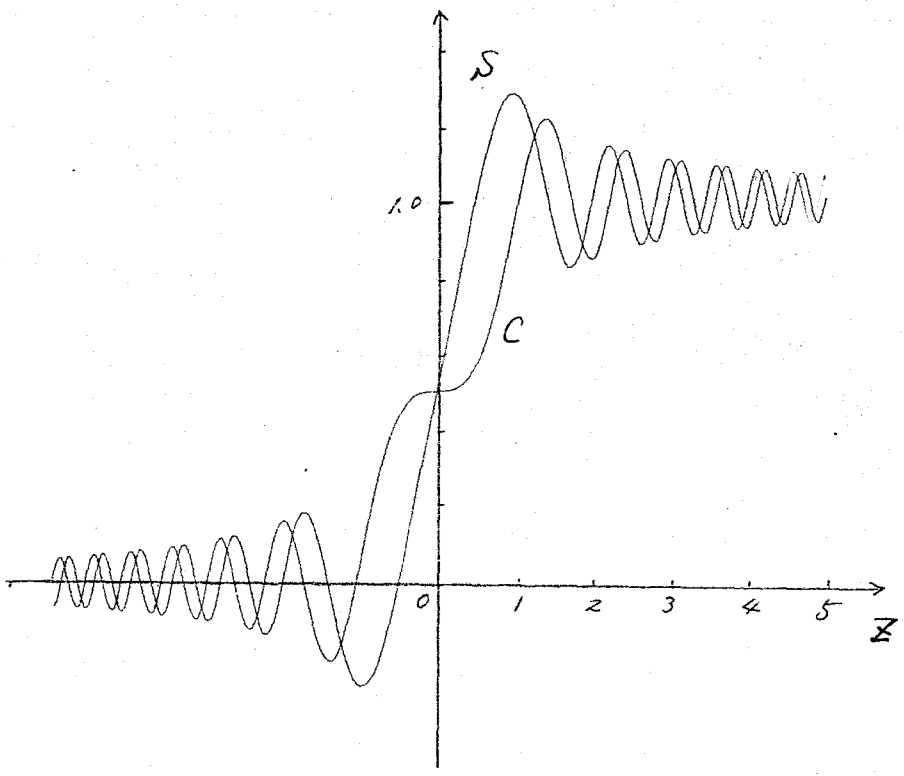

Fig. 5.1 Fresnel integral curves.

Fresnel integrals C(z) and S(z) are defined by

$$C(z) = \int_{-\infty}^{z} \cos\left(\frac{\pi}{2}t^2\right) dt$$

$$S(z) = \int_{-\infty}^{z} \sin\left(\frac{\pi}{2}t^2\right) dt$$

The assymptotic values are $C(\infty) = S(\infty) = 1$.

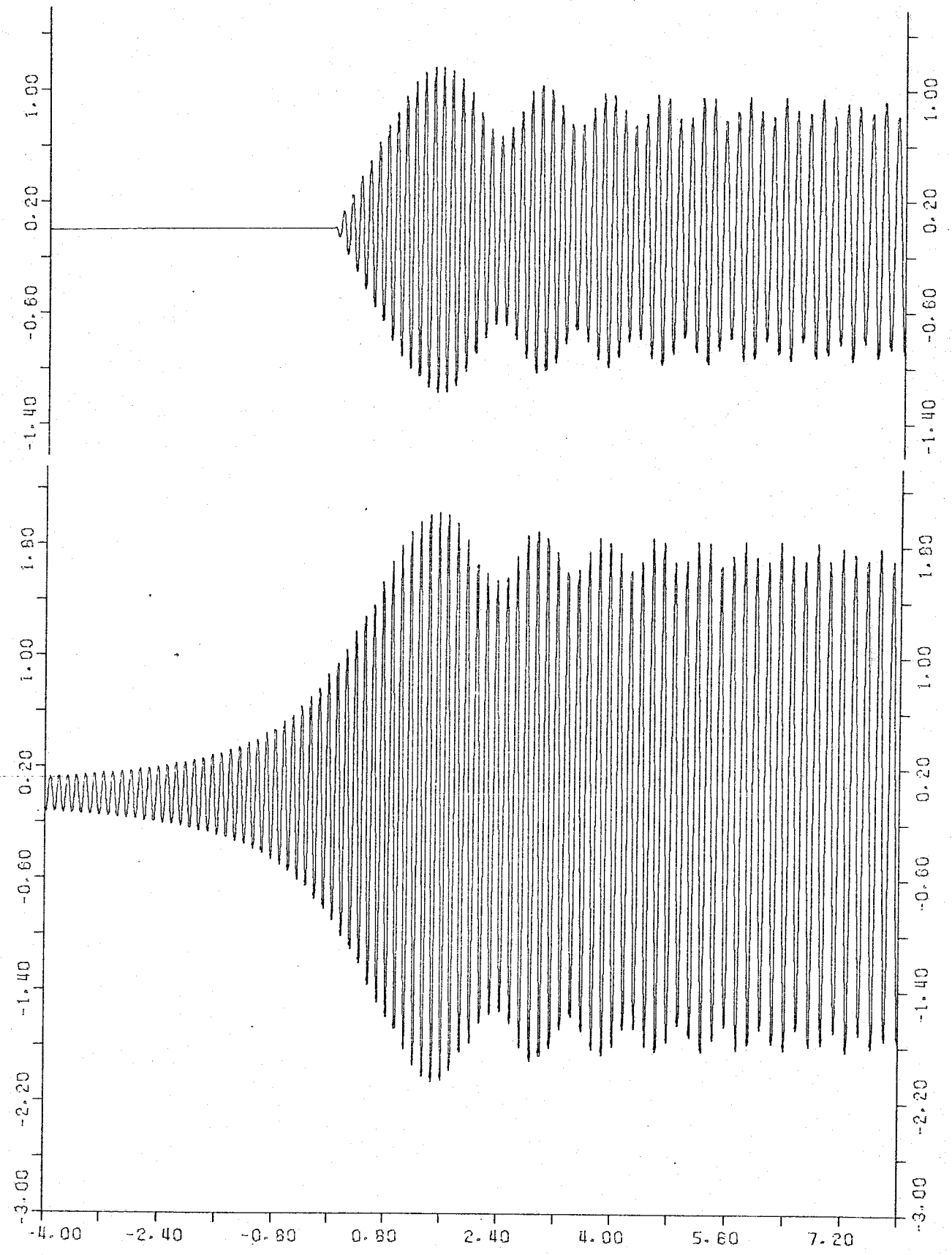

Fig. 5.2 Oscillation profiles given by Eq.(5.13), where the prameter $\beta=50$ is used.

(a) shows the case where a = 0, i.e., the oscillator is initially located at the resonance point, while (b) is the case where $a = -\infty$. In this case the envelope of the oscillation profile is given by the well-known Fresnel pattern.

later case corresponds to the stationary oscillation profile after the passage of sufficient time. Note that in order for the resonance oscillation to be enhanced it takes sufficient time. This is clear from that the later case with sufficient time before arrival at the resonance point exhibits much enhanced oscillation than the former case. It is also noted that the oscillation amplitude shows its peak value after arrival at the critical point and its envelope exhibits a Fresnel pattern defined by $(C^2+S^2)^{1/2}$ in the case where $\tilde{a}=-\infty$. We are interested in the flow effect on limiting the resonantly enhanced amplitude. Therefore, we will proceed using the oscillation form in the case where $\tilde{a}=-\infty$.

5.3 Inversion from Lagrangian to Eulerian Variables

The quivering distance defined by

$$\delta x_{os} = \int_0^t V_{os}\, dt$$

may be calculated from Eq.(5.13). By the use of the fact that the prameter β is much larger than unity and we are interested in the oscillation behaviour near the resonance point where η is order unity, then the displacement given by integrating Eq.(5.13) with respect to time η is shown approximately by the form

$$\delta\tilde{x}_{os} = -\sqrt{\frac{\pi}{8}}\,\frac{V_a}{V_0}\left[\sin(\beta\eta-\eta^2-\tilde{a}\beta)\cdot C\left(\sqrt{\tfrac{2}{\pi}}\eta\right) + \cos(\beta\eta-\eta^2-\tilde{a}\beta)\cdot S\left(\sqrt{\tfrac{2}{\pi}}\eta\right)\right] \qquad (5.14)$$

where in Eq.(5.13), $C(\sqrt{2/\pi}\tilde{a})$ and $S(\sqrt{2/\pi}\tilde{a})$ are neglected because $\tilde{a} \to \infty$, but the wave phase in the argments of the sin and cos functions are left. The normalization of δx_{os} is defined by $\delta\tilde{x}_{os} = \delta x_{os}/x_D$.

Let us consider to carry out inversion from Lagrangian to Eulerian variables. The relation (5.10) is rewritten in the nondimensional form

$$\tilde{x} = \delta\tilde{x}_{os}(\eta,\tilde{a}) + \eta \qquad (5.15)$$

Using this relation with Eq.(5.14) we can transform from Lagrangian coordinate $\tilde{a}$ to Eulerian coordinate $\tilde{x}$. For example, the wave profile at some time in the Eulerian frame is shown in Fig.5.3 for the oscillation velocity given by Eq.(5.13), where the prameter $v_0/v_d = 5.422$ is employed. It is apparent from this figure that the deformation of the oscillation profile from a linear-phase, sinusoidal one appears and the wave-breaking occurs in the underdense region where $\tilde{x} > 3$.

For the corresponding electric field, we can obtain $\tilde{E} = \delta\tilde{x}_{os}$ from Eq.(5.3)' with Eq.(5.12) in the same approximation used in obtaining Eq.(5.14). Here, the electric field is normalized as $\tilde{E} = -e\beta E/m\omega v_0$. The electron density perturbation, $\delta n = n_e - n_e(t=0)$, may be given by the continuity relation[12];

$$n_e(t=0) = n_e(x,t)\cdot\frac{\partial x}{\partial a}$$

$$\delta\tilde{n} = \frac{1}{1+\frac{\partial}{\partial\tilde{a}}(\delta\tilde{x}_{os})} - 1 \qquad (5.16)$$

where $\delta\tilde{n} = \delta n/n_e(t=0)$. The electric field and electron density perturbation are shown in Fig.5.4, where steepnings of the electric field and corresponding density bounchings with narrow highdense regions appear. It is noted that when and/or where the inequality, $\frac{\partial}{\partial\tilde{a}}(\delta\tilde{x}_{os})+1 < 0$, is satisfied, the transformation from Lagrangian to Eulerian variables does not remain

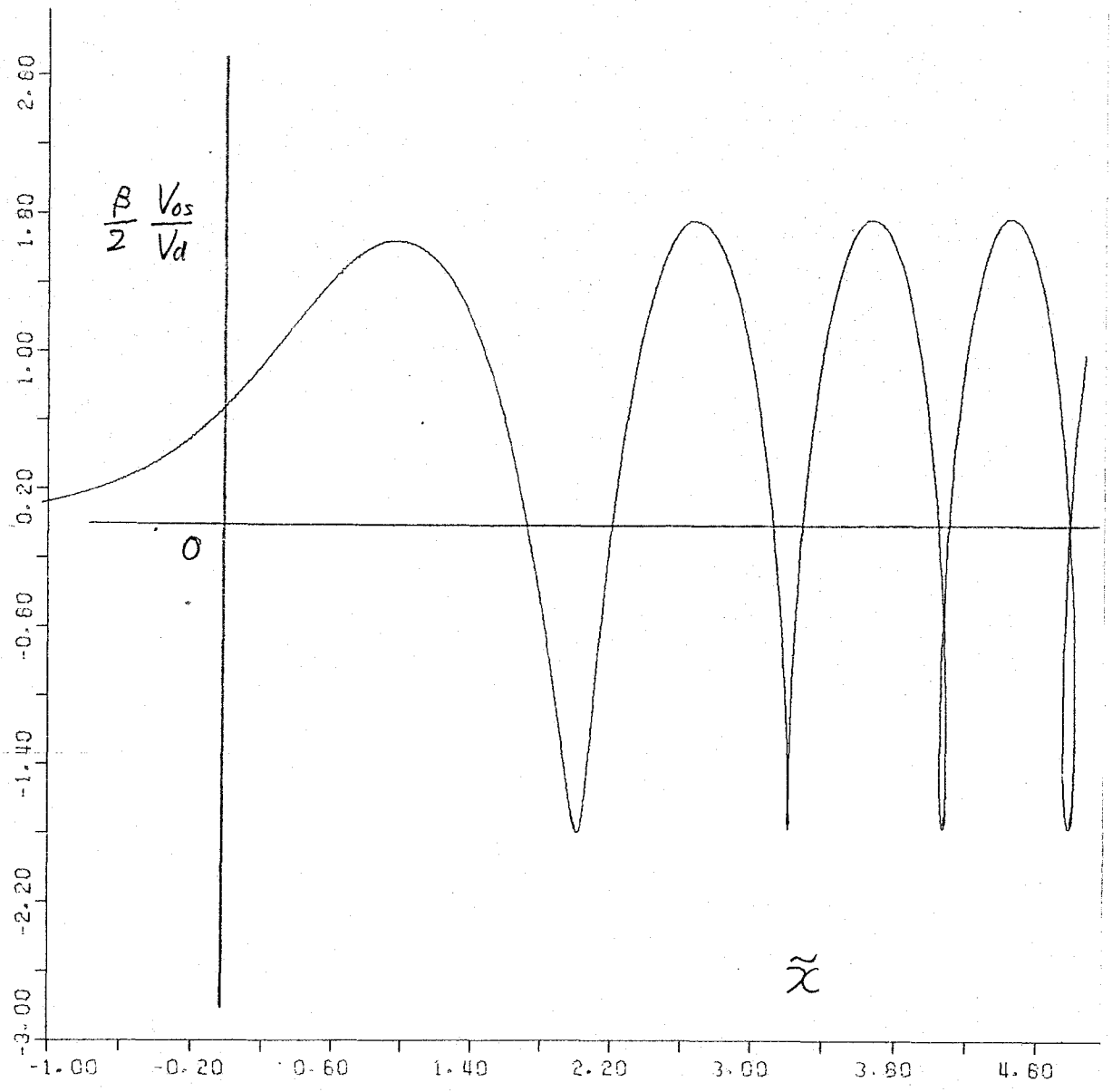

Fig. 5.3 Spatial profile for the oscillation velocity in the Eulerian frame with $v_0/v_d = 5.4$.
It is obvious from this figure that wavebreaking appears for $\tilde{x} > 3$.

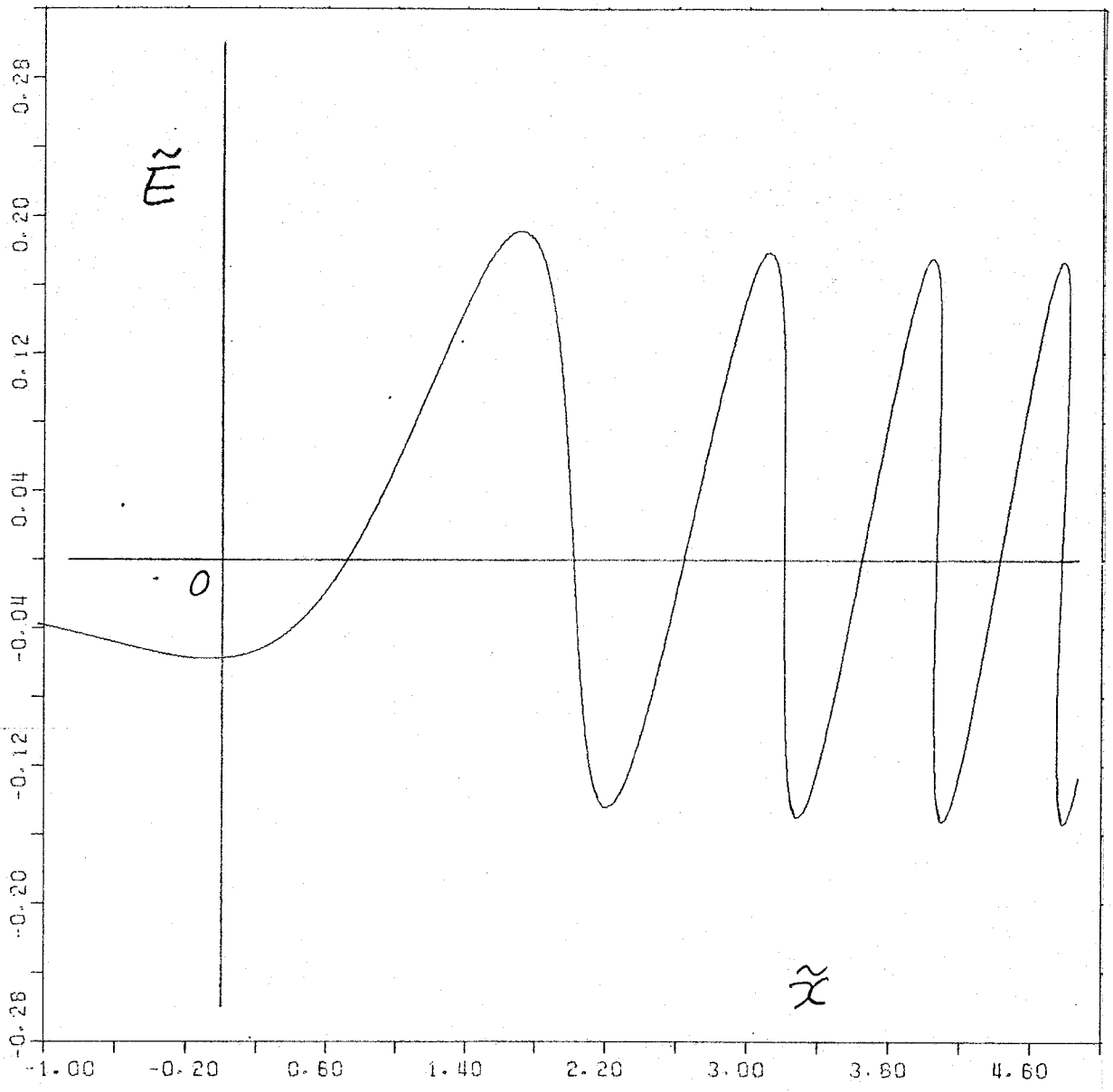

Fig 5.4.a Electric field profile with v_0/v_d = 5.4 corresponding to Fig.5.3.

"Steepnings" appear at the wave fronts.

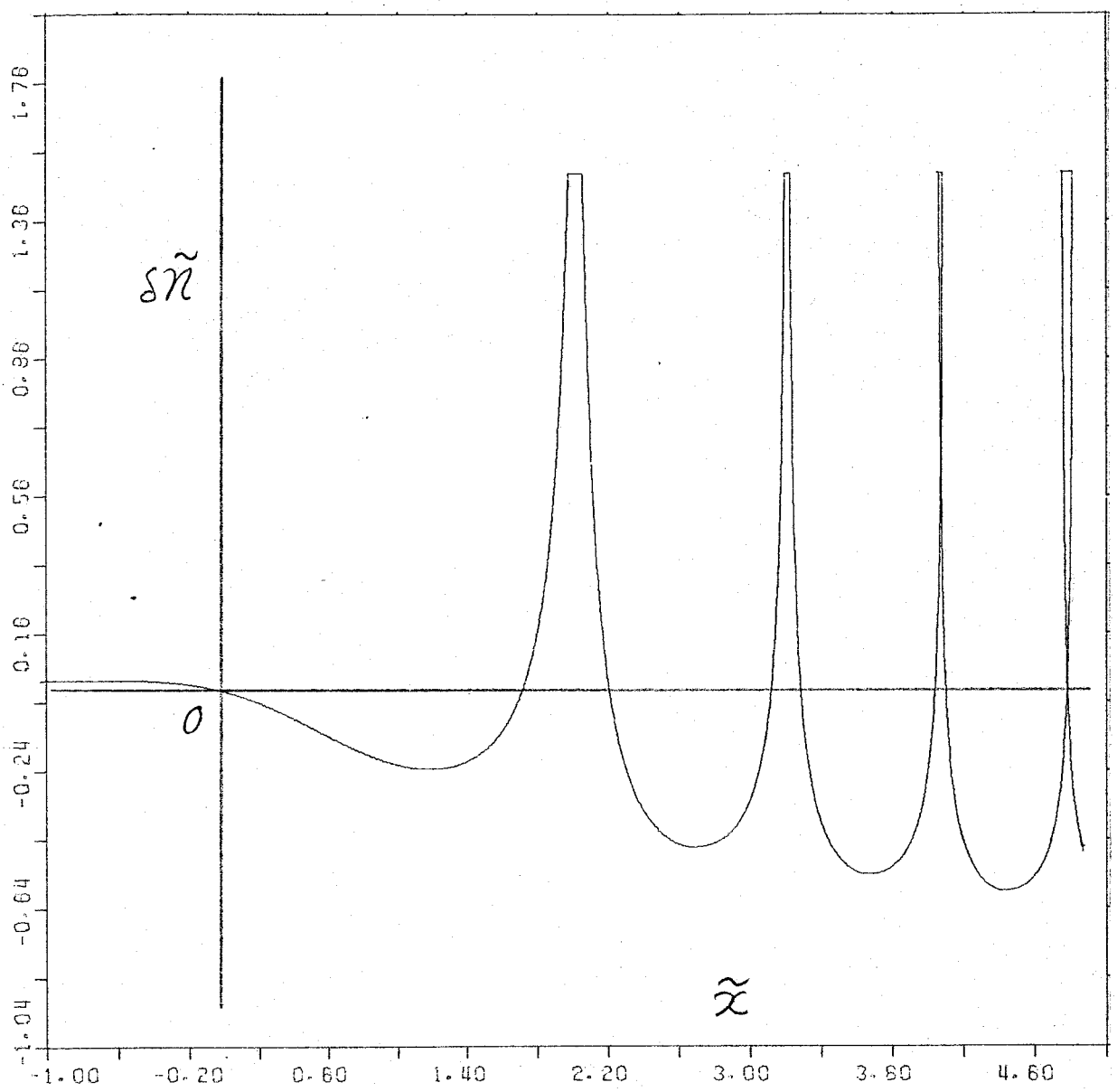

Fig 5.4.b Corresponding density profile.
"Bounchings" of electrons appear distorting the wave form from sinusoidal one.

unique for all time and space, therefore we must abandon the solutions in these reagions.

5.4 Wavebreaking Condition and Resonance Field Amplitude

As mentioned in the previous section, when an overtaking of the electron fluid elements appear, the phase mixing of the oscillation motions limits the wave amplitude to less value, as well as the Lagrangian formalism that has been employed in the present anarysis has no meaning mathmatically. As apparent from Fig.5.3 and 5.4, wavebreaking occurs predominantly in the underdense region. This may be explained as follows.

For a streaming cold plasma, its dispertion relation is readily shown as

$$(\omega - k u_0)^2 = \omega_p^2$$

where u_0 is a mean velocity, ω_p is a plasma frequency, and k is a wavenumber. Apply the dispertion relation to an inhomogeneous case, where $\omega_p = \omega_p(x)$. Then, the local wavenumber is given by $(\omega_0 - \omega_p)/u_0$ by assuming $\omega = \omega_0$: const. In our problem, as seen in the previous section the wave amplitude in the underdense region ($\omega_0 > \omega_p$) remains nearly constant. (see Fig. 5.2.b or Figs.5.3, 5.4.) Therefore,setting this amplitude as v_s,for instance, we can roughly estimate the wavebreaking conditions as

$$\frac{\omega}{k} = \frac{\omega_0}{\omega_0 - \omega_p} \cdot u_0 \lesssim v_s$$

$$\rightarrow \quad \omega_p \lesssim \left(1 - \frac{u_0}{v_s}\right)\omega_0 \qquad (5.17)$$

This ineequality means that if the phase velocity of the plasma wave becomes smaller than the oscillation vellosity, electron trapping by the large amplitude wave potential occurs, and the amplitude of this wave is limited. This is one of rather qualitative explanations for the wavebreaking phenomena. The inequality (5.17) says that the wavebreaking predominantly occures in the underdense region.

The above discussion for the wavebreaking condition is not so strict. The strict definition of wavebreaking is given by a breaking of Lagrangian formalism. The condition of this breaking is shown from the continuity relation as

$$\frac{\partial}{\partial \tilde{a}}(\delta\chi_{os}) \lesssim -1 \qquad (5.18)$$

for the present problem. Making use of Eq.(5.14), and minimaizing it over an its oscillation period, we obtain a local wavebreaking condition.

$$\frac{V_0}{V_d} \lesssim \frac{1}{2}\left\{\left[\sqrt{2\pi}\,\eta\cdot S\left(\sqrt{\frac{2}{\pi}}\eta\right)+\cos(\eta^2)\right]^2 + \left[\sqrt{2\pi}\,\eta\cdot C\left(\sqrt{\frac{2}{\pi}}\eta\right)-\sin(\eta^2)\right]^2\right\} \qquad (5.19)$$

where η corresponds to the coordinate of the oscillation center. The wavebreaking condition (5.19) is drawn in Fig.5.5. For the example in the previous section where $v_0/v_d=5.422$, it is evident from this figure that the wavebreaking condition

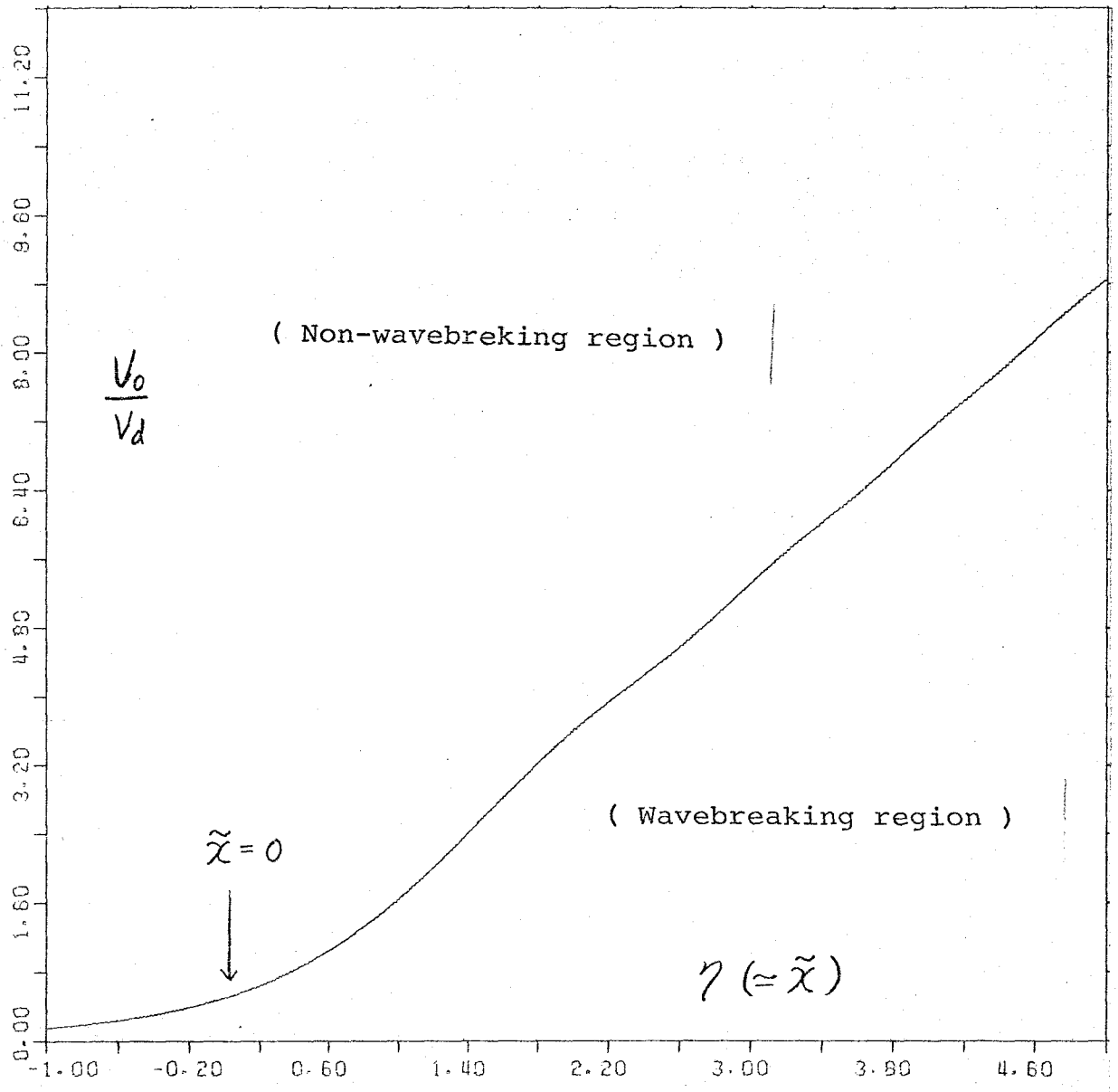

Fig. 5.5 Local wavebreaking condition given by Eq.(5.19).

s satisfied in the underdense region where $\eta \simeq \tilde{x} > 3$, as noted in the previous section.

Let us determine a peak amplitude of the present resonance field by taking into account the breaking condition. The peak amplitude v_{osp}, which has a direct relation to a maximum energy of hot electrons, is estimated from Fig.5.2.b as

$$V_{osp} = 2.1\,(L\omega/V_0)^{1/2}\cdot V_d \qquad (5.20)$$

$$\text{at } \eta = 1.53 \quad \text{or} \quad x \simeq 3\,(LV_0/\omega)^{1/2}$$

, when wavebreaking dose not occur at this point. However, in the case of $v_0/v_d < 2.7$, wavebreaking appears at this peak point. Therefore, we have to take it into account to get the peak amplitude. As the results, we can expect the following peak amplitudes for the streaming plasma.

$$V_{osp} = \begin{cases} 2.1\,(\omega L/V_0)^{1/2}\,V_d & \text{for } \dfrac{V_0}{V_d} > 2.7 \\ 1.3\,(\omega L/V_d)^{1/2}\,V_d & \text{for } \dfrac{V_0}{V_d} < 2.7 \end{cases} \qquad (5.21)$$

Thus, if the flow velocity is sufficiently large, the resonance field is saturated by the convection effect. On the other

hand, when the flow velocity is not so large, the wavebreaking occures predominantly to limit the peak amplitude of the resonance field.

5.5 Conclusion and Discussion

In the previous sections, we have focused only on the convection effect for the saturation mechanism which limits the resonance field amplitude to a finite value. We here intend to consider the other effects of the electron temperature dispersion and rest plasma wavebreaking, and to compare them in order to specify what exhibits the most significant effect for the resonance field and, in addition, for the hot electron temperature. The fomer effect[7] limits a localization of the resonance field by a wave dispersion coming from the electron pressure work. The later effect[2] is essentially the same with that described in the present analysis without the treatment of a time evolution for the resonance field. According to Ref.7, the resonance field saturated by the dispersion shows the profile given by an Airy function and its peak amplitude is

$$V_{osp} = 1.2 \left(\frac{\omega L}{v_e}\right)^{2/3} \cdot V_d \qquad (5.22)$$

where v_e is the electron thermal velocity. For the cold rest plasma, wavebreaking appears when the peak amplitude reaches

$$V_{osp} = \left(\frac{2\omega L}{V_d}\right)^{1/2} \cdot V_d \qquad (5.23)$$

as given in Ref.2.

Compareing these amplitudes given by Eqs.(5.21), (5.22),

and (5.23) and noticing that the most significant effect limits the peak amplitude to the lowest value, we obtain the following condition to the case where the flow effect is most significant.

$$\frac{V_0}{V_e} > 3.0 \left(\frac{V_e}{\omega L}\right)^{1/3}$$

$$\frac{V_0}{V_d} > 2.2$$

Note that $v_e/\omega L \sim \lambda_{De}/L$ is much smaller than unity. The diagram for the competition between these three effects is shown in Fig.5.6. To know where our plasma is located in this diagram is a drastic problem associated with hot electron generation. For the particle code simulation, it seems that the effect of flow is not included. However, in order to investigate the steady production of hot electrons, this effect can be expected to play the significant role in the actual laser produced plasma.

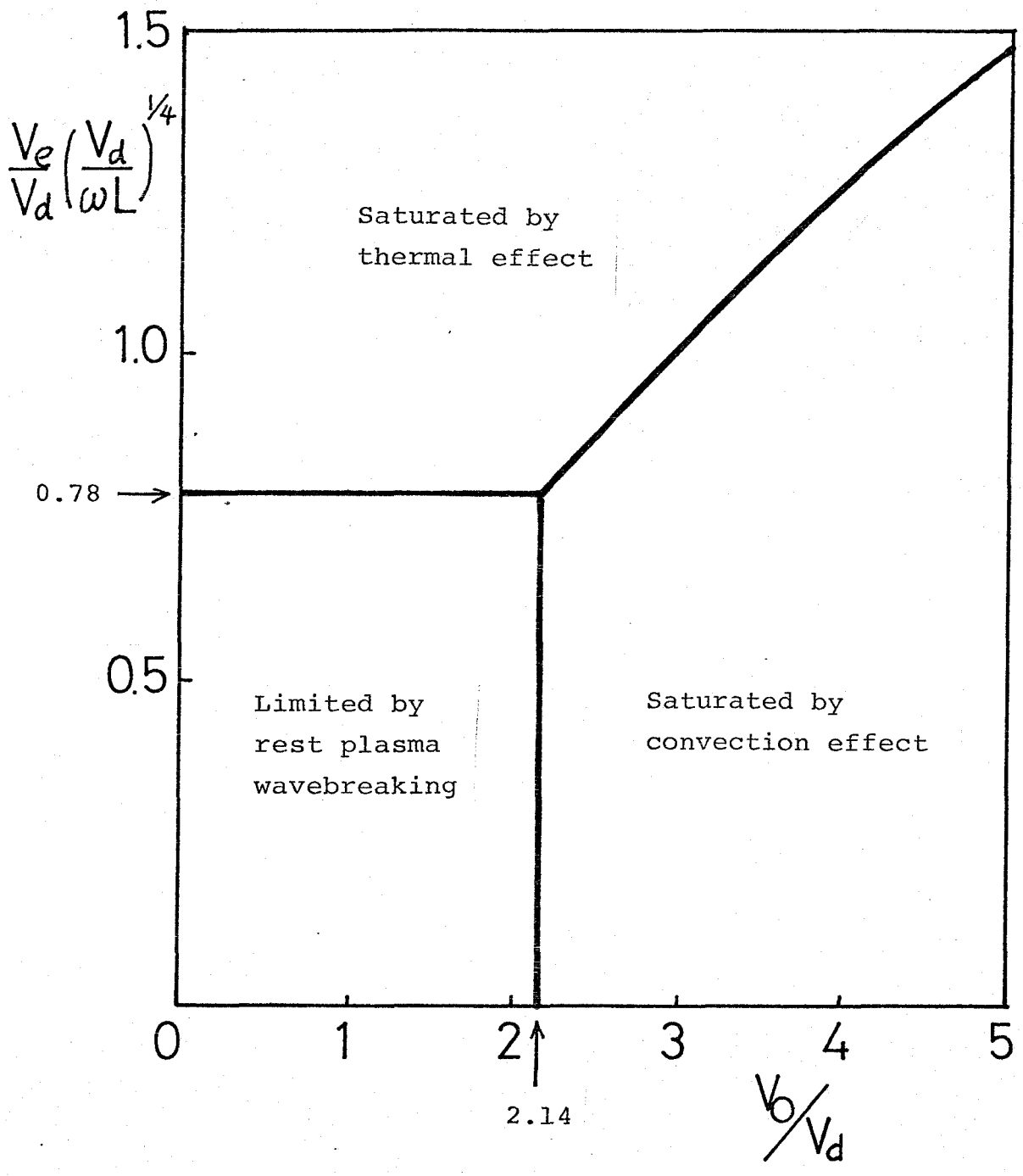

Fig. 5.6 Diagram for the competition between the effect of rest plasma wavebreaking, the thermal effect, and the convection effect.
Seculer growing of the resonance field is limited by the most effective mechanism.

References

1. J. M. Dawson, Phys. Rev. 113, 383(1959)
2. P. Koch and J. Albritton, Phys. Rev. Lett. 32, 1420(1974)
3. J. Albritton and P. Koch, Phys. Fluids 18, 1136(1975)
4. W. L. Kruer, Phys. Fluids 22, 1111(1979)
5. T. P. Coffey, Phys. Fluids 14, 1402(1971)
6. J. P. Freidberg, R. W. Mitchell, R. L. Morse, and L. F. Rudshinski, Phys. Rev. Lett. 28, 795(1972)
7. K. G. Estabrook, E. J. Valeo, and W. L. Kruer, Phys. Fluids 18, 1151(1975)
8. J. S. DeGroot and J. Tull, Phys. Fluids 18, 672(1975)
9. D. W. Forslund, J. M. Kindel, and K. Lee, Phys. Rev. Lett. 39, 284(1977)
10. K. G. Estabrook and W. L. Kruer, Phys. Rev. Lett. 40, 42(1978)
11. W. L. Kruer and K. G. Estabrook, "LLL Laser Progress Annual Report 1976," p.4.61.
12. R. C. Davidson, "Method in Nonlinear Plasma Theory," p.35, Eq.(12). (Academic, New York, 1972).

Chapter 6

Effects of Flow, Thermal Conduction, and Compressibility on Implosion Symmetry

6.1 Introduction

To achieve the laser fusion within practical laser energy, (10 $\sim$ 100 kJ), it is important to compress the fuel up to $10^3 \sim 10^4$ times solid density. Even if the achieved compression by spherically symmetric implosion is extremely high, unavoidable departures from symmetry limit the achievable compression. These departures from symmetry can arise from pellet asymmetries, from nonuniform laser illumination, and from hydrodynamic instability. The fusion pellets must be sufficiently symmetric so that the compression is not reduced by nonunuform motion of the pellet surface. Though a requirement to the pellet surface is severe, it is not inachievable.

The uniformity of laser energy deposition on a spherical pellet surface depends on the number of the laser beams, intensity distribution, and focusing condition. If any smoothing or averaging effects are absent, the nonuniformity of laser flux would lead to marked temperature and hence pressure variation in the pellet surface, causing nonuniform acceleration and destroying the spherically symmetric hydrodynamic motion. The effects of nonuniformity may be, however, very markedly alleviated by electron thermal condition through the conduction region. According to Ref. 1, the characteristic smoothing scale is of the order of thousands of microns for glass laser case. This scale is much larger than the pellet radius. Therefore, as long as the thermal condition is considerable, the conduction tends to make the pressure at the ablation surface much more symmetric than

might be expected from the laser energy distribution (see also Ref. 2). This smoothing effect essentially depends on enrgy transport problem, so that reduction or limitation of heat transport would reduce the smoothing effect.

We now turn to the question of hydrodynamic stability of the implosion. Principal x-t diagram for the implosion of a typical target is shown in Fig. 6.1. The typical target is constructed by three layers; say, fuel, high-Z pusher, and low-Z ablation. In the light of the classical problem of Rayleigh-Taylor instability, this instability can occur at I, II, and III in Fig. 6.1, and any perturbation of these surface will grow. At a plane interface the growth rate is given by

$$\gamma = (\alpha k g)^{1/2}$$

where α [$= (\rho_1-\rho_2)/(\rho_i+\rho_2)$] is an Attwood number, k is the wave number of the perurbation, and g is the acceleration of the corresponding surface. For the instabilities at II and III, the classical formula may give a correct growth rate without modification due to a diffuse boundary effect. However, for the instability at the ablation front (I in Fig. 6.1), this formula may not provide a well approximated value for growth rate since there exists the ablating flow across the front, the large thermal conduction, and so on. The stability analysis to the ablation front, which is characteristic for implosions in all inertia fusion schemes, is unavoidable problem to achieve supercompression.

On the effect of thermal conduction, Nuckolls et al.[4] suggested that the amplitude of the instability will be restricted by ablative "fire ploishing": any salient high-

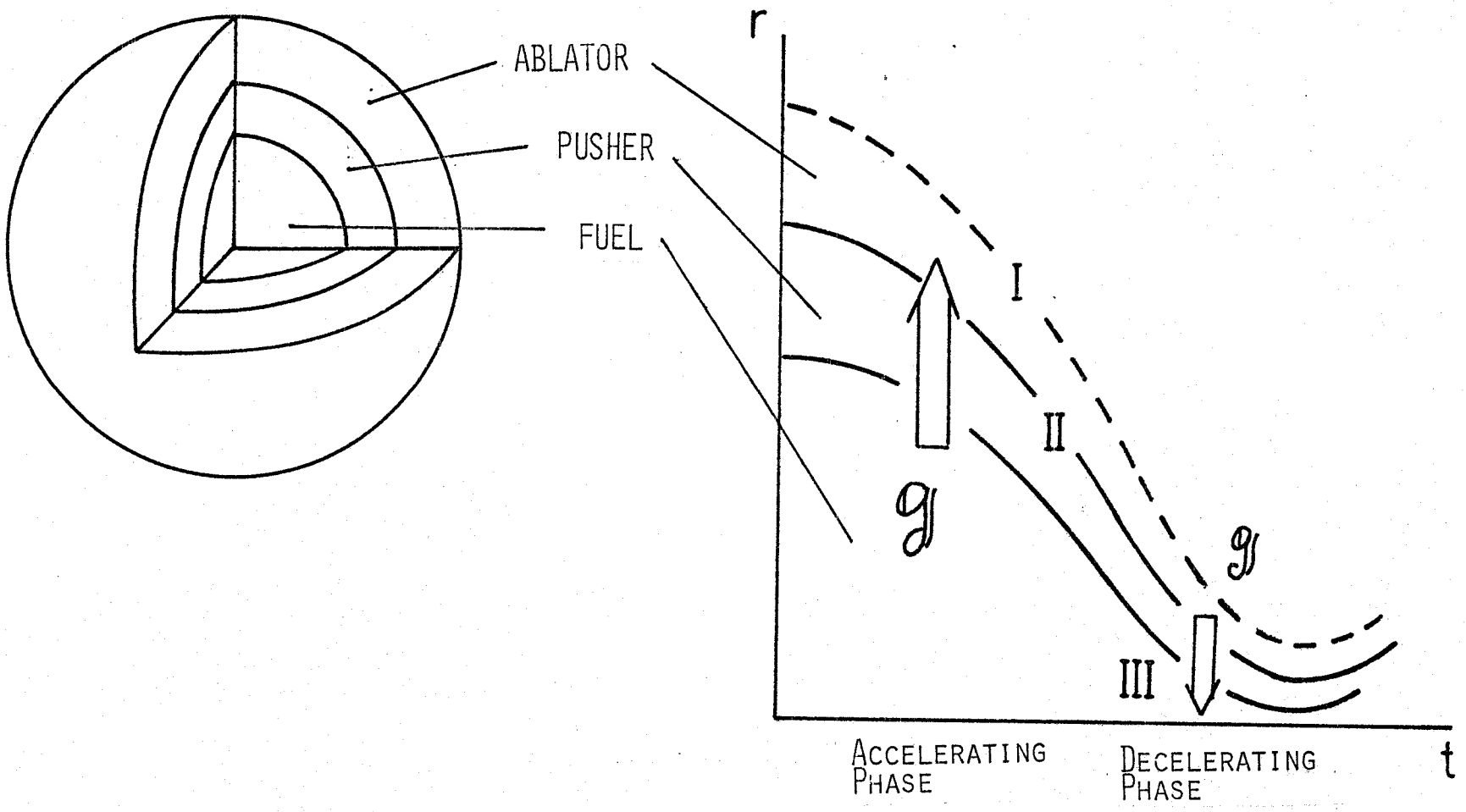

Fig. 6.1 Typical target structure (left figure) and principal x-t diagram for the implosion dynamics of this target (right figure)

The effective gravitations appear in twe phases, and these foces give rise to the Rayleigh-Taylor instabilities at three surfaces I, II, III.

density region will be nearer to the critical density surface where heat source exists and will thus be more rapidly ablated. In Refs. 5, 6, and 7, numerical analysis have been done using one-dimensional linear perturbation codes in which the analystic equations govering fluid dynamics are transformed into a set of linearized equations govering the time evaluation of peturbations, decoupled by an expansion in term of spherical or Fourier harmonics. Shiau et al. in Ref. 5 concluded that the ablation surface is not stabilized against small depatures from spherical symmetry. However, Henderson et al. in Ref. 6 found that for conditions relevant to laser fusion experiments the surface is positively stable. Moreover, Brueckner et al. in Ref. 7 showed that the ablation surface is stable, and they pointed out that the inconsistent result obtained in Ref. 5 is due to the fact that the temperature used in the analysis was much lowered for the thermal conduction effect to be effective to the ablation front stabilization.

The flow effect on reducing the classical Rayleigh-Taylor growth rate was pointed out by Bodner.[8] He carried out a model analysis by setting that the ablation front is assumed to be discontinuous surface and the flow across this front is sufficiently subsonic in both sides. He found that the effect of convectional flow reduces the classical gr owth rate to

$$\gamma = \sqrt{kg} - ku$$

where u_0 is the upstream flow velocity. Afanasev et al.[9] also pointed out that the convectional flow will carry the

growing pertubations to the stable region and the growth of pertubations may be reduced by the convection effect. Recently, Catto[10] analysed an ablating stabilization by considering the diffused, structured ablating plasma and he concluded that the most unstable modes, $k^2L^2 \gtrsim 1$, are insensitive to the ablation stabilization, where L is the density scale length at the ablation front.

In summarizing aspects on the ablation front stablity, it is convenient to refer the schematic representation given by Boris et al.[1] According to Ref. 11, the changes expected in the dispersion relation from the various effects at ablation front are represented schematically in Fig. 6.2. The upper curve (·····--) is the case of an ideal density discontinuity in an incompressible fluid. When finite density gradient scale length are taken into account in an incompressible fluid, the dispersion relation is modified at short wavelength (-·-·-·-). The growth rate is essentially constant and given as $\gamma=\sqrt{g/L}$ at shorter wavelengths, $k \gtrsim 1/L$. Addition of convection and finite thermal conduction tend to reduce the growth to zero at sufficiently short wavelength giving the (----) curve shown in the figure. The uppermost solid curve differs from the dashed curve by the addition of acceleration term which reduces the gravitational force to $g_{eff}=g-d^2/dx^2(u_0^2/2)$. Moreover, they say that the lower solid curve includes the further addition of dynamic stabilization for the most dangerous unstable modes. It seems to be optimistic to the ablation front stability. However, in order to achieve more symmetric implosion and

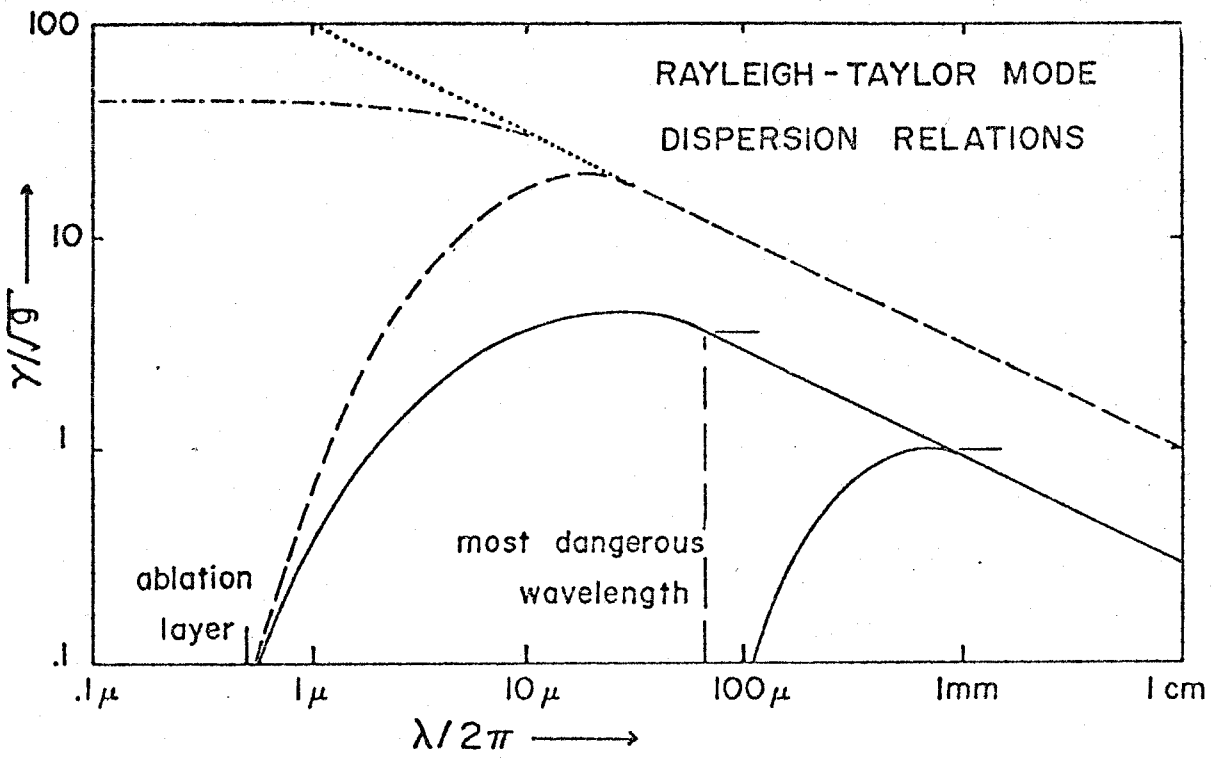

Fig. 6.2 Typical Rayleigh-Taylor dispersion relations given in Ref. 11.

also controll the stability of the ablation front, more investigations to the front stability are needed, especially, in the field of theoretical analysis. In this chapter, we intend to formulate this problem including the effects of compressibility, thermal conduction, ablation, and convection.

In Sec. 6.2, the linearized equations governing the evolution of the small perturbations are introduced with inclusion of the energy equation. Section 6.3 is devoted to investigate the thermal conduction, ablation and compressibility effects. It is concluded that in the case of short wavelength perturbations, the thermal conduction effect reduces the growth rate whereas ablation effect works in stabilization. In the case of the longwavelength perturbation, the effect of compressibility reduces the growth rate, but this effect is not so effective and the modification to the classical value is small. Moreover, in contrast to incompressible Rayleigh-Taylor formulation, it is found that the source term causing instabilities is not proportional to $-\nabla P \cdot \nabla \rho$[11] but proportional to $\nabla P \cdot \nabla T$. In Sec. 6.4, attention is focused on the effect of convective flow adopting a discontinuous model to the ablation front. It is found that the ablation front is unstable even if the gravitational filed is absent, say, the convection effect does not play the role of stabilization as shown in Refs. 8, 9, but induces a new type instability. However, when the flow velocity exceeds a sonic speed at the downstream, then it is found that this instability induced by the convection is stabilized, coupled with the effect of compressibility.

6.2 Basic Equation for Linear Perturbations

In the compressed region and/or near the ablation front, the hydrodynamics well describe the evolution of the motion of laser produced plasma. We carry out the stability analysis for the evolution of the small deviations from the equilibrium state. Basic Equations which describe the equilibrium state and also controll the evolution of the perturbations are

$$\frac{\partial}{\partial t}\rho + \nabla(\rho \mathbf{u}) = 0 \tag{6.1}$$

$$\rho\left(\frac{\partial}{\partial t} + \mathbf{u}\nabla\right)\mathbf{u} = -\nabla P + \rho \mathbf{g} \tag{6.2}$$

$$\frac{\partial}{\partial t}\left(\frac{3}{2}P + \frac{1}{2}\rho u^2\right) + \nabla\left(\frac{5}{2}P\mathbf{u} + \frac{1}{2}\rho u^2 \mathbf{u} + \mathbf{Q}\right) = \rho \mathbf{g}\cdot\mathbf{u} \tag{6.3}$$

where ρ, $\mathbf{u}$, and P are the mass density, velocity, and pressure, respectively and $\mathbf{g}$ means the graritational field coming from a inertia force in the frame moving with the ablation front. (see Fig.6.1.) The electron thermal conduction is denoted by the flux $\mathbf{Q}$ in Eq.(6.3). Here, the above equations are the equations of continuity (6.1), motion (6.2), and energy (6.3), respectively.

We simplify the problem by reglecting the effect of a spherical geometry and setting the equilibrium motion only

in the x direction and gravitational force is also in the same direction. Then the zeroth order equations for the equilibrium state are

$$\rho_0 u_0 = \text{const.} \tag{6.4}$$

$$\frac{1}{\rho_0}\frac{d}{dx}P_0 = g - \frac{d}{dx}\left(\frac{u_0^2}{2}\right) \tag{6.5}$$

$$\frac{d}{dx}\left(\frac{5}{2}P_0 u_0 + Q_0\right) + u_0\frac{d}{dx}P_0 = 0 \tag{6.6}$$

where subscript 0 means the zeroth quantities. Fig.6.3 is a schematic of the typical spatial behaviour of the zeroth variable in the vicinity of the ablation front.

In linearizing Eqs.(6.1) - (6.3), we assume that the perturbed quantities depend on the time and the transverse dimension y as

$$f_1(x,y,t) = f_1(x)\exp(\gamma t + iky) \tag{6.7}$$

where k is a wavenumber of the sinusoidal perturbation in the y direction. The linearized equation for Eqs.(6.1) - (6.3) are then

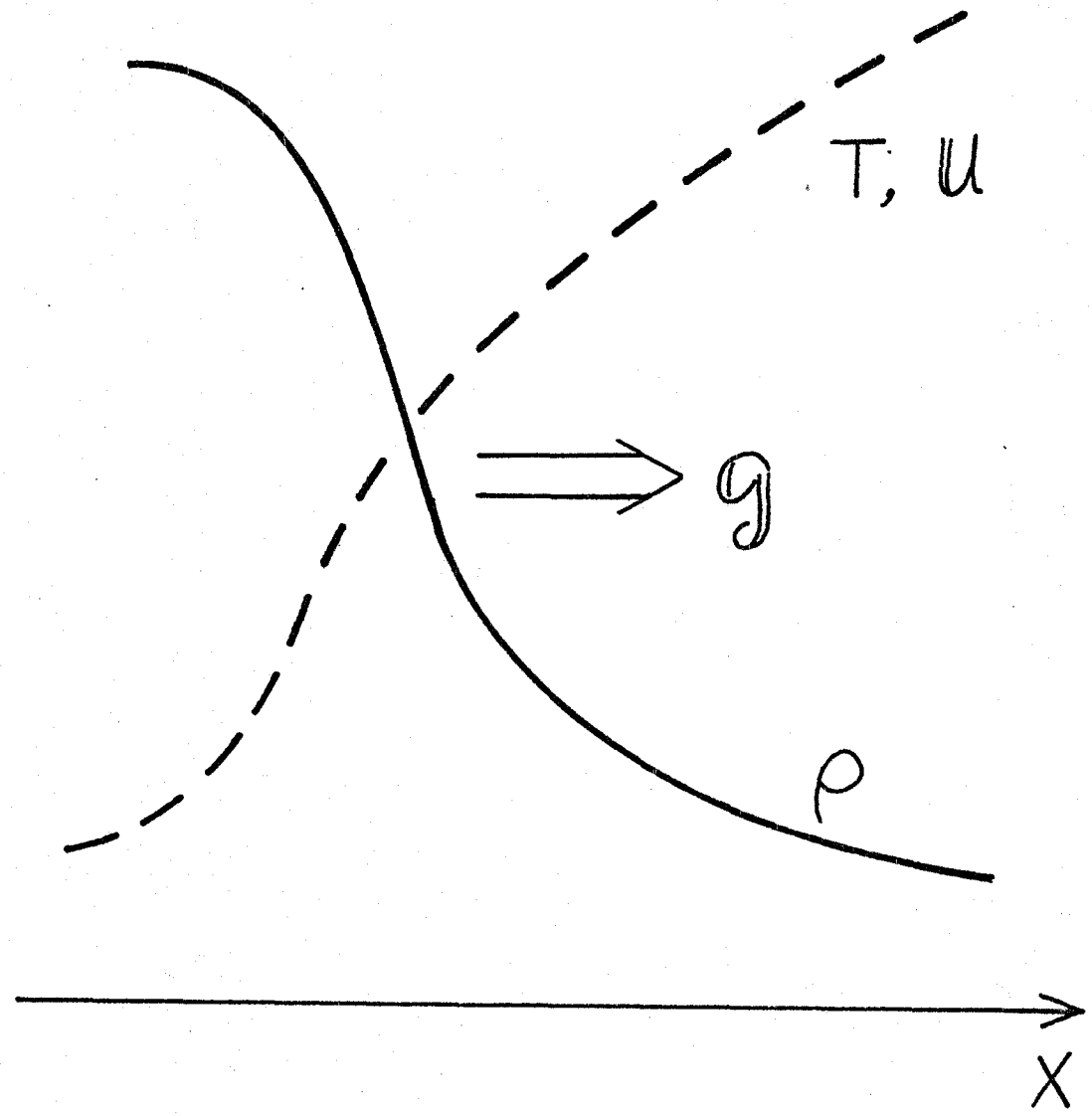

Fig. 6.3 Schematic profile near the ablation front.

$$\left(\gamma+\frac{dU_0}{dx}\right)\rho_1+\rho_0\frac{d}{dx}U_{x1}+ik\rho_0U_{y1}+U_{x1}\frac{d\rho_0}{dx}=-U_0\frac{d\rho_1}{dx} \tag{6.8}$$

$$\rho_0\left(\gamma+\frac{dU_0}{dx}\right)U_{x1}+\frac{dP_1}{dx}-\left(g-U_0\frac{dU_0}{dx}\right)\rho_1=-\rho_0U_0\frac{dU_{x1}}{dx} \tag{6.9}$$

$$\gamma\rho_0U_{y1}+ikP_1=-\rho_0U_0\frac{dU_{y1}}{dx} \tag{6.10}$$

$$\left(\frac{3}{2}\gamma+\frac{5}{2}\frac{dU_0}{dx}\right)P_1+\frac{5}{2}\frac{d}{dx}(P_0U_{x1})+\frac{5}{2}ik\rho_0U_{y1}+ikQ_{y1}$$
$$=-\frac{5}{2}U_0\frac{d}{dx}P_1-\frac{d}{dx}Q_{x1}-\left[\frac{\partial}{\partial t}\rho U^2+\nabla\frac{1}{2}\rho U^2U\right]_1 \tag{6.11}$$

where ρ_1, u_{x1}, u_{y1}, P_1, Q_{x1}, Q_{y1}, and $[\ ]_1$ are the first order perturbed guantities and the perturvations for thermal flux are given by $\mathbb{Q} = (Q_{x1}, Q_{y1}, 0)$. Hereafter, we take account of only the y-directional thermal flux peraturvation Q_{y1}, and neglect Q_{x1}. Since the thermal flux in the diffusion form is given by $\mathbb{Q} = -K\nabla T$ (where K is the thermal conductivity and T is the temperature defined by $T = P/\rho$), the perturbed flux Q_{y1} is

$$Q_{y1}=-ik\chi(P_1-T_0\rho_1) \tag{6.12}$$

where $\chi = K/\rho_0$ is the thermal diffusivity. In obtaining Eq.(6.12), we neglected the perturbation for K.

6.3 Termal Conduction, Ablation, and Compressibility Effects on Reducing the classical R-T Growth

By separating the convection effect from the effects of the compressibility, thermal conduction, and ablation, we consider only the later effects in this section. Here, the convection and ablation coming from the zeroth order flow are defined as follows. The former is the effect carrying the perturbation with the zeroth flow, which is denoted by the term $-u_0\frac{d}{dx}$ in Eqs. (6.8) - (6.11), whereas the later denotes a distortion of the equilibrium state because of the exsistence of the zeroth flow. The perturbation for the kinetic energy denoted by $[\ ]_1$ in Eq.(6.11) is neglected in this section, since we assume the flow is sufficiently sobsonic. Then, the right hand sides of Eqs.(6.8) - (6.11) can be set equal to zero. The reduced equations are

$$\gamma' p_1 + \frac{d}{dx}\varphi_x + \frac{k^2}{\gamma} p_1 = 0 \tag{6.13}$$

$$\gamma' \varphi_x + \frac{d}{dx} p_1 - \rho_1 A = 0 \tag{6.14}$$

$$\left(k^2\chi + \frac{5}{2}\gamma' - \gamma + \frac{5}{2}\frac{k^2 T_0}{\gamma}\right) p_1 + \frac{5}{2}\frac{d}{dx}(T_0\varphi_x) - k^2 T_0 \chi \rho_1 = 0 \tag{6.15}$$

where $\gamma' = \gamma + du_0/dx$, $\varphi_x = \rho_0 u_{x1}$, and $A = g - u_0\frac{d}{dx}u_0$. The perturbed velocity u_{y1} is eliminated using Eq.(6.10). Here, A denotes the effective gravitation when the ablation exsists.

Eliminating the pressure P_1 and the density ρ_1, we get the following differential equation for φ_x.

$$\frac{d}{dx} F \frac{d}{dx} \varphi_x - G \frac{d\varphi_x}{dx} + H \varphi_x = 0 \tag{6.16}$$

where

$$\begin{aligned} F &= k^2 T_0 \left(\chi + \frac{5}{2}\frac{\gamma'}{k^2}\right) / B \\ G &= \left[\frac{5}{2}\gamma' T_0 \frac{d}{dx}(\ln \rho_0) + (k^2\chi - \gamma) A\right] / B \\ H &= \frac{d}{dx}\left(\frac{5}{2}\frac{\gamma'}{B}\frac{dT_0}{dx}\right) + \frac{5}{2}\frac{A}{B}\frac{k^2}{\gamma}\frac{dT_0}{dx} - \frac{\gamma'}{\gamma}k^2 \\ B &= (k^2 T_0 + \gamma\gamma')\left(\chi + \frac{5}{2}\frac{\gamma'}{k^2}\right) - \frac{\gamma^2\gamma'}{k^2} \end{aligned} \tag{6.17}$$

Equation (6.16) is rewritten in the Sturm-Liouville form.

$$\frac{d}{dx}\left(F S \frac{d}{dx}\varphi_x\right) + H S \varphi_x = 0 \tag{6.18}$$

here

$$S = \exp\left(-\int^x \frac{G}{F}\, dx\right)$$

We obtain the folloiwng form for S by using the zeroth relation (6.5)

$$S = P_0^{(1+\frac{2}{5}k^2\chi/\gamma')^{-1}} P_0^{\frac{2}{5}(\frac{\gamma}{\gamma'} - \frac{k^2\chi}{\gamma'})/(1+\frac{2}{5}\frac{k^2\chi}{\gamma'})} \tag{6.19}$$

By multiplying Eq.(6.18) by the complex conjugate φ_x^* and integrating over the x space from the negative infinite to positive infinite, the following variational formulation is obtained.

$$\gamma\gamma' = \frac{\int_{-\infty}^{\infty} \frac{k^2 A \frac{d}{dx}\ln T_0}{f_c f_T - \frac{2}{5}\gamma^2/k^2 T_0} |\varphi_x|^2 S\, dx}{\int_{-\infty}^{\infty} \left(\frac{f_T}{f_c f_T - \frac{2}{5}\gamma^2/k^2 T_0} \left|\frac{d\varphi_x}{dx}\right|^2 + k^2 \frac{\gamma'}{\gamma} |\varphi_x|^2 \right) S\, dx} \tag{6.20}$$

$$f_c = 1 + \gamma\gamma'/k^2 T_0$$

$$f_T = 1 + \frac{2}{5}\frac{k^2}{\gamma'}\chi \tag{6.21}$$

where we used the fact that φ_x is bounded at $\pm\infty$. We

neglected the first term in H of Eq.(6.17), because the variation and/or the jump of the derivative for T_0 is sufficiently small within our interest. In the above formula, f_c and f_T provide the modifications. due to the compressibility and thermal conduction, repectively. It is obvious from Eq. (6.20) that the region where $A\frac{dT_0}{dx} > 0$ is unstable.

Thus, by making use of Eq. (6.18) or (6.20) the stability analysis proceeds. We here consider the two limiting case.s One is the case of much shorter y-directional wavelength than the scale length L of the zeroth order variables (diffuse boundary problem), and the other in the case of much longer wavelength (discontinuous boundary problem).

Case-A ($kL \gg 1$)

When the y-directional wavelength is much shorter than the scale length L of the zeroth variables, the unstable mode may be localized over the unstable region and local approximation may be good for the analysis. In this limiling case, Eq.(6.18) reduces to the approximate form

$$\frac{d}{dx}\left(\frac{1}{P_0}\frac{d}{dx}\varphi_x\right) + \frac{1}{P_0}\left(\frac{A/\gamma}{\frac{2}{3}\chi k^2 + \gamma'}\cdot\frac{1}{T_0}\frac{dT_0}{dx} - \frac{\gamma'}{\gamma}\right)k^2\varphi_x = 0 \qquad (6.22)$$

In this equation, the spatial extent of the wave function directly depends on the unstable source term, which is given

by the term propotional to $A \cdot dT_0/dx$. Near the ablation front, the temperature varies very rapidly, while the pressure is kept nealy constant. Thus, the variation of P_0 in Eq.(6.22) can be neglected.

Let us set the temperature profile as

$$\frac{1}{T_0}\frac{dT_0}{dx} = \frac{1}{L}\cosh^2(\alpha x) \tag{6.23}$$

where L is the ninimum local scale length of the temperature profile, which may be given y rhe scale length near the thermal wave front, and α is some value corresponding to the width of the ablation structure. Then, Eq. (6.22) reduced to

$$\frac{d}{dx^2}\varphi_x + \left(\frac{A/\gamma}{\frac{2}{5}\chi k^2 + \gamma'}\frac{1}{L}\cosh^2(\alpha x) - \frac{\gamma'}{\gamma}\right)k^2\varphi_x = 0 \tag{6.24}$$

The solution of this eigenvalue problem is given in the textbook of Landau and Lifshitz[12]. And the eigenvalue is, in this case, expressed as

$$\frac{\gamma'}{\gamma}k^2 = \frac{\alpha^2}{4}\left[\sqrt{1 + \frac{4A}{(\frac{2}{5}\chi k^2 + \gamma')\gamma L}\frac{k^2}{\alpha^2}} - (1+2n)\right]^2 \tag{6.25}$$

where n=0, 1, 2, 3, ...,. The most unstable mode is obtained when n=0. This is evident setting $\gamma' = \gamma$ in the above equation. The relation(6.25) provide us with the growth rate γ. For large k, Eq.(6.25) may be approximated to the following quadratic equation

$$\gamma'^2 + \frac{2}{5} k^2 \chi \gamma' - \frac{A}{L} = 0 \qquad (6.26)$$

or simply

$$\gamma \approx \frac{A}{\frac{2}{5} k^2 \chi L} - \frac{dU_0}{dx} \qquad (6.27)$$

It is found from these results that the effect of thermal conduction reduces the growth rate, not stabilizes the instability, and the effect of the ablation gives the reduced gravitational force $g - U_0 \frac{dU_0}{dx}$ instead of g and also plays a characteristic role to cut the unstable mode spectrum when $\frac{dU_0}{dx}$ is sufficiently large.

If we neglect the effect of thermal conduction, Eq. (6.26) gives

$$\gamma = \sqrt{A/L} - \frac{dU_0}{dx} \qquad (6.28)$$

This points out that the well-known growth rate $\sqrt{A/L}$ [10] is reduced by dU_0/dx due to the additional ablation effect.

Case-B ($kL \ll 1$)

When the y-directional wavelength k is sufficiently large compared with the scale length of the zeroth order variable near the ablation front, then the unstable mode extends on the spatial scale of not L but rather k^{-1}. When this is the case, the problem becomes that for the discontinuous equilibrium state. In the discontinuous problem, the Source which gives rise to the instability is localized at the discontinuous surface, while the unstable mode extends over the upperdense (region I) and lowerdence (region II) regions where the growth variable are almost homogenious respectively. For $kL \ll 1$, by neglecting the effects of the ablation and the thermal conduction, the variational form given by Eq.(6.20) reduces to

$$\gamma^2 = \frac{\int_{-\infty}^{\infty} \frac{k^2 g \frac{d}{dx} T_0}{1+\frac{3}{5}\gamma^2/k^2 T_0} |\varphi_x|^2 P_0^{-\frac{3}{5}} dx}{\int_{-\infty}^{\infty} \left(\frac{1}{1+\frac{3}{5}\gamma^2/k^2 T_0} \left|\frac{d\varphi_x}{dx}\right|^2 + k^2 |\varphi_x|^2 \right) \frac{P_0^{2/5}}{\rho_0} dx} \qquad (6.29)$$

The corresponding growth rate will be calculated using maximization method for the given test function as follows. Let us set the wave function as the form

$$\varphi_x = \varphi_0 \begin{cases} \exp(K_1 x) & x<0 \\ \exp(K_2 x) & x>0 \end{cases} \qquad (6.30)$$

in the upperdense region ($x < 0$) and the lowerdense region ($x > 0$), respectively. Moreover, for simplicity, we assume that the temperatures T_{01} in $x < 0$, T_{02} in $x > 0$, satisfy the relation $T_{01} \ll T_{02}$ and the pressure P_0 varies very gradually in space compared with k^{-1}. Then, the integrations of Eq.(6.29) may be carried out to give

$$\gamma^2 = \frac{k^2 g \left(\frac{1}{1+\frac{3}{5}\gamma^2/k^2 T_{01}} + 1 \right) \frac{1}{2} \left(\frac{1}{\rho_{02}} - \frac{1}{\rho_{01}} \right)}{\left(\frac{K_1}{1+\frac{3}{5}\gamma^2/k^2 T_{01}} + \frac{k^2}{K_1} \right) \frac{1}{2\rho_{01}} + \left(K_2 + \frac{k^2}{K_2} \right) \frac{1}{2\rho_{02}}} \qquad (6.31)$$

Here, we made use of the fact that the numerator of Eq.(6.29) involves a delta function given by dT_0/dx at the discontinuous surface, $x = 0$. The maximization for γ^2 in Eq. (6.31) with respect to K_1 and K_2 provides us with the well approximated growth rate. With the corresponding values

$$K_1 = k \left(1 + \frac{3}{5} \frac{\gamma^2}{k^2 T_{01}} \right)^{1/2}$$

$$K_2 = k \qquad (6.32)$$

we obtain the following growth rate in the case where $\rho_{01} \gg \rho_{02}$

$$\gamma^2 = \frac{1}{2}\left(1 + \frac{1}{1+\frac{3}{5}\gamma^2/k^2T_{01}}\right)kg \qquad (6.33)$$

This results show that when k is sufficiently small satisfing the relation $\gamma/k \lesssim \sqrt{\frac{5}{3}T_{01}}$ (sound speed in the upperdense region), then disturbances of the unstable mode cannot propagate rapidly, therefore the extent of this perturbation at the upperdense regeion is reduced to that obtained in Eq.(6.32), and the corresponding growth rate is also reduced as obvious from Eq.(6.33). It is found, however, that the reduction of the incompressible growth rate $\gamma=\sqrt{kg}$ due to the compressibility effect is not so drastic even when $\gamma^2 \gtrsim k^2T_{01}$, as long as $\gamma^2 < k^2T_{02}$. And it may be rather important that when the extent of the unstable mode is large, the zeroth equilibrium state in the upperdense ($x < 0$) and the lowerdense ($x > 0$) regions may be distorted due to the gravitational force so that the variations of P_0, T_0, and ρ_0 over the extent of the unstable mode should be taken into account for the integrations in Eq. (6.29).

The effect of the compressibility on reducing the classical growth rate is not so drastic by itself, but as shown in the following section, this effect plays a significant role together with the convection effect.

6.4 Effect of Convection on Stabilization and Destabilization

In this section, we consider the discontinuous problem to the ablation front stability (see Fig.6.4) including the effects of convention and compressibility but excluding the effect of the thermal conduction which is not essential for the discussion of this section. The effect of ablation is also not essential in such a discontinuous model. For simplicity, we do not consider the energy equation (6.11) and set $P_1=T_0\rho_1$. This assumption is reasonable for region II, where the thermal conduction is large enough to give the temperature perturbation $T_1 = 0$, but not for region I, where the adiabatic assumption $P_1=5/3T_0\rho_1$ is rather resonable. However, this effect does not change the following discussion so much that we set $P_1=T_0\rho_1$ hereafter. Then, Eqs. (6.8) - (6.10) for the perturbations are rewritten as

$$\left(\gamma+\frac{dU_0}{dx}+U_0\frac{d}{dx}\right)\rho_1+\rho_0\frac{d}{dx}U_{x1}+ikU_{y1}+U_{x1}\frac{d\rho_0}{dx}=0 \tag{6.34}$$

$$\rho_0\left(\gamma+\frac{dU_0}{dx}+U_0\frac{d}{dx}\right)U_{x1}+T_0\frac{d}{dx}\rho_1-\frac{1}{\rho_0}\frac{dP_0}{dx}\rho_1=-\rho_0U_0\frac{dU_{x1}}{dx} \tag{6.35}$$

$$\rho_0\left(\gamma+U_0\frac{d}{dx}\right)U_{y1}+ikT_0\rho_1=0 \tag{6.36}$$

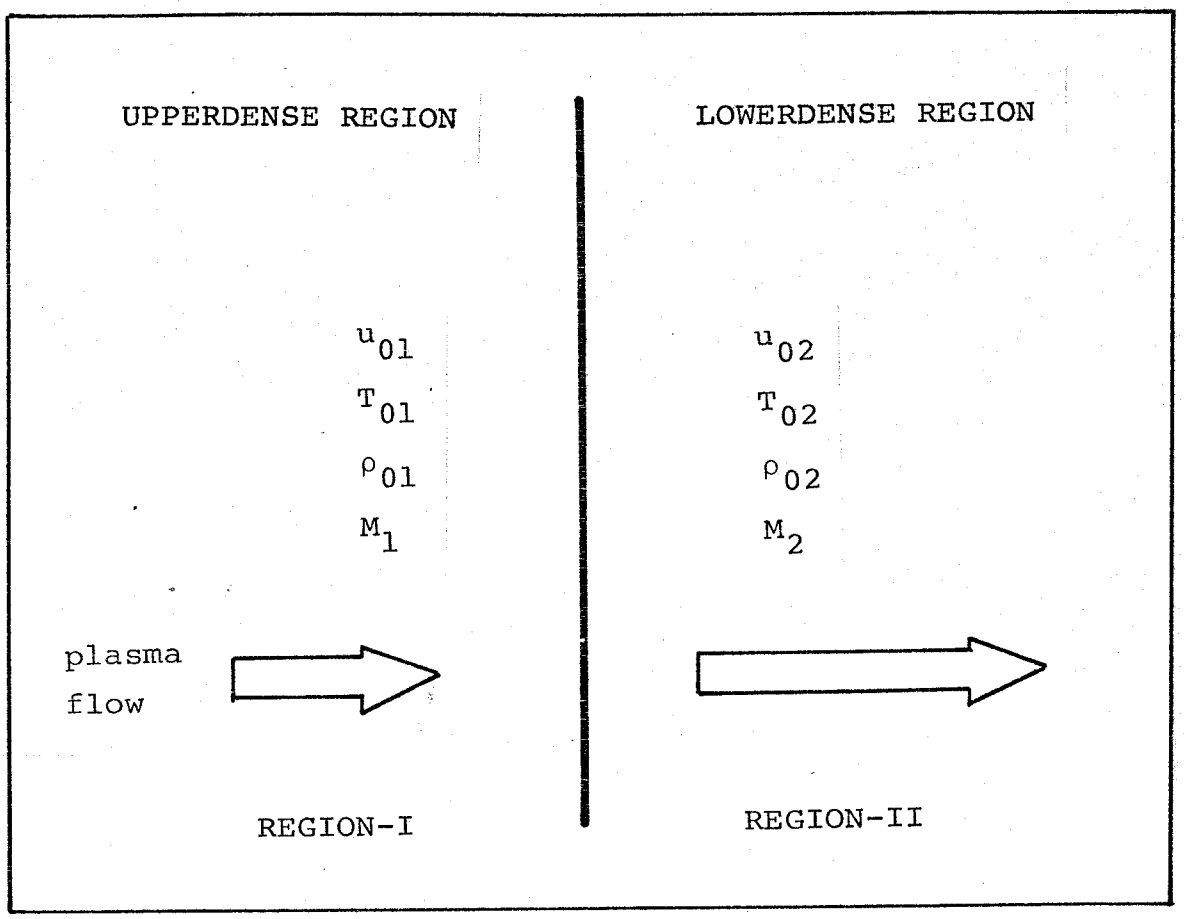

Fig. 6.4 Geometry for jump conditions to the zeroth quantities. The flow velocity, temperature, density, and Mach numbers are defined by u_{01}, T_{01}, ρ_{01}, and M_1 in the upperdense region I, while u_{02}, T_{02}, ρ_{02}, and M_2 in the lowerdense region II.

We assume that the gravitational force is not so strong to distort the zeroth variables and hence the instability mode in the regions I and II. Thus, by neglecting the spatial variations of the zeroth variables in the both regions, the characteristic equation for the unstable mode is

$$(\gamma + u_0 K)\left[(u_0^2 - T_0)K^2 + 2\gamma u_0 K + k^2 T_0 + \gamma^2\right] = 0 \qquad (6.37)$$

where $K = d/dx$. After solving this equations, the perturbed mode is given by the form proportional to $\exp(KX)$. In region I with high density, low temperature, and sufficiently subsonic flow, the meaningful solution of Eq.(6.37) is

$$K = \left[\left(1 + \frac{\gamma^2}{k^2 T_{01}}\right)^{1/2} + M_1\left(\frac{\gamma^2}{k^2 T_{01}}\right)^{1/2}\right]\cdot k \quad (\equiv k_1) \qquad (6.38)$$

and in region II with low density, high temperature, and subsonic flow, K is

$$K = -\frac{\gamma}{u_{02}} \qquad (6.39)$$

$$K = \frac{1}{1-M_2^2}\left[\left(\frac{\gamma^2}{k^2 T_{02}}\right)^{1/2} - \left(1 - M_2^2 + \frac{\gamma^2}{k^2 T_{02}}\right)^{1/2}\right]\cdot k \quad (\equiv k_2) \qquad (6.40)$$

where M_1 and M_2 are the Mach numbers at the region I and region II, respectively, It is noted that the extent of the perturbation in region I given by Eq.(6.38) is identical to that given by K_1 in Eq.(6.32), say, the modification of the spatial extent is mainly due to the compressibility in the regeon I, whereas in the region II, a new mode $X = -\gamma/u_{02}$ which is due to cirect effect of convection appears, and the surface mode(6.40) is drastically modified, when the flow is supersonic, $M_2 > 1$.

According to these three modes, the amplitudes of the perturbations in the vicinity of the discontinuous surface are obtained from Eqs.(6.34) - (6.36) as

$$
\begin{aligned}
u_{x1} &= A \\
u_{y1} &= i\frac{k}{k_1}A \\
p_1 &= -\frac{\rho_{01}}{c_{01}}\left(\frac{\gamma}{k_1 c_{01}} + M_1\right)A
\end{aligned}
\tag{6.41}
$$

at x = -0 in region I, and

$$
\begin{aligned}
u_{x1} &= B + C \\
u_{y1} &= i\frac{k}{k_2}B - i\frac{\gamma}{k u_{02}}C \\
p_1 &= -\frac{\rho_{02}}{c_{02}}\left(\frac{\gamma}{k_2 c_{02}} + M_2\right)B
\end{aligned}
\tag{6.42}
$$

at x = +0 in region II, respectively. Here, $C_{01}=\sqrt{T_{01}}$ and $C_{02}=\sqrt{T_{02}}$, and k_1 and k_2 are k of Eqs(6.38) and (6.40), respectively. A is the amplitude of the x-directional perturbed velocity for the mode(6.38). B and C are amplitudes of the modes (6.40) and (6.39), respectively. Note that the perturbation corresponding to the mode(6.39) is a transverse one, say, $\rho_1 = 0$. The perturbations have been specified by the tree constants A, B, and C as described above. In order to obtain the dispasion relation to the unstable mode we use the following consevation laws given by integrating Eqs(6.34) - (6.36) across the perturbed discontinuous surface. The intergral are carried out over the infinitesimal range from ξ-0 to ξ+0, where ξ means the x-diredtional displacement of the discontinuous surface. Then the consevation laws of mass, x-momentum, and y-momentum flows are

$$\left[\rho_1 u_0 + \rho_0 (u_{x1} - \gamma\xi)\right]_{-0}^{+0} = 0 \tag{6.43}$$

$$\left[\rho_1 u_0^2 + 2\rho_0 u_0 u_{x1} - \rho_0 u_0 \gamma\xi + p_1 + g\rho_0 \xi\right]_{-0}^{+0} = 0 \tag{6.44}$$

$$\left[u_{y1} + ik u_0 \xi\right]_{-0}^{+0} = 0 \tag{6.45}$$

where $[\ ]_{-0}^{+0}$ means the Poisson bracket. When the thermal conduction is included, to find out relation between ξ and the other 1-st order quantities becomes the most important problem to

get a correct dispersion relation, since the discontinuous surface corresponds to that of the temperature profile for the ablation front. However, in the present case, where the effect of thermal conduction is excluded and attention is limited to the compression and convection effects, the temperature discontinuity follows the perturbation in the upperdense region, because in this region the tharmal perturbation follows that of the other quantities. Therefore, we set that

$$\xi = \int_0^t u_{x1}\, dt \Big|_{at\ x=-0}$$

$$= \gamma \cdot A \tag{6.46}$$

By sybstituting Eqs.(6.41)and (6.42) into Eqs.(6,43) - (6.46), we obtain the following dispersion relation

$$\begin{vmatrix} M_2^2 \frac{k}{k_1} X^2 - M_1 X & 1 - M_2^2 - M_1(1+M_2^2)\frac{k}{k_2} & 1 \\ \frac{1+M_2^2}{1-M_2^2}\frac{g}{k T_{01}} - \frac{k}{k_1}X^2 - M_1 & 1 + \frac{M_1}{M_2^2}\frac{k}{k_2}X & 0 \\ M_2^2 - M_1(1+M_2^2)\cdot\frac{k}{k_1}X & \frac{k}{k_2} & M_1\frac{1+M_2^2}{M_2^2}X \end{vmatrix} = 0 \tag{6.47}$$

where $x = \gamma/kC_{01}$ and the jump relations for zeroth quantities across the discontinuous surface are used under the assumytin $M_1 \ll 1$. When we obtain the solution to the dispersion relation Eq.(6.47), we consider the following three cases;
(I) $M_1, M_2 \ll 1$, (II) $M_1 \ll 1$, $M_2 \lesssim 1$, and
(III) $M_1 \ll 1$, $M_2 > 1$.

Case-I ($M_1, M_2 \ll 1$)

In general, the ablation front satisfies the condition for the upstream. First of all, we here consider the case where the flow is also sufficiently subsonic in the lowerdense region. In this case, as long as the gravitational force is not so strong, the imcompressible condition provides us with a good approximation, which will become appear from the resultant growth rate. By setting $k_1 = k$, $k_2 = -k$, the dispersion relation(6.47) reduces to the following graduratic form.

$$(u_{01}+u_{02})\gamma^2 + 2ku_{01}u_{02}\gamma - ku_{01}u_{02}\left[g\left(\frac{1}{u_{01}} - \frac{1}{u_{02}}\right) + k(u_{02}-u_{01})\right] = 0 \qquad (6.48)$$

This dispersion relation is identical to that obtained by Landau[13]. In the circumstance where $u_{01} \ll u_{02}$, Eq. (6.48) yields

$$\gamma = \sqrt{kg + k^2 u_{01}u_{02}} \qquad (6.49)$$

It is significant to emphasise that a new type instability appears at the ablation front due to the convection and the ablation front is unstable even if the gravitational field is absent. This result is inconsistent with those of Bodner[8] and Afanas'ev et al[9].

Case-II ($M_1 \ll 1$, $M_2 \lesssim 1$)

When the downstream velocity appriaches sound speed, as is apparent from the previous result, the growth rate of thisinstability increases. In this case, the assumption of imcompressible fluid is not adequate in the region I. In region II, the flow effect distorts the perturbalation mode. We make use of the approximate form

$$k_1 = \sqrt{1+X^2}\cdot k$$

$$k_2 = (1-M_2^2)^{1/2} k$$

for k_1 and k_2 to obtain the dispersion relation

$$\frac{X^2}{1+X^2} = \frac{1+M_2^2}{1-M_2^2}\frac{g}{kT_{01}} + \frac{M_2^2}{(1-M_2^2)^{1/2}}$$

In this case, the essential feature for the qualitative dis-

noted that the effect of convection gives rise to the growth rate of order kC_{01} [$x \sim O(1)$].

Case-III ($M_1 \ll 1$, $M_2 > 1$)

As apparent from Eq.(6.40), the evanisent wavenumber in the region II (k_2) becomes a complex value and exhibits an oscillating decay property, when the flow velocity grows up to a supersonic one in this region. The dispersion relation, in this case, may be shown by the form

$$\frac{X^2}{1+X^2} = \frac{1+M_2^2}{1-M_2^2}\cdot\frac{g}{kT_{01}} + 2\cdot\frac{M_2^2}{M_2^2-1}$$

When the gravitational force is absent, it is readily verify that the growth rate x given by this relation becomes a pure imaginary value for $M_2 > 1$. This indicates that the unstable mode is stabilized by the convectional effect when the flow velocity exceeds a sonic speed. This is a drastic result due to the exsistence of the convective flow across the discontinuous surface. More rigorous result to Eq.(6.47) is shown in Fig.6.5 When the gravitational force is not so strong, the gravitational instability is also attenuated by the convection effect.

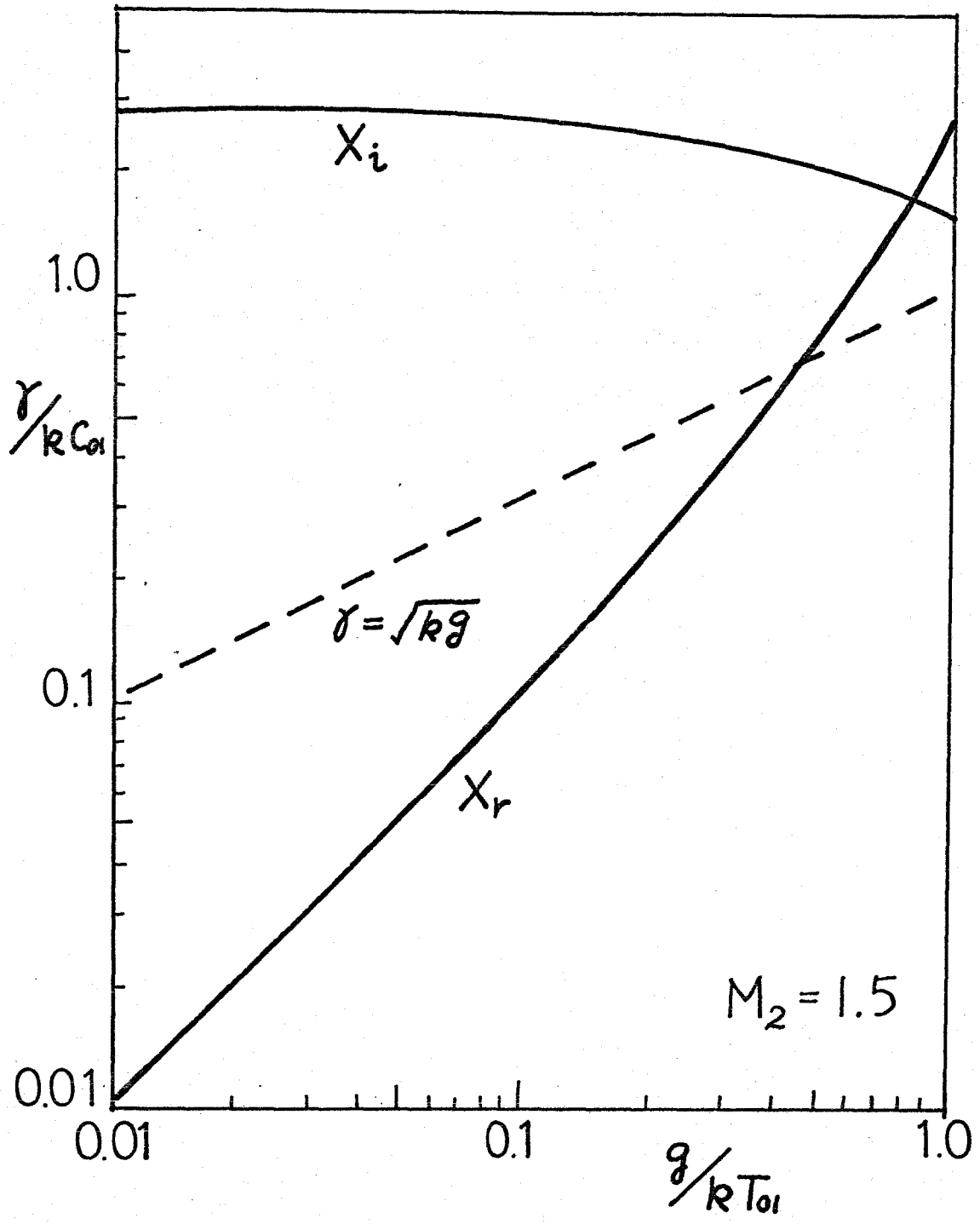

Fig. 6.5 Growth rate given by the dispersion relation Eq.(6.47) for the case-III with M_2=1.5.
Here, X_r, X_i are the real and imaginary parts of the growth rate X ($=\gamma/kC_{01}$). Even when the gravitational force exsists, the real growth rate (X_r) is reduced compared with that given by the classical Rayleigh-Taylor instability in the interesting region where $g/kT_{01}<<1$.

6.5 Conclusion and Discussion

The stability analyses to the accelerating ablation front have been carried out, focusing our attention on the compressibility, thermal conduction, ablation, and convection effects. The conventional linearization method was employed to describ the evolution of the perturbations in the continuity, momentum, and energy equations. It was found that these coupled equations reduces to the second order linear differential equation, when the convection effect is neglected. Moreover, in this case the tractable variational representation to the growth rate was also obtained. As the results, it was found that (1) the source term which causes instabilities is not proportional to $-\nabla P \cdot \nabla \rho$ but proportional to $\nabla P \cdot \nabla T$, when the energy equation is included in the analyses; (2) the y-directional thermal conduction reduces the growth rate, but does not stabilize the instabilities; (3) the ablation effect play the significant role that it reduces the gravitation to the smaller value, $g_{eff} = g - u_0 \frac{d}{dx} u_0$, and also stabilize the shortwavelength perturbations by providing the growth rate with the additional negative term $-du_0/dx$, and (4) the effect of compressibility becomes important for longer wavelength perturbations, but it is not so drastic as long as the compressibility is effective only in the upper dense region but not in the under-dense region. (This condition is satisfied for the lase inplosion in general.)

In order to investigate the convection effects, the stability analysis was carried out by assuming ablation front

discontinuous. It was found that this effect causes the new type instability without the gravitational force in this case of subsonic flow. However this mode is stable for the case where the flow is supersonic at the downstream. These results are essential for the stability of the ablation front where the flow velocity varies from subsonic to supersonic in space with the finite transition region. Therefore, in order to discuss some quantitative aspects to the practical stability problems of the ablation front, it is necessary to extendthis analysis to the diffused boundary model. In this case, the other effects described above will inevitablly couple to this problem directly. This problem is now in investigation and results will be presented near feature.

References

1. K. A. Brueckner and S. Jorna, Rev. Mod. Phys. 46, 325 (1974)
2. D. B. Henderson and R. L. Morse, Phys. Rev. Lett. 32, 355(1973)
3. S. Chandraseckhar, "Hydrodynamic and Hydromagnetic Stability," Chap.X. (Clarendon, Oxford, 1961).
4. J. Nuckolls, L. Wood, A. Thiessen, and G. Zimmerman, Nature 239, 139(1972)
5. J. N. Shiau, E. B. Goldman, and C. I. Weng, Phys. Rev. Lett. 32, 352(1973)
6. D. B. Henderson, R. L. MaCrory, and R. L. Morse, Phys. Rev. Lett. 33, 205(1974)
7. K. A. Brueckner, S. Jorna, and R. S. Janda, Phys. Fluids 17, 1554(1974)
8. S. Bodner, Phys. Rev. Lett. 33, 761(1974)
9. Yu. F. Afanas'ev, N. G. Vasov, E. G. Gamalii, O. N. Krokhin, and V. B. Rosanov, JETP Lett. 23, 567(1976)
10. P. J. Catto, Phys. Fluids 21, 30(1978)
11. J. P. Boris and J. H. Orens, in "Digest of Technical Papers presented at Topical Meeting on ICF. Feb.29, 1978, SanDiego, Calfornia," p.Thcl-1.
12. L. D. Landau and E. M. Lifshitz, "Quantum Mechanics," 3rd ed., p.73. (Pergamon, Oxford, 1977).
13. L. D. landau and E. M. Lifshitz, "Fluid Mechanics," p.478.(Problem.1). (Pergamon, Oxford, 1963)

Chapter 7

Conclusions

In the present paper, the implosion and ablation mechanisms were investigated in Chap.2 and 3 and its stability was also considered in Chap.6. For the absorption and transport problems, Chaps. 4 and 5 were devoted to analyses of the linear conversion and the transport of the hot electrons.

In Chap.2, the stationary deflagration structure was investigated using the one fluid two temperature hydrodynamic equations. The width of this deflagnation is given by $\Delta x=0.32 \quad (M/m)^{1/2} \, l_{ep}$ in terms of the electron mean free path at the rear, l_{ep}. The structure near the ablation front shows a good agreement with that of the well-known thermal wave. The deflagration is characterized by the steep gradients of the density, flow velocity, and temperatures and also by the almost constant prsesure. The density at the Chapman-Jouguet point is found to be important for compression, because the implosion efficiency is proportional to the square root of this density.

In Chapter 3, the self-similar ablating motion was investigated using the same equations employed in Chap.2, when the absobed laser energy increases with the form $I_{ab} = \phi_0 t^{\beta}$. The time dependect dynamics of the ablation phenomena is obtained uniquely by the use of the energy conservation law. It is pointed out that the response between the absorbed power and the ablation pressure is different in time, and in order to maintain the constant pressure the increase of the absorbed power in proportion to $t^{1/5}$ is necessary. In contrast to the case of the staisionary model analysis, the self-similar solution soes not shown any singularity at the

sonicpoint and it gives us the reasonable structure over the expanding region.

In Chapter 4, the electrostatic field generation and the corresponding hot electron heat flux reduction were investigated including the appearance of the ion wave turbulence near the cut-off. The collisionless Vlasov equation for hot selections and fluid equations with the anomalous collision effects for cold electrons were used. As the results, it is found that a large electrostatic potential, say, $|e\phi/T_h| = 1$ or 2 is built up and only about 10 % (spherical) or 20 % (plane) of the free streaming flux limit can penetrate into the core region.

In Chapter 5, the resonantly driven plasma wave was investigated to the case where plasma flow exsists through the resonance point. Maxwell equation and the momentum equation of the cold electron fluid were used, and to avoid the nonlinearity coming from the convection, the Lagrangian description was employed for the large amplitude wave oscillation. It is pointed out that wavebreaking appears predominantly in the underdense region, and when the current velocity is sufficiently large the resonance field amplitude is limited by the flow effect without occurence of wavebeaking.

In Chapter 6, the stability analyses to the accelerating ablation front was shown, focusing our attention on the compressibility, thermal conduction, ablation, and convection effects. The hydrodynamic equations including the energy equation were used. It is poined out that the inclusion of the temperature perturbation provides us with the instability souce proportional to $\nabla P \cdot \nabla T$, not $-\nabla P \cdot \nabla \rho$. The effect

of thermal conduction reduces the growth rate of the small wavelength perturbation, while the ablation effect play the role of not only redicing the growth rate but also cutting the unstable spectrum for sufficiently large wavenumber perturbation. The effect of convection is found to be drastic for the ablation front stability. When the flow across the ablation front is subsonic, this effect causes a new type instability even when the gravitational force is absent. On the otherhand, when the flow becomes supersonic in the downstream, this convection instability becomes stable, and instability is caused only by the gravitational force.

Throughout these investigations,the ablation phenomena, which play the foundamental role in the implosion process, became clear, and the stability of the ablation front was also clarified. In conection with the hot electron generation, the effect of the flow on influencing the linear conversion processes and the hot electron transport inhibition due to the self-generated electrostatic field were also pointed out.

Acknowledgements

The author would like to express his sincere thanks to Professor Chiyoe Yamanaka and Dr. Kunioki Mima for their valuable guidances and continuous encouragements in carrying out the present study. The author wishes to express his sincere thanks to Professor Hitoshi Kinoshita, Professor Masataro Nishimura, Professor Yoshio Inuishi, Professor Katsunobu Hujii, Professor Yutaka Suzuki, Professor Masahiro Yokoyama, Professor Sadao Nakai, and the late Professor Kazuo Kawabe for their kind guidances in my graduate school.

The author would like to express his thanks to Professor Toshiya Taniuti, Dr. Katsunobu Nishihara, Dr. Takashi yabe for their valuable discussion and useful suggestions. Moreover, the author wishes to express his thanks to Dr. Tatsuhiko Yamanaka, Dr. Takatomo Sasaki, Dr. Yoshiaki Kato, Dr. Takayasu Mochizuki, Dr. Yasukazu Izawa, Dr. Yoneyoshi Kitagawa, Dr. Masafumi Matoba, Dr. Kunio Yoshida, Dr. Kazuo Imasaki, and Zunichi Mizui of Nagoya University for their great interest and important suggestions in their respective fields.

Finally, The author wishes to express his thanks to Miss. Yumi Watanabe, Miss Mika teraura, and my sister, Junko Takabe for their fine typing of this manuscript.

PUBLISHED PAPERS

1) Deflagration Waves in Laser Compression I
by H. Takabe, K. Nishihara and T. Taniuti
J. Phys. Soc. Japan 45, 2001 (1978)

2) Deflagration in Laser Plasma
by H. Takabe and K. Nishihara
Technol. Rept. Osaka Univ. 28, 35 (1978)

3) Computer Simulation on Laser Plasma Compression
by N. Kimura, T. Taguchi, K. Hosokawa, H. Takabe,
K. Nishihara and C. Yamanaka
Technol. Rept. Osaka Univ. 28, 193 (1978)

4) Reduction of Hot Electron Energy Transport by
Electrostatic Field
by H. Takabe and K. Mima
Kakuyugo-Kenkyu, 41, 15 (1979) (in Japanese)

5) Hot Electron Energy Flux Limitaiton by Electrostatic
Field
by H. Takabe and K. Mima
Physics of Fluid (Received at June 1, 1979)

6) Ablation and Compression Mechanism in Laser Fusion
Plasma (An Approach with Self-Similar Solutions)
by H. Takabe, T. Yabe and K. Nishihara
Laser-Kenkyu, 7, 4 (1979) (in Japanese)

学会発表

1). レーザー爆縮におけるディフラグレーションの構造
物理学会 山口大 1977年 4月

2). レーザー噴出プラズマの相似解
物理学会 東京理科大 1977年 10月

3). シース電場による高速電子の熱輸送への影響
物理学会 東北大 1978年 4月

4). 二成分電子を含出レーザー噴出プラズマの構造
物理学会 静岡大 1978年 10月

5). Rayleigh-Taylor 不安定への流れ及び圧縮性の効果
物理学会 愛媛大 1979年 10月

6). Wavebreaking への流れの効果
物理学会 愛媛大 1979年 10月